Title
New modalities of strain-control of ferroelectric thin films

Journal
Journal of Physics Condensed Matter, 28(26)

ISSN
0953-8984

Authors
Damodaran, Anoop R
Agar, Joshua C
Pandya, Shishir
et al.

Publication Date
2016-07-06

DOI
10.1088/0953-8984/28/26/263001

Peer reviewed

New modalities of strain-control of ferroelectric thin films

2016 J. Phys.: Condens. Matter 28 263001

(http://iopscience.iop.org/0953-8984/28/26/263001)

IOP Publishing Journal of Physics: Condensed Matter

J. Phys.: Condens. Matter **28** (2016) 263001 (36pp) doi:10.1088/0953-8984/28/26/263001

Topical Review

New modalities of strain-control of ferroelectric thin films

Anoop R Damodaran[1,3], Joshua C Agar[1,3], Shishir Pandya[1], Zuhuang Chen[1,2], Liv Dedon[1], Ruijuan Xu[1], Brent Apgar[1], Sahar Saremi[1] and Lane W Martin[1,2]

[1] Department of Materials Science and Engineering, University of California, Berkeley, Berkeley, California, USA

[2] Materials Science Division, Lawrence Berkeley National Laboratory, Berkeley, California, USA

E-mail: lwmartin@berkeley.edu

Received 5 December 2015, revised 23 February 2016
Accepted for publication 24 February 2016
Published 17 May 2016

Abstract

Ferroelectrics, with their spontaneous switchable electric polarization and strong coupling between their electrical, mechanical, thermal, and optical responses, provide functionalities crucial for a diverse range of applications. Over the past decade, there has been significant progress in epitaxial strain engineering of oxide ferroelectric thin films to control and enhance the nature of ferroelectric order, alter ferroelectric susceptibilities, and to create new modes of response which can be harnessed for various applications. This review aims to cover some of the most important discoveries in strain engineering over the past decade and highlight some of the new and emerging approaches for strain control of ferroelectrics. We discuss how these new approaches to strain engineering provide promising routes to control and decouple ferroelectric susceptibilities and create new modes of response not possible in the confines of conventional strain engineering. To conclude, we will provide an overview and prospectus of these new and interesting modalities of strain engineering helping to accelerate their widespread development and implementation in future functional devices.

Keywords: ferroelectrics, thin films, epitaxy, strain

(Some figures may appear in colour only in the online journal)

1. Introduction

As early as the 1970s, research on ferroelectric thin films was underway to integrate functionalities found in ferroelectrics into microelectronic devices, microelectromechanical systems, and optical devices [1–10]. Initial work focused primarily on addressing some of the challenges associated with the higher leakage and losses when reproducing bulk-like ferroelectric responses in thin films [11–15]. By the 1990s, ferroelectric thin films were finding wide-spread application in memories, rf/microwave devices, pyroelectric (thermal), and piezoelectric (stress) sensors and actuators [6, 16–19]. Accelerated by advances in the synthesis of ferroelectric thin films with controlled chemistry and epitaxy [20–22], researchers sought to leverage these abilities to impose epitaxial strain, achieving complex control of crystal and domain structures, and ultimately ferroic responses inconceivable in the bulk [23–29]. The search for knowledge in this space has developed symbiotically with new advanced characterization techniques, and has driven the development of theoretical, computational, and modeling tools enabling the study and selection of these materials across expansive length- and time-scales and under various external perturbations [29–41]. The results have provided a detailed understanding of ferroelectricity including: new routes to control materials and phenomena, the discovery of new ferroelectric phases (some not stable or known in bulk form),

[3] These authors contributed equally to this work.

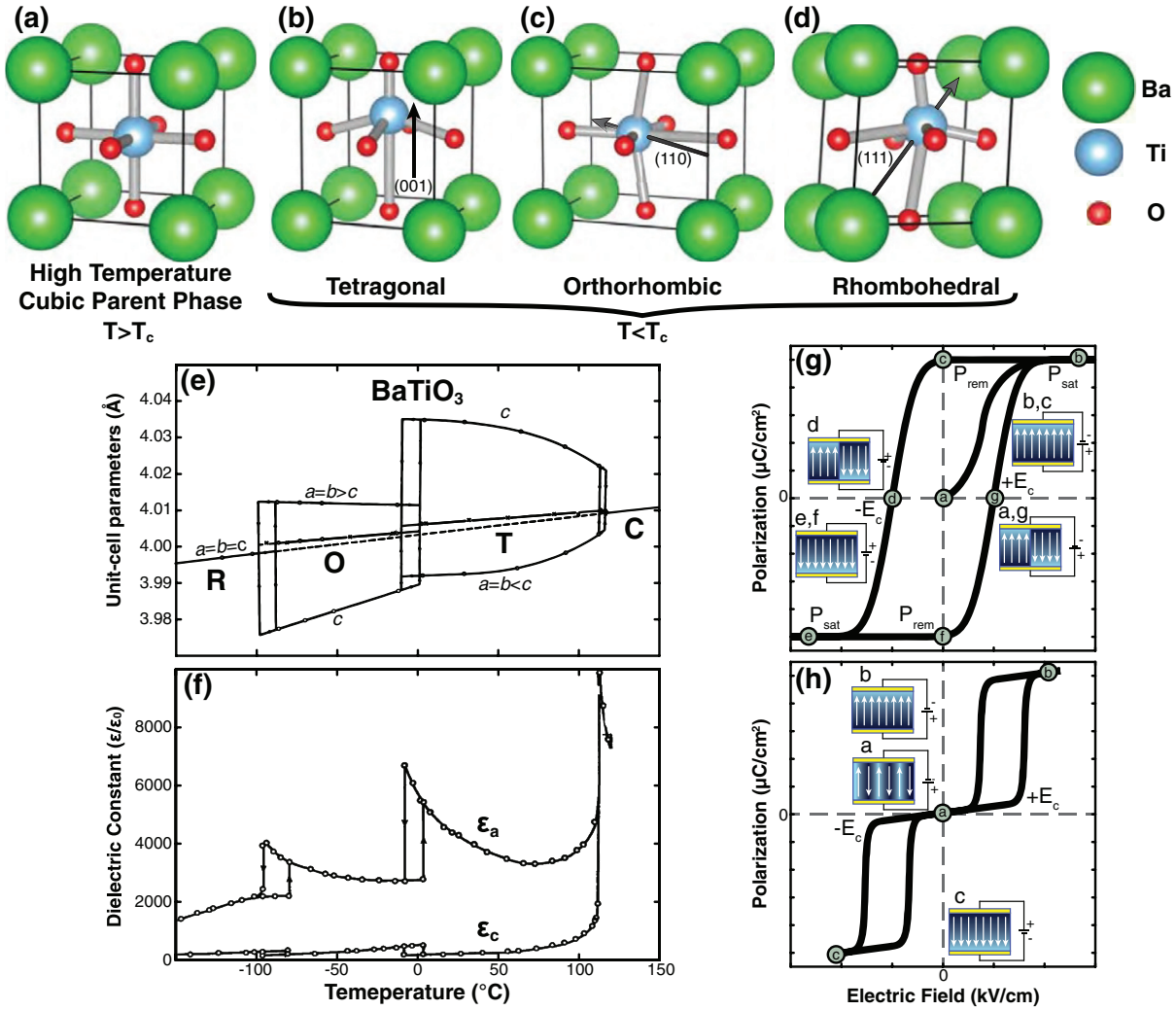

Figure 1. Schematic depiction of the crystal structure of polymorphic states of $BaTiO_3$ including (a) ideal perovskite structure (cubic, paraelectric parent phase), (b) tetragonal phase with polarization along [001], (c) orthorhombic phase with polarization along [110], and (d) rhombohedral phase with polarization along [111]. (e) Temperature-dependent evolution of the unit-cell lattice parameters and ferroelectric phase transitions (Reprinted from [52] by permission of Taylor & Francis Ltd, www.tandfonline.com) and (f) associated dielectric response in $BaTiO_3$ (Reprinted figure with permission from [53]. Copyright 1949 by the American Physical Society). (g) A typical ferroelectric hysteresis loop of polarization as a function of applied electric-field starting from a virgin polydomain state with zero net macroscopic polarization to a monodomain state that can be switched hysteretically between states with downward- and upward- pointing polarization. (h) A typical antiferroelectric hysteresis loop, for $E > E_C$ the system transforms to a ferroelectric phase.

new physics, and exciting possibilities for future applications. In this review, we provide a synopsis of the major developments and achievements in the last few years in the area of strain engineering of ferroelectric thin films (for a historical perspective we recommend several excellent reviews [16, 25, 26, 42]) with a strong emphasis on work blazing a new trail in terms of methods and control of strain engineering, understanding of strain effects, and routes to develop new functionalities and improved performance in ferroelectric-based microelectronic devices.

2. Physics of ferroelectrics

Ferroelectrics are materials that possess two or more stable states with a spontaneous polarization (or an electric dipole moment per unit volume) even in the absence of an applied electric field and can be reversibly switched between these states by the application of an electric field [43–45]. The ferroelectric polarization is strongly susceptible to electrical, mechanical, and thermal excitations yielding large dielectric, piezoelectric, and pyroelectric responses. To achieve such unique properties requires a specific combination of crystallographic and atomic-scale symmetry that limits ferroelectricity to only 10 of the 32 crystallographic classes [45, 46]. Perovskites with chemistry ABX_3, represented by 8 corner-sharing A-site cations with six face-sharing anions (typically oxygen), and a central B-site cation located inside the anion octahedron are one of the most widely studied crystallographic structures that exhibit ferroelectricity. At high temperatures the perovskite structure is centrosymmetric and exists in the paraelectric phase. Upon cooling, the perovskite structure can undergo structural distortions, most commonly related to octahedral rotations (typically quantified in terms of the Goldschmidt tolerance factor [47]) and/or ferroelectric distortions which can give rise to a spontaneous polarization (P_s) and ferroelectricity below the Curie temperature (T_c). To understand ferroelectricity requires consideration of the atomic orbitals and their interaction. For

instance, typically ferroelectric distortions can occur as the result of a symmetry breaking distortion of the *B*-site cation within the anion octahedra. *B*-site driven ferroelectricity results from an effect known as the second order Jahn–Teller effect which occurs when mixing between the *d* orbitals of the *B*-site cation and the oxygen 2*p* orbitals results in the formation of a non-degenerate ground state with a low-lying excited state [48–50]. This mixing (or hybridization) of the atomic orbitals generates a displacement in the position of the *B*-site cation ultimately giving rise to ferroelectricity. In general, *B*-site-driven ferroelectricity exists nearly exclusively in perovskites wherein the *B*-site cation possesses d^0 formal valence, as these orbitals can readily mix with the O 2*p* orbitals and the empty *d*-shell reduces columbic repulsion. $BaTiO_3$ is the prototypical example of a *B*-site driven ferroelectric wherein the Ti 3*d* orbitals hybridize with the O 2*p* orbitals, while the Ba 5*p* orbitals remain stereochemically inactive [31]. Additionally, the *A*-site cation can also contribute significantly to ferroelectricity [31, 51]. For instance, in Pb-based systems the 6*s* electrons of the Pb cation hybridize with the O 2*p* orbitals. This hybridization causes the electrons to become localized, inducing ferroelectricity [31]. Such *A*-site-driven ferroelectricity tends to give rise to a larger and more temperature stable ferroelectric distortions [31].

At various temperatures, pressures, and/or chemical compositions competition between sources of symmetry breaking exists, resulting in the possibility of structural phase transitions. For example, in bulk $BaTiO_3$, there are many temperature dependent phase transitions which can occur upon cooling from high temperature. First, there is a paraelectric–to-ferroelectric transition at 120 °C, where the material goes from a cubic lattice ($Pm\bar{3}m$ symmetry, figure 1(a)) to a tetragonal structure ($P4mm$ symmetry, figure 1(b)). This transition is accompanied by the development of a spontaneous macroscopic polarization along the tetragonal *c* axis (i.e., [001]). Upon cooling further, the $BaTiO_3$ crystal has additional phase transitions, including an orthorhombic phase ($mm2$ symmetry) at 0 °C with spontaneous polarization along the two-fold [110] (figure 1(c)) and a rhombohedral phase ($R3m$ symmetry) at −70 °C with spontaneous polarization along the three-fold [111] (figure 1(d)). These ferroelectric phase transitions in bulk $BaTiO_3$ tend to be of first-order meaning they are accompanied by the release of latent heat and a discontinuous and hysteretic change in lattice parameters (figure 1(e)) [52] and dielectric response (figure 1(f)) [53]. When ferroelectrics are grown as thin films, it is more common for ferroelectric transitions to be second-order (continuous transitions without any latent heat) as a result of the substrate imposed elastic boundary conditions. These ferroelectric transitions are particularly interesting as large anomalies in ferroelectric susceptibilities (theoretically approaching infinity in second order transitions) can be achieved. In turn, it is generally desirable to design materials to operate near these phase transitions for maximum response.

Once below the T_C, ferroelectric materials can exhibit multiple degenerate ferroelectric distortions (or polarization states) and can be switched between these states by the application of an external electric field. This switching process is typically represented in the form of a macroscopic ferroelectric hysteresis loop (figure 1(g)). Alternativly, the spontaneous polarization can be driven by octahedral rotations to order in an anti-parallel manner at the unit-cell level (i.e. antiferroelectricity). Antiferroelectrics exhibit no macroscopic spontaneous polarization, yet can be driven to behave like a ferroelectric when an electric field is applied; thereby producing a double hysteresis loop (figure 1(h)). As previously mentioned, the presence of a spontaneous polarization gives rise to coupled piezoelectric (linear coupling of stress-polarization and/or electric field-strain), pyroelectric (coupling of temperature-polarization), and electrocaloric (coupling of electric field-entropy) responses which are important for a wide variety of sensing, energy conversion, and device applications. While both pyroelectricity and piezoelectricity have less restrictive symmetry requirements than ferroelectricity (existing in 10 and 20 of the 32 crystallographic classes, respectively) these responses tend to be particularly large in ferroelectric materials making them interesting to study.

While ferroelectrics can exist with a single polarization variant (monodomain) it is more common to form domains (i.e., small volumes of uniform polarization direction) to minimize depolarization fields (ferroelectric) and to accommodate elastic strain (ferroelastic). In the bulk these domain structures are complex and difficult to control, however, epitaxial thin films provide a convenient platform to controllably orient and control domain structures. Such strain-based approaches to domain engineering are of significant interest as the presence of these domain structures can significantly influence ferroelectric susceptibilities, and has even been proposed as a route to achieve new types of devices where the domain wall is the functional element [16, 54–62].

3. Conventional misfit-strain control of ferroelectrics

Ferroelectric susceptibilities are strongly dependent on temperature, pressure, strain, and composition. The ability to controllably modify the structure of bulk ferroelectrics for device applications, however, is rather limited as devices can typically only operate over a narrow temperature and pressure range, and these ceramic materials structurally fail under modest strains (typically $<0.1\%$ under both compressive and tensile strains), limiting routes to control these material primarily to chemistry. The epitaxial growth of perovskite ferroelectric thin films on lattice mismatched single-crystal substrates, however, relaxes the limitation of strain engineering, allowing an additional knob, apart from composition and akin to pressure, to engineer phase and domain structures providing an enormous phase space for materials design [22, 26, 42, 63]. Furthermore, the geometry and simplicity of epitaxial single-crystal thin films provides a model platform to design systematic studies of both intrinsic (i.e., the bulk, unit-cell level, response of the polarization to an applied stimulus) and extrinsic (i.e., interfaces, domain walls, surfaces, phase boundaries, defects, etc.) responses. This interest in strain engineering has led to the development of high-quality perovskite substrates with a wide range of lattice parameters (3.68–4.17 Å) suitable for imposing various degrees of epitaxial strain (figure 2, bottom section) [27, 64–84]. Additionally,

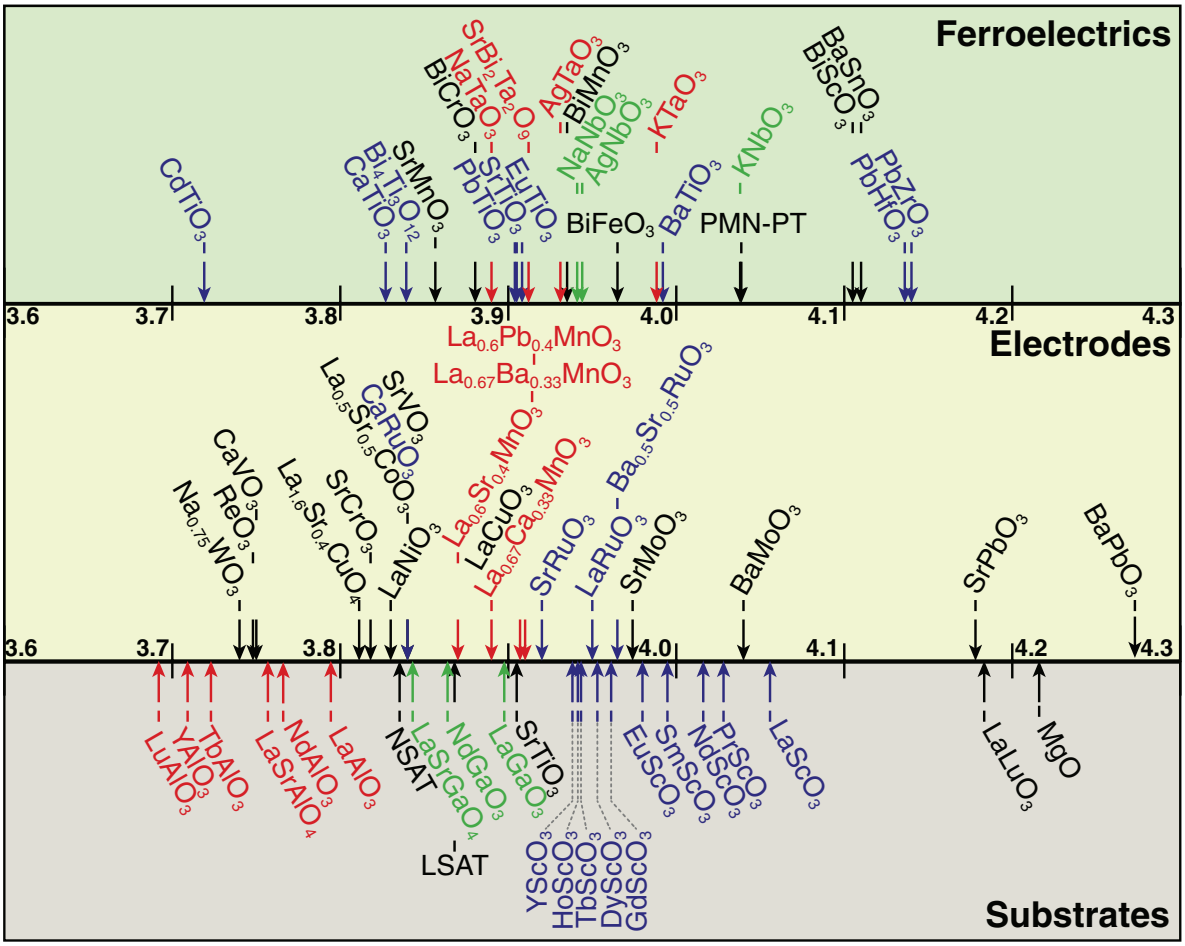

Figure 2. Survey of lattice parameters of commercially available substrate materials (bottom section), a select list of perovskite electrode materials (middle section), and ferroelectric, incipient ferroelectric, and anti-ferroelectric materials (top section).

techniques have been developed to assist in controlling the epitaxy including specialized surface treatments [85–90] that allow for the control of the interface chemistry and *in situ* monitoring/control of the growth processes at the sub-unit-cell level [21, 22]. These technologies have facilitated the design of ferroelectric heterostructures, devices, and superlattices where the thickness of the individual perovskite layers are precisely controlled to have "atomically" sharp interfaces (note that perfect interfaces are difficult, if not impossible, to achieve in practice, but intermixing of only 1-2 unit cells is perceived as possible).

To utilize ferroelectric thin films in devices requires bottom electrodes that are compatible with the epitaxy and allows for the retention of strain. In this regard, several conductive perovskite bottom electrode materials have been implemented (figure 2, middle section) [91, 92]. The diverse set of available single-crystal substrates and conductive bottom electrodes provide a convenient platform upon which an expansive range of perovskite ferroelectric films (figure 2, top section) [62, 93–103] can be grown, controllably oriented, strained, and probed. Most theoretical and experimental studies of epitaxial strain control have focused on (001)-oriented ferroelectric films (due in most part to the prevalence of the pseudo-cubic (001)-cut of commercial substrates and relative ease of growth) and, thus, we will focus primarily on such structures.

3.1. Lattice mismatch strain, size, and interface effects in ferroelectrics

The development of modern strain engineering was aided, in part, by pioneering theoretical predictions for misfit strain-temperature phase diagrams by researchers in the late 1990s based on phenomenological thermodynamic models [33, 104, 105]. Such phase diagrams predicted the ability of mechanical boundary conditions (or epitaxial strain) to change the order of the ferroelectric phase transitions, alter T_C, and possibly engineer novel low-symmetry ferroelectric phases unachievable in the absence of strain. In turn, a range of ferroelectric phases and domain structures were predicted creating an expansive and diverse nomenclature to describe these phases (figure 3(a)). While strain-induced enhancements of some tens of degrees in the T_C of ferromagnets [106, 107] and superconductors [108, 109] had been observed, these phenomenological models predicted much larger enhancements in ferroelectrics. These models even predicted the possibility of using epitaxial strain to stabilize ferroelectricity in $SrTiO_3$, a quantum paraelectric (figure 3(b)) [20, 26, 110, 111]. To experimentally realize these predictions, researchers developed and utilized an array of rare-earth scandate perovskite substrates and subsequently demonstrated the power of

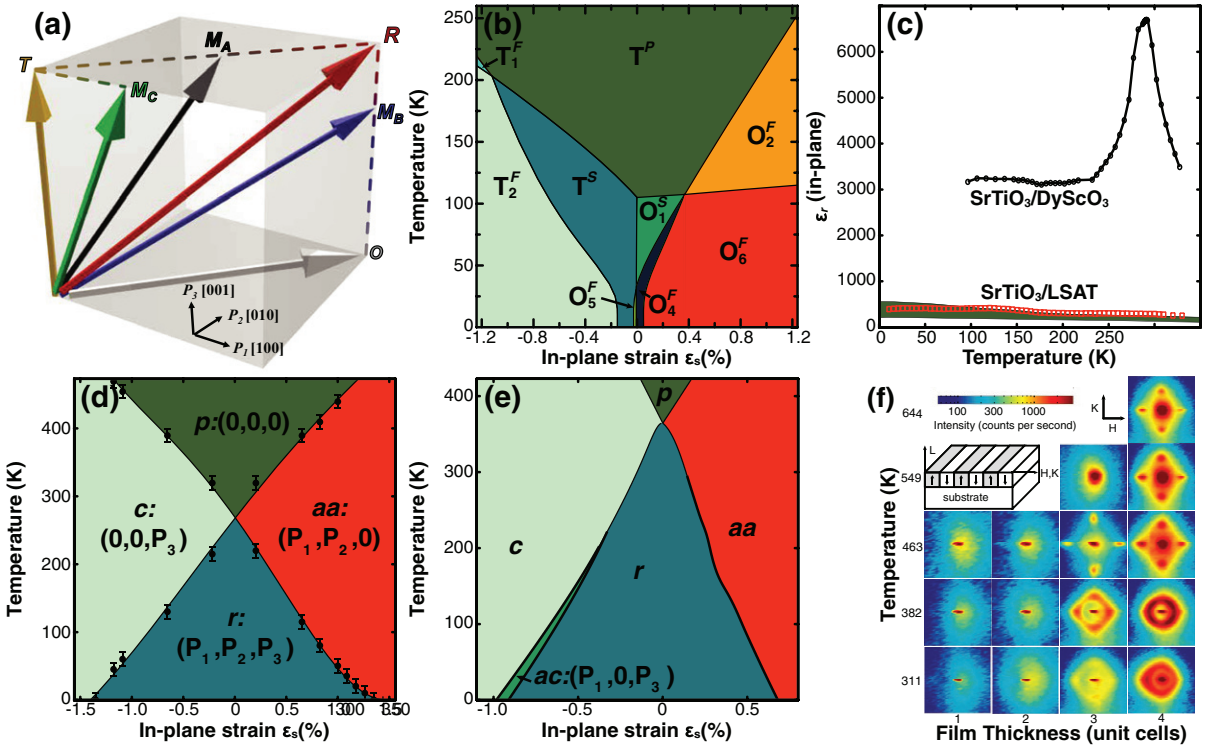

Figure 3. (a) Diagram showing the various nomenclatures used to describe ferroelectric phases based on their polarization direction. Tetragonal (T): $T(c)$ $P_1 = P_2 = 0$, $P_3 \neq 0$; $T(a_1)$ $P_2 = P_3 = 0$, $P_1 \neq 0$; $T(a_2)$ $P_1 = P_3 = 0$, $P_2 \neq 0$. Monoclinic (M): $M_C(ca)$ $P_1 \neq 0$, $P_2 = 0$, $P_3 \neq 0$; $M_A(r)$ $P_1 = P_2 \neq 0 < P_3 \neq 0$; $M_B(r)$ $P_1 = P_2 \neq 0 > P_3 \neq 0$; $M_C(ca^*)$ $P_1 = 0$, $P_2 \neq 0$, $P_3 \neq 0$; $M_C(aa*)$ $P_1 \neq 0$, $P_2 \neq 0$, $P_3 = 0$. Orthorhombic (aa): O $P_1 = P_2 \neq 0$, $P_3 = 0$. Rhombohedral (R): R $P_1 = P_2 = P_3 \neq 0$. (b) Phase-field predictions for the misfit-strain-temperature phase diagram for (001)-oriented $SrTiO_3$ assuming a monodomain state for all structural and ferroelectric phases (Reprinted with permission from [20]. Copyright 2008 John Wiley and Sons. Adapted with permission from [111]). The letters T, O, R, and M used in the phase notations indicate tetragonal, orthorhombic, rhombohedral, and monoclinic crystallographic symmetries, respectively. The superscript 'P,' 'S,' or 'F' indicates whether the phase is paraelectric, antiferrodistortive, or ferroelectric, respectively. (c) Temperature-dependent in-plane dielectric constant (ε_r) at a measurement frequency (f) of 10 GHz for 50 nm thick films of $SrTiO_3$ on $DyScO_3$ (110) and $(LaAlO_3)_{0.29}(Sr_{0.5}Al_{0.5}TaO_3)_{0.71}$ (001) substrates corresponding to epitaxial strains of +0.9% and –0.9%, respectively (Reprinted with permission from [112]. Copyright 2004 Nature Publishing Group). (d) and (e) $BaTiO_3$ temperature-stress diagram comparing *ab initio* predictions (Reprinted with permission from [126]. Copyright 2004 by the American Physical Society) with those from phenomenological thermodynamic calculations (Reprinted from [33] by permission of Taylor & Francis Ltd, www.tandfonline.com). (f) In-plane diffuse x-ray scattering profiles about the $PbTiO_3$ 303-diffraction condition for various thicknesses and temperatures. In each case the region shown extends ±0.2 reciprocal lattice units in the in-plane reciprocal space coordinates H and K. The broadening of the central Bragg peak in the H direction is due to instrumental resolution limits. Inset shows orientation of stripe domains (Reprinted with permission from [153]. Copyright 2004 AAAS Publishing).

strain-effects in controlling/inducing ferroelectricity [112, 113]. By applying biaxial tensile strains of ~1% to (001)-oriented $SrTiO_3$ thin films grown on $DyScO_3$ substrates, researchers were able to induce room-temperature ferroelectricity (figure 3(c)) [112, 114]. Likewise, application of a few percent compressive strain to $BaTiO_3$ resulted in the enhancement of the ferroelectric transition temperature by 500 °C and remnant polarization by ~250% [113].

This initial work motivated intense theoretical and experimental investigations of epitaxial-strain effects on the structure and response of a range of perovskite ferroelectrics including: $Ba_xSr_{1-x}Ti_xO_3$, $PbTiO_3$, $PbZr_xTi_{1-x}O_3$, $BiFeO_3$, and many others. Various computational methods including first-principles density functional theory (DFT) [30, 31, 38, 115–120], atomic-scale simulations (effective Hamiltonian methods [34, 121–126], molecular dynamics simulations [35, 37, 127–132], and Monte Carlo simulations [133–136] etc.) are now being employed in addition to continuum Landau-based thermodynamic models (including numerical phase-field [111, 137–141] as well as phenomenological Ginzburg–Landau–Deveonshire (GLD) models) to understand and predict ferroelectric phenomena at the nanoscale. First-principles-based, finite-temperature phase diagrams [126] have been obtained and match qualitatively well with those produced via phenomenological thermodynamic models [33] for prototypical systems including $BaTiO_3$ (figures 3(d) and (e), respectively). These models are particularly useful to predict the nature of the ferroelectric phases that form under epitaxial strain. One somewhat unexpected observation from these studies was that the strain dependence varies significantly across ferroelectric systems with $BiFeO_3$ and $LiNbO_3$ showing rather weak strain dependence compared to other ferroelectrics (i.e., $BaTiO_3$, $PbTiO_3$, etc.) [142, 143]. In $BiFeO_3$, for instance, it has been shown that the weak strain-dependence of spontaneous polarization is related to the competing polar cation displacements and a tendency for antiferrodistortive rotations [144]. Furthermore, it was shown that these antiferrodistortive rotations destabilize ferroelectricity decreasing the T_C of $BiFeO_3$ with increasing compressive strain [145–147]. These discoveries highlight the importance of macroscopic

phenomenological models and microscopic first-principles calculations in unraveling the nature of ferroelectric phenomena. Today, efforts are underway to develop multiscale-simulation strategies that bridge various theoretical/modeling approaches across several decades of length- and time-scales ushering in a new era of "ferroelectric oxides by design."

Along with epitaxial strain, the role of electrical boundary conditions in controlling ferroelectric thin films has been extensively explored. Such electrostatic considerations become especially important in ultrathin films, where there has been much debate about the existence of a critical thickness for ferroelectricity. Foundational work suggested a critical thickness of 10 nm is needed to stabilize a strongly polar phase [45, 148, 149], however, this notion has been challenged. As early as 1999 it was observed using scanning probe-based studies that a stable out-of-plane ferroelectric polarization can exist in epitaxial thin films of $PbZr_xTi_{1-x}O_3$ only 10 unit-cells thick [150]. This was followed by several theoretical investigations predicting stable ferroelectric ground states in ultrathin films [115, 151, 152]. Subsequent experimental investigations using synchrotron-based X-ray diffraction of ultrathin $PbTiO_3$/$SrTiO_3$ (001) heterostructures revealed a critical thickness of only 3 unit cells for stable out-of-plane ferroelectric polarization and a $T_C \approx 250$ °C (figure 3(f)) [153]. Furthermore, the absence of ferroelectricity at thicknesses < 3 unit cells was thought to arise from an antiferrodistortive $c(2 \times 2)$ surface reconstruction of the $PbTiO_3$ surface, rather than an intrinsic thickness-related effect [154]. It was also noted in these studies that in the absence of metal electrodes, depolarization effects that destabilize ferroelectricity were mitigated by the formation of periodic domains of alternating polarity (inset, figure 3(e)) resulting in satellite peaks around the $PbTiO_3$ 303-diffraction condition in X-ray scattering experiments. The lateral dimensions for these domains were only 1.2–4 nm (i.e., <10 unit cells) holding the promise of being able to achieve ferroelectric memory devices with ultrahigh densities approaching tens of Tb cm^{-2} [155–158].

There has also been renewed focus on understanding the origin and impact of dead layers at ferroelectric-metal interfaces on the performance of ultrathin ferroelectric devices (ferroelectric film thickness of <10 nm) [159–161]. In general, diminished dielectric performance of ultrathin ferroelectrics has been addressed *via* the concept of a so-called "dead layer" wherein a parasitic low permittivity layer at the ferroelectric-electrode interface can detrimentally impact device performance. The true nature of the dead layer either as an unavoidable and/or inherent feature of any dielectric-metal interface [162–166], or a manifestation of extrinsic effects arising from defects and imperfections [167–172] from thin-film growth and processing, has been a matter of debate. Recent theoretical studies suggest the crucial role of the local chemical environment wherein interfacial ferroelectricity formed between *A*-site terminated perovskites and simple metals can result in an overall enhancement of the ferroelectric instability [173]. Numerous studies were undertaken to resolve this seeming contradiction between theory and experiments, with a current proposition that the nature of the specific bonds intrinsic to the ferroelectric-electrode boundary can dictate ferroelectric behavior at the nanoscale [174].

In general, these studies reveal how computational modeling and experimental design can be utilized to manipulate the electrical and elastic boundary conditions in epitaxial thin films. Using these tools, researchers can deterministically tune phase transition temperatures and phase competition, realize metastable phases, and much more—all of which can dramatically impact ferroelectric susceptibilities and enable the creation of new ferroelectric functionalities. Such work provides the foundational tools to strain-engineer ferroelectric thin films.

3.2. Strain-tuning ferroelectric domain structures and properties

In addition to altering the crystal structure there has been significant interest in how strain can tune ferroelastic domain structures which can dramatically influence ferroelectric susceptibilities and functionality [16, 54–61]. In the case of ferroelectric thin films, the possibility of applying an epitaxial strain to suitably orient and simultaneously engineer self-organized ferroelectric nanostructures makes it promising for nanolithography, nonlinear optical, and other applications which rely on nanoscale ordered structures [175–177]. Ferroelectrics form domains to minimize the total free energy of the system, including elastic, electrostatic, and domain-wall (or gradient) energies. Mechanical compatibility requirements for stress-free domain walls [63, 178–180], and electrostatic compatibility [45, 63, 181] requirements for uncharged domain walls are crucial in determining ferroelectric domain structures. Typically these effects impose strong restrictions on the domain-wall geometries (denoted as the angle between the polarization vectors in adjacent domains) limiting the domain structures primarily to a select few (e.g., 90° and 180° domain walls in tetragonal ferroelectrics; 60°, 90°, 120°, and 180° domain walls in orthorhombic ferroelectrics; and 71°,109°, and 180° domain walls in rhombohedral ferroelectrics) [63, 178–180, 182]. More specifically, ferroelectric 180° domains generally form to compensate the depolarization field resulting from imperfect screening of the polarization charge [155, 183] and non-180° or ferroelastic domains generally form to accommodate elastic energy due to film-substrate interactions (i.e., lattice-mismatch, epitaxial strain) [184, 185]. Domain-wall energy (significant at thickness <10 nm) typically favors monodomain configurations, however, as the thickness increases, the strain energy begins to dominate. As a result, the domain patterns that form depend upon the nature of the ferroelectric phase and can be engineered by controlling the strain *via* appropriate choice of substrate, the nature of charge compensation at the top and bottom electrodes, the film thickness, among other features.

To experimentally probe such complex domain patterns, experimentalists have increasingly relied on scanning probe-based piezoresponse force microscopy (PFM), X-ray diffraction, and transmission electron microscopy (TEM)-based techniques to image and manipulate ferroelectric domain structures at the nanoscale [186–193]. At the same time, analytical models based on thermodynamic analysis [32, 194–197], 3D

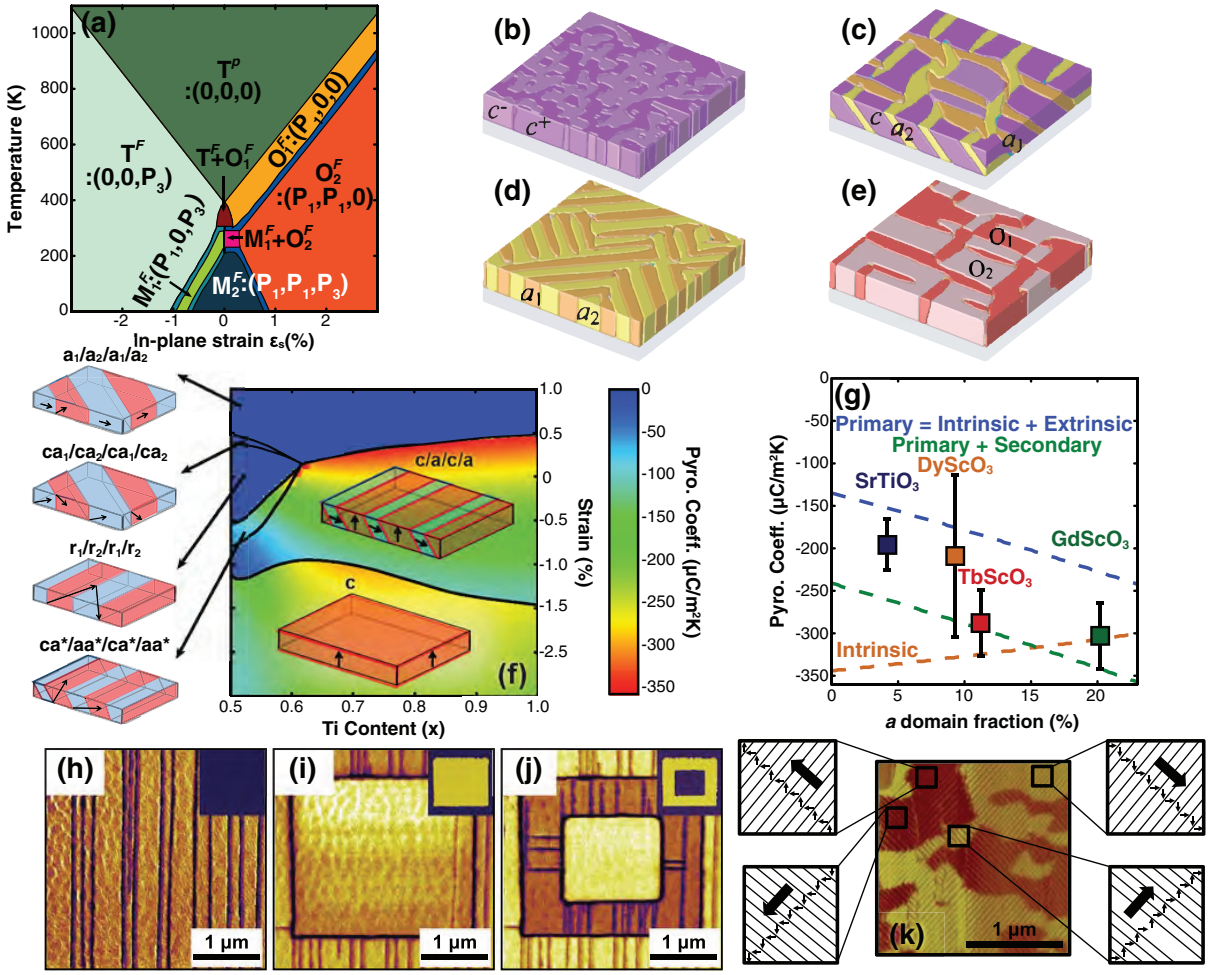

Figure 4. (a) Phase diagram of $BaTiO_3$ films as a function of temperature and misfit strain, with T^P (tetragonal paraelectric), T^F (tetragonal ferroelectric), O^F (orthorhombic ferroelectric), and M^F (monoclinic ferroelectric) phases noted, and (b)–(e) representative domain morphologies in $BaTiO_3$ films at different temperatures and misfit strains (Reprinted with permission from [203]. Copyright 2006 AIP Publishing LLC). (f) Strain-composition phase diagram for $PbZr_{1-x}Ti_xO_3$ thin films showing the pyroelectric coefficient at 300 K for the various equilibrium polydomain states (adapted from [212]). (g) The measured pyroelectric coefficient (squares) as a function of percentage of *a* domains in polydomain $PbZr_{0.2}Ti_{0.8}O_3$ thin films. The orange line represents the intrinsic response and the green line represents the primary response (intrinsic + extrinsic) calculated using polydomain GLD theory. The blue line indicates the trend expected assuming an average thermal expansion coefficient of $10.9 \times 10^6\ K^{-1}$ (Adapted from [213]. Copyright 2012 by the American Physical Society). PFM amplitude and phase (inset) images showing the sequence of 180° switching from (h) the initial 'parallel' *c*/*a* domain structure with homogeneous phase to (i) monodomain *c* domain with further switching leading to the creation of (j) ferroelastic *a* domains oriented both vertically and horizontally (Reprinted with permission from [214]. Copyright 2014 AIP Publishing LLC). (k) Lateral PFM phase images (scale bar range, 0–70°) of areas of $2 \times 2\ \mu m^2$ of an in-plane polarized 30 nm-thick $Pb_xSr_{1-x}TiO_3$ film. Four types of areas are observed (marked by the black squares), defining coarse-scale 'superdomains'. The polarization orientation in the nanodomains is represented by arrows for the four types of domain variants (Reprinted with permission from [220]. Copyright 2014 Nature Publishing Group).

phase-field simulations [138, 140, 198], and first-principles, effective Hamiltonian-based atomic level simulations [199, 200] have been employed to predict domain formation and their influence on the response of ferroelectric films as a function of misfit strain, film thickness, electrostatic boundary conditions, etc. Phase diagrams have been constructed for a variety of ferroelectric systems including $PbTiO_3$ [137], $PbZr_{1-x}Ti_xO_3$ [139, 201, 202], $BaTiO_3$ [203], $SrTiO_3$ [111], $BiFeO_3$ [204], and others. These theoretical approaches provide a fertile starting point by which understanding and the design of desired functionalities in ferroelectric materials can occur. As an example, a rich phase diagram with the presence of multi-domain tetragonal, orthorhombic, rhombohedral, and monoclinic phases with several narrow regions of phase coexistence is predicted for strained $BaTiO_3$ (figure 4(a)). For instance, as one traverses from the compressive to tensile misfit strain regimes near room temperature, the domain structure can evolve from purely *c* domain to $c/a_1/c/a_2$, then to a_1/a_2 twins, and finally to O_1/O_2 twins (figures 4(b)–(e), respectively). Systematic studies of misfit-strain effects on epitaxial $BaTiO_3$ thin films, however, have been limited by the lack of perovskite substrates with suitable lattice parameters which have been only recently made available. Consequently, most experimental studies of misfit-strain effects on the formation and control of nanoscale domain structure have been conducted on ferroelectrics with relatively small in-plane lattice parameters ($a < 3.96$ Å) including Ti-rich compositions of $PbZr_{1-x}Ti_xO_3$ and the room-temperature multiferroic, $BiFeO_3$.

The phase diagram for Ti-rich versions of $PbZr_{1-x}Ti_xO_3$ (strongly tetragonal ferroelectrics) reveal a systematic strain-dependent evolution from monodomain and out-of-plane polarized *c* domains at large compressive strains, to multidomain *c*/*a*/*c*/*a* domain structures (consisting of alternating *c* domains and in-plane polarized *a* domains) at reduced compressive or tensile strains, and finally to completely in-plane polarized a_1/a_2 domains at large tensile strains and such structures have been demonstrated in several experiments [59, 205–207]. The various domain configurations have been shown to possess dramatically different susceptibilities that can be optimized based on the desired application. For instance, based on a combination of phenomenological and experimental approaches (figures 4(f) and (g), respectively) [208–213], researchers utilized strain-control to demonstrate a significant contribution from the motion of 90° ferroelastic domain walls to the dielectric and pyroelectric susceptibilities of (001)-oriented $PbZr_{0.2}Ti_{0.8}O_3$ heterostructures. These studies revealed that ~50% of the room-temperature permittivity arises from 90° domain wall motion and under thermal excitation additional contributions from the thermal mismatch strains must also be considered. Recently, researchers have also demonstrated rather-compliant ferroelastic *c*/*a* domain structures in low defect density, slightly tensile-strained $PbZr_{0.1}Ti_{0.9}O_3$ films grown on $SrRuO_3$-buffered $DyScO_3$ (110) substrates (figures 4(h)–(j)) [214] that are not pinned by dislocations and other defects [59, 215–217]. It was further shown that these *a* domains can be locally created and annihilated by applying out-of-plane electric fields using a PFM tip, allowing one to envision new types of agile electronic devices based on concepts of domain wall conductivity where the circuit paths can be modified during operation. In this case, the annihilation of *a* domains was attributed to the combined effect of the out-of-plane electric field and the creation of temporary charged 90° domain wall sections during 180° switching [206, 214–216]. On the other hand, the creation of an *a* domain is related to the opposite piezoresponse from oppositely-poled domains when a tip-bias is applied at a 180° domain wall. Such opposite piezoresponse at the c^+/c^- domain boundary gives rise to a net elastic strain (piezostrain) that drives *a* domain formation [214, 218]. In a separate set of experiments focusing on domain control [219], the orthorhombic nature of the $DyScO_3$ (110) substrate was utilized to engineer ultrafine *c*/*a* domain patterns of conductive *a* domain stripes that were only 10 nm wide but extended tens of microns in length in an insulating *c* domain matrix. Until recently, studies on the high-tensile strain regime of the phase diagram for tetragonal $PbZr_xTi_{1-x}O_3$ were limited by the availability and cost of larger lattice parameter substrates. To overcome these challenges, researchers resorted to Sr-alloying (0–35%) of $PbTiO_3$ and achieved large biaxial tensile stains for films grown on $DyScO_3$ (110) [220]. Using a combination of synchrotron-based X-ray reciprocal space maps and PFM, the formation of the predicted a_1/a_2 twin domain pattern with purely in-plane components of polarization was confirmed. It was also noticed that quasi-periodic nanoscale a_1/a_2 twin motifs (with periodicity of 20–80 nm depending on the film thickness) formed larger mesoscopic domain patterns or "superdomains" at micron-sized length scales with the effective in-plane component of polarization along the [110] and $[1\bar{1}0]$ (figure 4(k)). Such complex hierarchical domain patterns with flux closure at two different length scales have also been reported in epitaxial $PbZr_xTi_{1-x}O_3$ thin films grown on tensile $SmScO_3$ (110) [221, 222]. It has been suggested the hierarchical domain patterns that form at the macroscale mimics, on average, the ground-state ferroelectric phase predicted by monodomain models. Additional theoretical and experimental studies on the formation of ordered hierarchical patterns, and the ability to self-assemble highly-ordered motifs of these structures at desired length scales could enable new functionalities and applications.

Strain-tuning of domain structures in epitaxial thin films of $BiFeO_3$ has also received significant attention in the last decade. $BiFeO_3$, in bulk-form, is a rhombohedrally-distorted perovskite (*R*3*c*) exhibiting antiferromagnetism that is coupled with ferroelectric order [223, 224]. It is one of just a few single-phase multiferroics and has been the center of intense scientific study due to its lead-free nature, large ferroelectric polarization, and room-temperature multiferroism [225]. In general, rhombohedral ferroelectrics are spontaneously polarized along the <111> giving rise to four structural variants and eight possible domain variants that are separated by 71°, 109°, or 180° domain walls. Previous theoretical and experimental work studying domain configurations of (001)-oriented rhombohedral ferroelectric thin films have demonstrated energetically-degenerate stripe-domain patterns with either 71° or 109° domain boundaries that form along the $\{101\}_{pc}$ or $\{100\}_{pc}$ (where "pc" refers to pseudo-cubic notation), respectively [182]. The surface structure for the two possible domain patterns are distinctly different, with the 71°-stripe domains possessing a flat surface topography and the 109°-domain variants showing a distinct puckered surface structure (figures 5(a)–(d) and (e)–(h), respectively). Studies have leveraged several novel routes including substrate lattice parameter, orientation, vicinality (or miscut), electrostatic boundary conditions, thickness of bottom electrodes, etc. to tune the structure. In 2006, researchers grew 1D nanoscale arrays of 71° domain walls in epitaxial $BiFeO_3$ films on $SrRuO_3$-buffered $DyScO_3$ (110) [226]. Such down-selection to a 2-variant domain structure has since been shown to be related to the oxygen-octahedral tilts and shear distortions associated with the orthorhombic symmetry of the substrate [227]. Such control was also demonstrated for films grown on cubic $SrTiO_3$ (001) substrates, whereby progressively adjusting the magnitude and the tilt-direction of the substrate-miscut, it was possible to synthesize films that were 4-variant stripe, 2-variant stripe, and monodomain [228–231]. Controlling domain structures has led to a range of exciting observations including correlation of different domain structures to variations in remanent polarization [231, 232], exploration of domain effects on fatigue lifetimes [233], achievement of deterministic control of switching pathways [234], and much more (for a recent review see [28]). Phase-field studies [204] have provided additional insights on how elastic constraints, electrical boundary conditions, lattice anisotropy, and other effects,

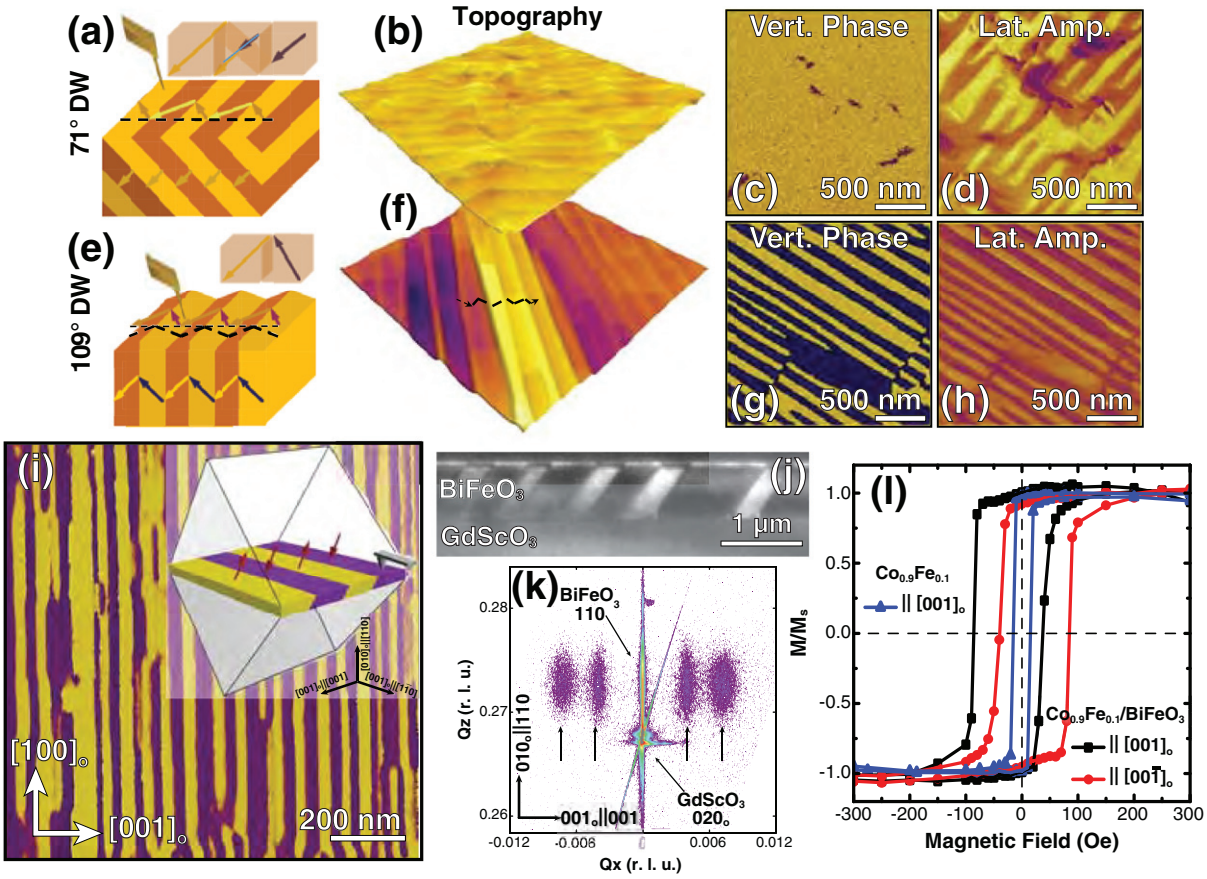

Figure 5. (a) Schematic illustration, (b) surface topography, (c) vertical phase, and (d) lateral amplitude images of 71°-striped $BiFeO_3$ possessing a flat surface topography and (e) schematic illustration, (f) surface topography, (g) vertical phase, and (h) lateral amplitude images of 109°-domain variants $BiFeO_3$ showing a puckered surface structure. (i) Lateral PFM phase image of $BiFeO_3$ with 180° domain structure; the inset shows a schematic illustration of the domain structure where the arrows represent the directions of the spontaneous polarization. (j) Cross-sectional, dark-field TEM image (top) and RSMs (bottom) about the 020_O-(110-) diffraction conditions of $GdScO_3$ (pseudocubic $BiFeO_3$) with the x-ray beam incident along the $[001]_O$, of a 14 nm thick $BiFeO_3/GdScO_3$ $(010)_O$ heterostructure with a 180° domain structure. Arrows indicate the positions of satellite peaks due to the periodic domain structure. (k) Room-temperature, in-plane magnetic hysteresis loops for a $Pt/Co_{0.9}Fe_{0.1}/BiFeO_3/GdScO_3$ $(010)_O$ heterostructure with a 180° domain structure (measured along in-plane $[001]_O$). A loop of similarly grown $Pt/Co_{0.9}Fe_{0.1}/GdScO_3$ $(010)_O$ heterostructure is shown for comparison. (Figures (i)-(l) are adapted with permission from [241]. Copyright 2015 American Chemical Society).

can be leveraged to engineer desired architectures in $BiFeO_3$ films. In 2009, researchers were able to use controlled strain and electrostatic boundary conditions to select between 1D arrays of purely 71° and 109° domain walls [235, 236]. Such selective control of ordered domain variants is important for next-generation spintronic-devices based on magnetoelectric multiferroics (such as $BiFeO_3$) and it has been shown that the density and nature of domain-walls that form are correlated to the overall magnetic moment of $BiFeO_3$ thin films, as well as to the exchange bias between $BiFeO_3$ and metallic ferromagnets [237–240]. It was only recently, that the 180° domain wall version of 1D-stripe domain patterns was stabilized. Using a combination of PFM (figure 5(i), lateral PFM image) and cross-sectional TEM-based studies (figure 5(j)), researchers showed that epitaxial $BiFeO_3$ films (thickness <35 nm) grown on $GdScO_3$ (010) spontaneously ordered into 1D arrays of 180° stripe domains with $\{11\bar{2}\}$ domain walls (inset, figure 5(i)) [241]. Symmetric reciprocal space mapping (RSM) studies (figure 5(k)) about the $GdScO_3$ 020_o-diffraction condition for a 14 nm thick film revealed two orders of satellite peaks along the $[001]_o$ corresponding to a dense domain periodicity of 20 nm. Additional magnetic studies (figure 5(l)) revealed exchange bias and exchange enhancement in $Co_{0.9}Fe_{0.1}/BiFeO_3$ heterostructures based on $BiFeO_3$ films with the 180° stripe-domain architecture, suggesting their contribution to pinned, uncompensated spins that give rise to exchange bias. This was further confirmed by X-ray magnetic circular dichroism (XMCD) studies, which demonstrate that films with predominantly 180° domain walls have larger magnetization than those with primarily 71° domain walls.

In all, these studies summarize the advances made in strain control of ferroelectric domain architectures over the last decade. Such control is important as ferroelectric domain morphologies affect not only susceptibilities, but also impact the overall ferroelectric device performance and reliability. Furthermore, the controlled synthesis of films with highly-ordered and simplified domain wall configurations will serve as the foundation to investigate and understand new functionalities such as electronic conduction, reduced optical band-gaps, magnetism, etc. that emerge at ferroelectric domain walls.

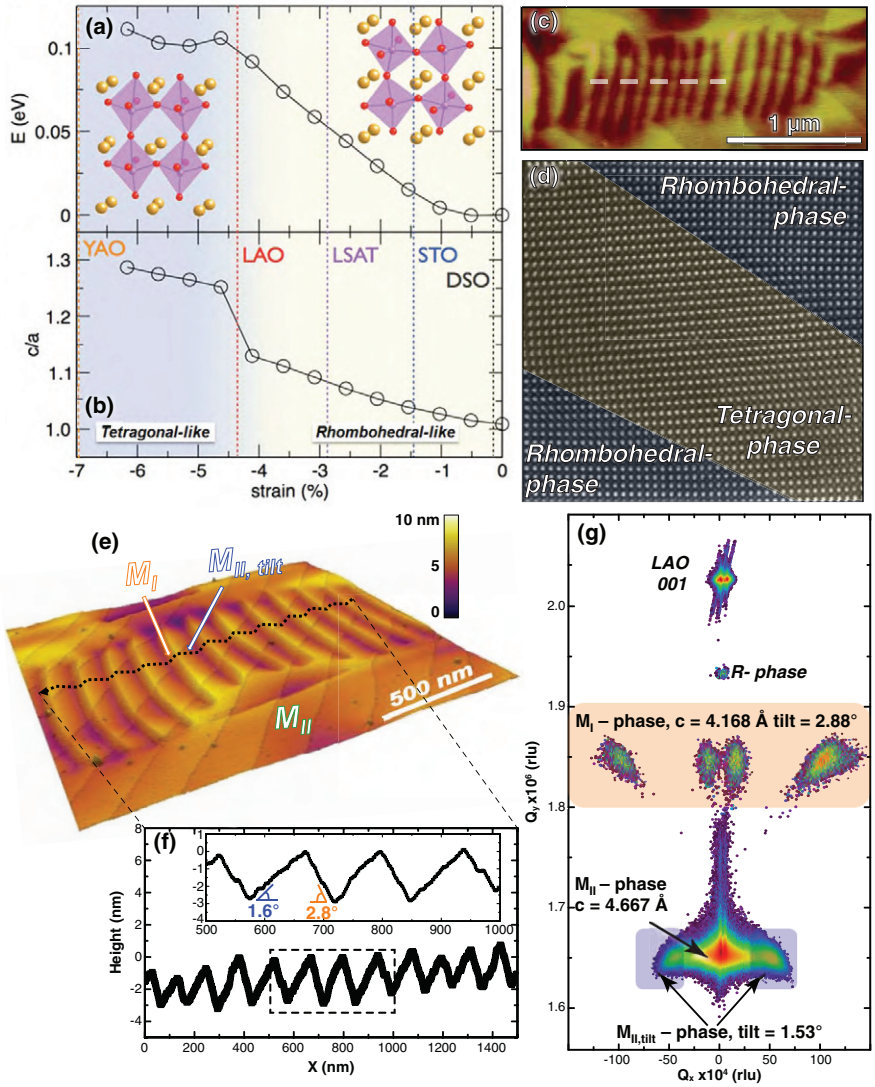

Figure 6. Evolution of the (a) energy and (b) *c/a* lattice parameter ratio of $BiFeO_3$ as a function of in-plane strain. This data shows the presence of two phases—both with monoclinic symmetry—the highly-distorted *T*-like phase (left) and an *R*-like phase derived from the parent phase. The lattice mismatch between a number of commonly used and tested oxide substrates are shown as dashed lines (Reprinted with permission from [249]. Copyright 2009 AAAS Publishing). (c) High-resolution AFM image of a mixed-phase region, and (d) high-resolution TEM image of the boundaries between *R*- and *T*-like regions (Reprinted with permission from [249]. Copyright 2009 AAAS Publishing). A smooth transition between phases is observed; no dislocations or defects are found at the interface. (e) AFM topography and (f) line-trace along the dashed line of a 140 nm thick $BiFeO_3/LaAlO_3$ (001) thin film. (g) RSM about the 002-diffraction condition of $LaAlO_3$ for a 130 nm-thick $BiFeO_3/LaAlO_3$ (001) thin film (Adapted from [262]. Copyright 2011 John Wiley and Sons).

3.3. Stabilizing polymorphic ferroelectric phases

Recent theoretical first-principles [242] and experimental investigations [225, 243–247] of phase transitions in bulk $BiFeO_3$ have reported numerous temperature- and pressure-induced ferroic transitions, including phases with complex structures indicative of the presence of complex-tilt systems and off-center cation displacements, as well as insulator-to-metal transitions that occur at high-temperature and -pressure regimes. These complexities are also reflected in the temperature-misfit strain phase diagram for epitaxial thin films of $BiFeO_3$ that reveal several competing phases of reduced symmetry. Over the years, thin films of $BiFeO_3$ have been strained on essentially every possible oxide substrate (spanning from 6.6% compressive strain on $YaAlO_3$ (110) to 1.4% tensile strain on $PrScO_3$ (110)) and semiconductor wafers such as Si and GaN. Various low-symmetry phases including tetragonal (*P*4*mm*), triclinic, monoclinic M_C (*Cm*), monoclinic M_A (*Cm*), rhombohedral (*R*3*c*), monoclinic M_B (*Cc*), and orthorhombic (*Ima*2) phases form as one transitions from compressive to tensile strains. For a detailed summary of this complex phase evolution, the reader is directed to a recent review [248]. Here, for brevity, we focus on films under high compressive strains of >4.5% that result in the coexistence [249] of low-symmetry rhombohedral- and tetragonal-like phases. These mixed-phase structures are akin to the technologically significant morphotropic phase boundaries (MPB) (or chemically-induced structural instabilities that occur in complex lead-based mixed perovskites such as $PbZr_xTi_{1-x}O_3$ (PZT) and $(x)PbMg_{1/3}Nb_{2/3}O_3$–$(1-x)PbTiO_3$ (PMN-PT) at $x = 0.52$ and $x = 0.33$, respectively) [250–252]. Recently, it has been shown

that MPB's are the consequence of inherent structural instabilities. Materials which are single-phase under ambiet conditions can be driven to exhibit phase competition by non-ambient pressures and temperature [253]. These approaches can be used to achieve MPB-like materials in environmental-friendly, lead-free compositions [254]. The discovery of such exotic strain-induced MPB-like features in thin films of $BiFeO_3$ has caused tremendous excitement as a potential lead-free route to circumvent the limitations on susceptibilities in epitaxially-clamped ferroelectric thin films [255]. Intense studies focusing on the origin of such complex phase-coexistence, as well as the implications for piezoelectric, optical, and multiferroic properties and applications have been undertaken.

The first signs of the presence of a tetragonal *P*4*mm* phase of $BiFeO_3$ with a giant polarization of ~150 $\mu C\ cm^{-2}$ was observed in polycrystalline films deposited on $Pt/TiO_2/SiO_2/Si$ substrates [256–258]. Subsequent theoretical [142, 259] and experimental studies [260] confirmed the existence of this tetragonally-distorted phase. *Ab initio* calculations exploring the role of epitaxial strain on $BiFeO_3$, showed that under compressive strains of >6%, a new super-tetragonal phase (derived from a structure with *P*4*mm* symmetry, $a \approx 3.665$ Å and $c \approx 4.655$ Å) with a giant *c/a* ratio of ~1.27 and highly-enhanced spontaneous polarization is stabilized (figures 6(a) and (b)) [249, 261]. For films grown on $LaAlO_3$ substrates (compressive misfit-strain of ~4.5%), a mixed-phase structure [249] with a distinctive stripe-like surface morphology (figure 6(c)) was observed. High-resolution TEM images (figure 6(d)) across these stripe-like features revealed the coexistence of a parent rhombohedral-like and the predicted super-tetragonal-like phases. Despite the large lattice mismatch between the two phases, the interface was found to be coherent without any evidence of dislocations indicating a gradual deformation of the structure at the interface over a length scale of ~10 unit cells. Subsequent studies [262] helped uniquely identify the various phases present and their nanoscale spatial distribution. In this work, a careful comparison was drawn between the complex topographical features (various tilted facets of the nanostructure (figure 6(e)) which produce an asymmetric saw-tooth surface structure (figure 6(f)) embedded in a flat, plateau-like matrix), and the crystallographic tilts that were measured from symmetric RSM about the 001-diffraction condition of the $LaAlO_3$ substrate (figure 6(g)). In turn, it was shown that the mixed-phase regions in these films are made up of an intimate mixture of highly-distorted, monoclinic phases—a monoclinic version of the tetragonal phase ($M_{II,tilt}$) with $c \approx 4.67$ Å which is tilted ~1.5° from the surface normal and an intermediate, monoclinic (actually triclinic) phase (M_I) with $c \approx 4.17$ Å which is tilted ~3° from the surface normal in the opposite direction. It was also noted that the flat plateau-like regions are comprised of an untilted version of the M_{II} phase. Finally, on occasion, a peak corresponding to the bulk-like $BiFeO_3$ parent rhombohedral (R) phase (with $c \approx 3.97$ Å) can occur in small fractions (although it is not part the AFM scanned area in these studies). Over the years, considerable details regarding the structure and symmetry of the phases present have emerged [261, 263–280] with several different names (including T', *T*-like, and Tri-2 for the M_{II}-phase and S', Tri-1, and M_R for the M_I-phase) being used to refer to the various phases. Furthermore, temperature- and thickness-dependent studies have revealed a complex evolution including a breakdown of this strain-stabilized metastable mixed-phase structure to non-epitaxial microcrystals of the parent rhombohedral structure of $BiFeO_3$, matching predictions of thickness evolution for strain-stabilized metastable phases [281–283]. To explain the energetics of the mixed-phase structure a detailed thermodynamic and elastic domain theory which includes contributions from interdomain elastic, electrostatic, and interface energies has been developed [284].

Electric field-dependent studies on the MPB-like, mixed-phase structures have demonstrated enhanced electromechanical responses in the mixed-phase regions that are potentially promising for piezoelectric applications. Scanning probe-based local ferroelectric switching studies [262] exposed the hysteretic nature of the electric-field response in the mixed-phase films (figure 7(a)). In particular, these studies revealed a number of important features: (1) large surface strains (4–5%) occur as the material transforms from a mixed-phase structure to the highly-distorted monoclinic M_{II}-phase, (2) transformations between these two states are reversible, and (3) there are numerous pathways to achieve large electromechanical responses in these materials—including routes which do not require ferroelectric switching. Furthermore, single-point spectroscopic piezoresponse studies [285] confirmed the reduced activation voltage for electric-field driven phase transformation as compared to ferroelectric switching and demonstrated a pathway to write complex "rosette" structures that can have implications for future devices. Similar piezoresponse studies [286] on macroscopic capacitor structures revealed a highly-enhanced d_{33} of ~115 pm V^{-1} for the mixed-phase $BiFeO_3$ films as compared to a d_{33} of ~30 pm V^{-1} and ~50 pm V^{-1} for the pure tetragonal-like and rhombohedral-like versions, respectively (figure 7(b)). *In situ* TEM biasing studies coupled with nanoscale electrical and mechanical probing [286], suggest that these large strains result from the field-driven motion of boundaries separating the two phases in the mixed-phase region and highlight the potential of materials with nanoscale phase boundary as a substitute for lead-based materials in future piezo-actuators. There has also been considerable interest in the implications of these strain-driven structural transitions on the multiferroic properties of $BiFeO_3$. X-ray magnetic circular dichroism-based photoemission electron microscopy (figure 7(c)) coupled with macroscopic magnetic measurements have revealed enhanced spontaneous magnetization in the mixed-phase structures [287]. These measurements demonstrate that the intermediate monoclinic M_I-phase possess enhanced magnetic moment as compared to the parent phase, which has been attributed to its piezomagnetic coupling to the adjacent tetragonal-like phase. Moreover, there have been several reports [271, 288–291] of near room-temperature ferroelectric and magnetic phase transitions in these highly-strained versions of $BiFeO_3$, which, along with the overall structural softness of the mixed-phase films, make them highly susceptible

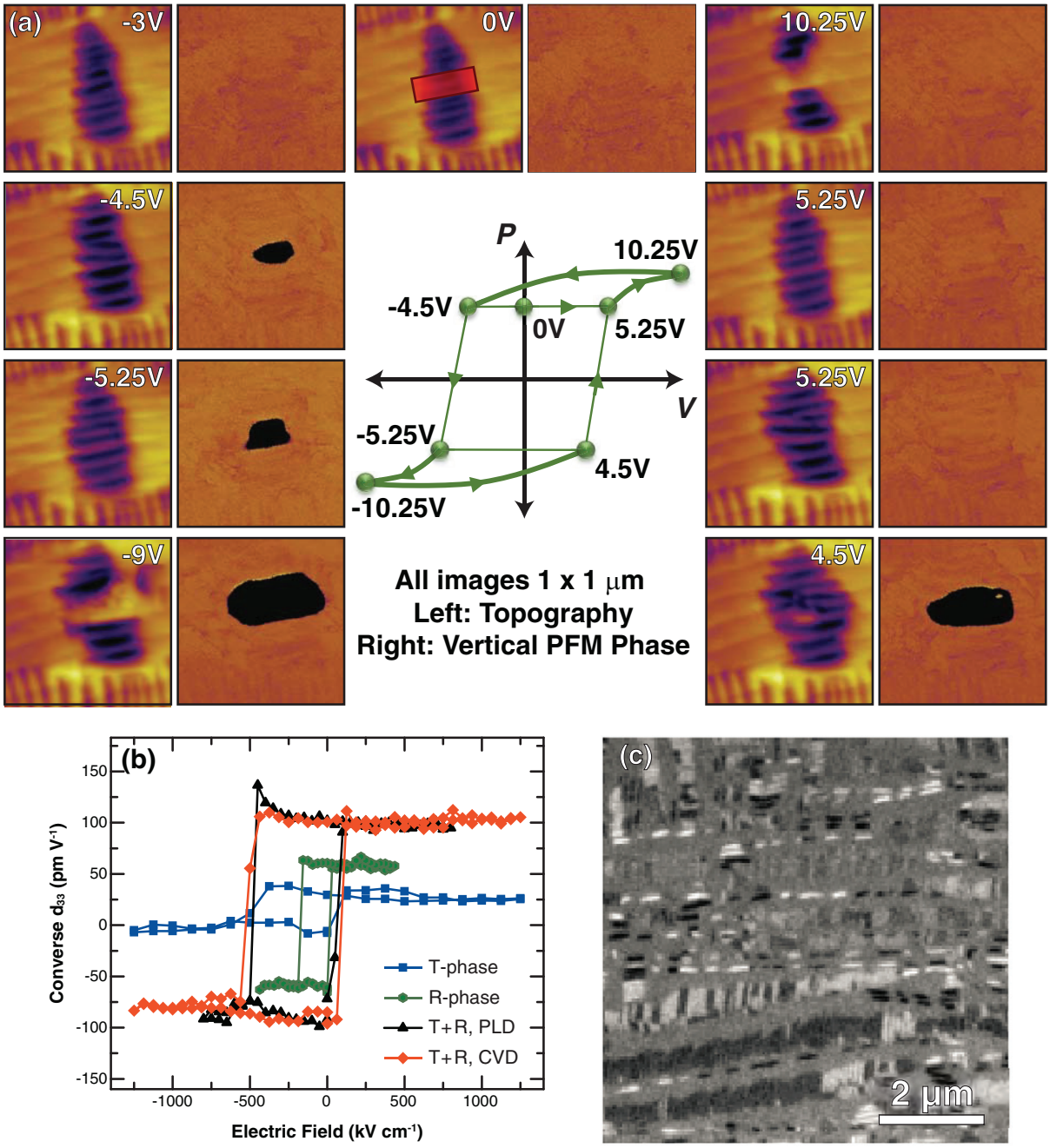

Figure 7. (a) AFM image (left) and vertical PFM image (right) of a 100 nm $BiFeO_3/La_{0.5}Sr_{0.5}CoO_3/LaAlO_3$ (001) film in the as-grown state (0 V) and after being poled in the box at various voltages (all images are 1 × 1 μm). At the center is a schematic hysteresis loop that shows the pathway to enhanced electromechanical responses (Adapted from [262]. Copyright 2011 John Wiley and Sons). (b) Piezoelectric hysteresis loops from *T*-like (blue curve), *R*-like (green curve) and mixed-phase (purple and orange curves) $BiFeO_3$ thin films, grown by pulsed-laser deposition (PLD) and chemical vapor deposition (CVD), measured in capacitors with a diameter of 32 μm (Reprinted with permission from [286]. Copyright 2011 Nature Publishing Group). (c) XMCD-PEEM image of a mixed phase $BiFeO_3$ film (Reprinted with permission from [287]. Copyright 2011 Nature Publishing Group).

to applied fields and promising for large magnetoelectric effects [266].

3.4. Ferroelectric superlattices

Superlattices of perovskite oxide materials offer many opportunities to develop enhanced physical properties and new functionalities [292]. By combining ferroelectrics with other functional oxides in a superlattice structure, the ferroelectric properties of the system can be tailored by rationally engineering the relative thicknesses of the ferroelectric and non-ferroelectric layers and the boundary conditions (i.e., epitaxial strain, electrostatic coupling, size effects, interfacial effects, etc.) [293]. In this regard, theoretical calculations of superlattice structures have spurred interest in how to create new artificial ferroelectrics with enhanced properties and unusual polarization profiles [117, 294–299], and have driven experiments to realize these predictions in two-component

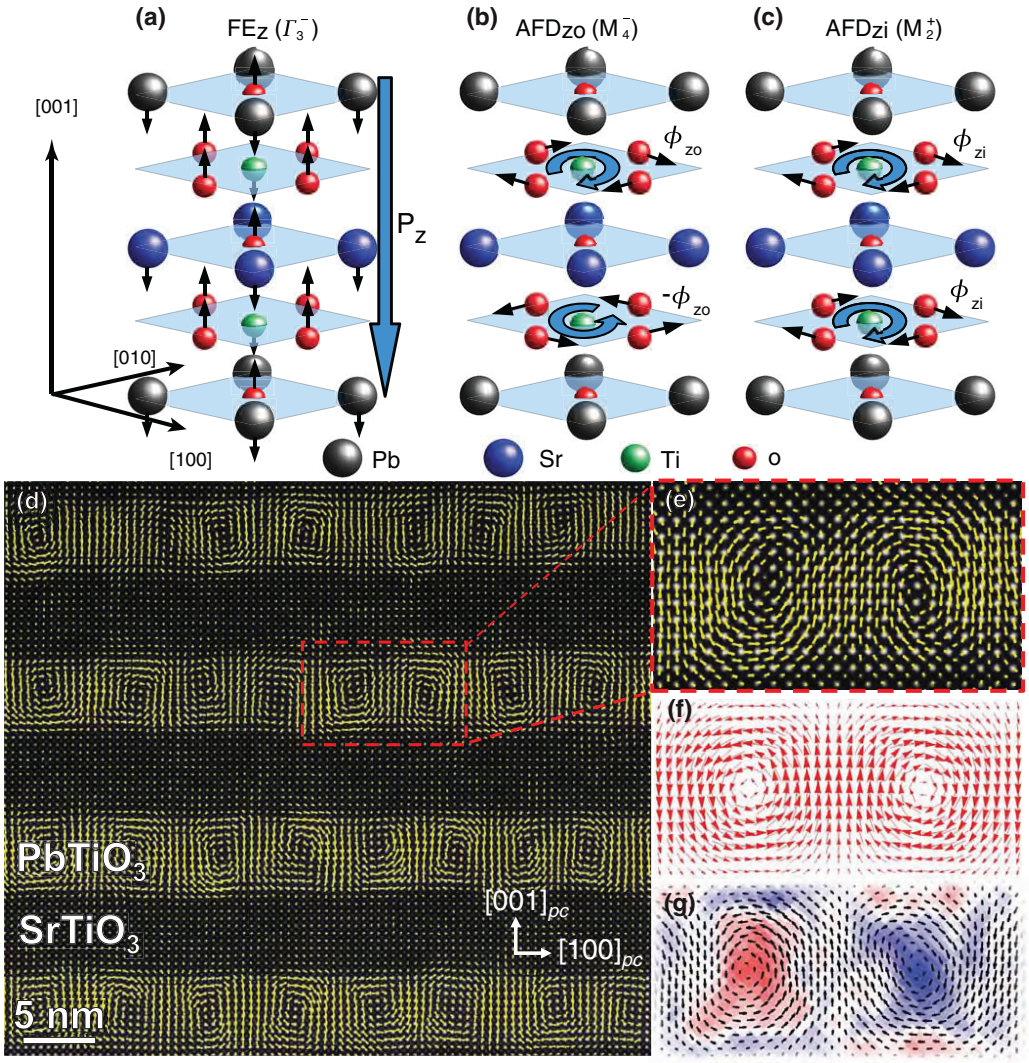

Figure 8. In short-period $PbTiO_3/SrTiO_3$ superlattices, the ferroelectric mode (a) FE_z, couples to two antiferrodistortive modes (b) AFD_{zi} and (c) AFD_{zo}, inducing an improper ferroelectric state. The particular set of structural distortions that condenses is sensitive to biaxial strain and thus other ground states with different couplings can be engineered (Reprinted with permission from [306]. Copyright 2008 Nature Publishing Group). (d) Observation of vortex/anti-vortex structures in intermediate periodicity $(PbTiO_3)_{10}/(SrTiO_3)_{10}$ superlattices using cross-sectional, atomic-scale imaging using STEM (the overlaid polarization vector maps represent the locally extracted polar distortion). (e) A magnified image of a single vortex/anti-vortex pair where the polarization state within such pairs can be visualized. (f) Phase-field simulations of the same superlattice structure also predicting the vortex/anti-vortex pairs. (g) The curl of polarization ($\nabla \times \boldsymbol{P}$) for a single vortex pair, extracted from the cross-section STEM polarization vector map (Reprinted with permission from [324]. Copyright 2016 Nature Publishing Group).

[300–311] and three-component ferroelectric superlattices [312, 313]. For instance, first-principle calculations have predicted that the spontaneous polarization of $BaTiO_3$ can be significantly enhanced by creating superlattices with $SrTiO_3$ (which is paraelectric in the bulk), wherein the $SrTiO_3$ layers become tetragonal and are driven to possess nearly the same polarization as the $BaTiO_3$ layers [117]. These predictions were experimentally validated in 2005 [313] in a three-component $BaTiO_3/SrTiO_3/CaTiO_3$ superlattice where two of the components, $SrTiO_3$ and $CaTiO_3$ are parelectric materials. Furthermore, by preserving the epitaxial strain and combining heterointerfacial couplings, an overall 50% enhancement in ferroelectric polarization of the superlattice with respect to similarly grown pure $BaTiO_3$ films was demonstrated. The use of three different components results in inversion symmetry breaking in the superlattice, which, in turn, allows the presence of built-in fields that result in an asymmetry in the two polarization states [295, 312]. This extra degree of freedom for controlling the physical properties of complex-oxide superlattices has been leveraged to create ferroelectricity in $NdMnO_3/SrMnO_3/LaMnO_3$ superlattices comprising entirely of non-ferroelectric layers [314]. More recently, $PbTiO_3/SrTiO_3$ ferrroelectric-paraelectric superlattices have attracted significant attention. First, in ultrashort period superlattices, researchers observed the formation of a new "improper" ferroelectricity. Using first-principle calculations, it was demonstrated that the observed recovery of ferroelectricity in $(PbTiO_3)_1/(SrTiO_3)_1$ superlattices can be explained by a complex ground state arising from an unexpected coupling (so called "trilinear coupling") between antiferrodistortive and ferroelectric instabilities (figures 8(a)–(c)) [306]. More interestingly, in such ultrashort-period superlattices, the ferroelectric polarization is not the primary order parameter and it couples linearly with two antiferrodistortive distortions in a way similar to improper

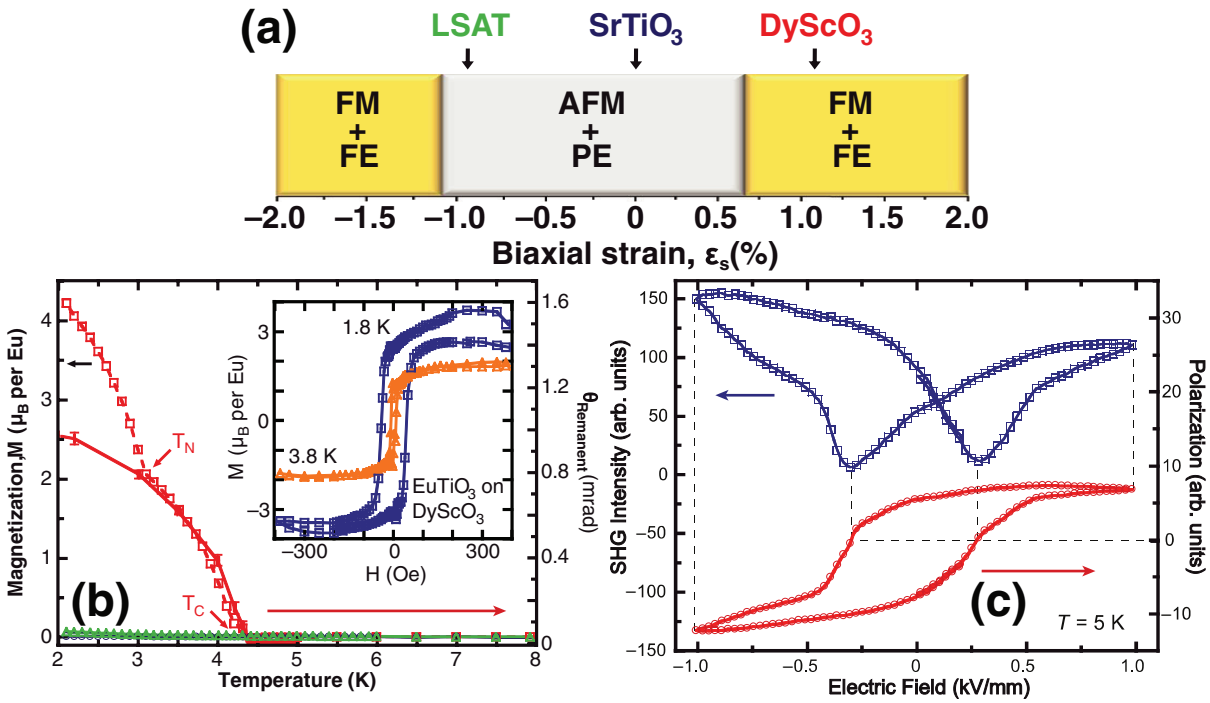

Figure 9. Strain-driven multiferroism in $EuTiO_3$ epitaxial thin films. (a) Predicted effect of epitaxial strain on $EuTiO_3$. (b) Temperature-dependence of the magnetization measured using both MOKE and SQUID magnetometry. (c) SHG hysteresis loop (blue) and corresponding polarization loop (red) for $EuTiO_3$ on $DyScO_3$ (110) at 5 K. The data reveals that epitaxial $EuTiO_3$ thin films on $DyScO_3$ are ferroelectric and ferromagnetic below 5 K. (Reprinted with permission from [328]. Copyright 2010 Nature Publishing Group).

ferroelectrics. This interesting observation holds the potential to achieve many useful properties such as large temperature-independent dielectric constants and insensitivity to depolarization-field-driven ferroelectric size effects that are common in improper ferroelectrics [292, 315]. The trilinear coupling of several structural instabilities at interfaces presents a new strategy for designing ferroelectric and multiferroic materials (and need not be restricted to the $PbTiO_3/SrTiO_3$ system) [316, 317].

In addition to such exotic interfacial coupling, by rationally tuning the thickness of each component and the epitaxial strain, recent works on ferroelectric/paraelectric superlattices have demonstrated the ability to: tune the magnitude of the polarization and transition temperatures [305], vary the tendency for formation of 180° stripe nanodomains [308], enhance dielectric [308] and piezoelectric response [311], produce exotic field-dependent domain and polarization changes [318], induce new phenomena in new superlattice varieties [306, 310], and give rise to complex flux-closure domain structures [319]. Theoretical studies have also predicted that the complex interplay between strain, depolarization, and gradient energies in ferroelectric/paraelectric heterostructures under confined geometries can stabilize non-trivial polarization modes such as vortices and skyrmions [297, 320–323]. By tuning the superlattice periodicity of $PbTiO_3/SrTiO_3$ superlattices grown on $DyScO_3$ (110) substrates to intermediate length scales (tens of unit cells), researchers have been able to observe ordered arrays of vortex-like structures (figures 8(d)–(g)) [324]. The observation of such exotic inhomogeneous polarization modes promises phase diagrams rich in topological textures [325], akin to those of liquid crystals, and the emergence of new functionalities [326].

3.5. Novel polar materials by design

Strain engineering of complex-oxides thin films is being increasingly explored to produce novel polar and ferroelectric states that are unstable at standard pressures and temperatures. The inherent sensitivity of ferroelectric instability to lattice strain can be exploited to stabilize novel ferroelectrics and multiferroics where the ferroelectric state is often destabilized due to the existence of magnetism [26, 27]. A flagship example in recent years is $EuTiO_3$. In 2006, first-principles work predicted that epitaxial strain could transform $EuTiO_3$, which is neither ferroelectric nor ferromagnetic in the bulk, into a ferroelectric-ferromagnet [327]. The work predicted that appropriately strained $EuTiO_3$ thin films should be simultaneously strongly ferromagnetic ($M_s \approx 7\ \mu_B$/Eu) and ferroelectric ($P_s \approx 10\ \mu C\ cm^{-2}$). These values are orders of magnitude higher than any known ferroelectric-ferromagnet and are comparable to the best materials that are solely ferroelectric or ferromagnetic. To test these predictions, commensurately-strained $EuTiO_3$ films were grown on three substrates: $(LaAlO_3)_{0.3}(Sr_2TaAlO_6)_{0.7}$ (001), $SrTiO_3$ (001), and $DyScO_3$ (110) to impart −0.9%, 0%, and +1.1% biaxial strain, respectively (figure 9(a)). Experimental measurements (figures 9(b) and (c)) confirmed that the $EuTiO_3/DyScO_3$ heterostructures were simultaneously ferromagnetic and ferroelectric, while on the other substrates it was not [328]. These studies exemplify the opportunity to use strain to simultaneously control multiple order parameters and as a viable route to create new multiferroics. In this regard, appropriate materials tend to be those that (1) possess a ground state in the absence of strain that is antiferromagnetic and paraelectric, (2) are at the brink of a

ferroelectric transition (incipient ferroelectrics), and (3) possess a large spin-phonon coupling [327]. Other exciting examples of the strain-induced ferroelectricity/ferromagnetism include: quantum paraelectric $SrTiO_3$ [112, 305] and $KTaO_3$ [329]; ferromagnetic $BiMnO_3$ (although first-principles calculations and structural refinements have recently brought the ferroelectric/multiferroic nature into question) [100, 330–332]; antiferroelectric $PbZrO_3$ [333]; antiferromagnetic $CaMnO_3$ and $SrMnO_3$ [328, 334]; and even simple rock-salt binary oxides, BaO and EuO [335].

While these routes to strain-tune ferroelectrics have been successfully implemented to alter the crystal and domain structures and responses, these approaches have been somewhat conventional in design. In turn, there is significant room to diverge from these conventional approaches expanding the possibility of structures, responses, and effects that can be achieved. In the following section we will explore some of these more exotic and unconventional routes that have been employed to impose strain on ferroelectric materials.

4. Unconventional strain control of epitaxial ferroelectrics

There is a growing trend to push beyond what can be induced *via* conventional, biaxial strain and to explore the limits of what can be achieved using new types of strain. This transition to new types of strain acknowledges a number of limitations with traditional strain control of materials: (1) The magnitude of the strain that can be applied before the onset of relaxation is generally relatively small (1–2% typically); (2) The thickness of a coherently-strained film must be maintained below a critical thickness for strain relaxation typically rendering films unsuitable for high-voltage applications; and (3) There is a lack of continuous tunability arising from the limited number of substrates. These factors put stringent limits on our ability to manipulate the properties and enhance performance on demand. With this in mind, researchers have explored a wide array of novel approaches to create enhanced strain states. Although there are many interesting examples, here we highlight just a few.

4.1. Thermal mismatch strain

Beyond misfit strain, differences in thermal expansion coefficients (TEC) between a film and substrate can result in large, in-plane thermal mismatch strains upon cooling from growth temperature to ambient conditions [184, 336–340]. These effects can be particularly important as thermal mismatch strains can impose significant strains even in the absence of lattice-mismatch. In turn, this enables the extension of strain engineering to thicker films which is important for high-power/voltage ferroelectric and piezoelectric applications. While the presence of these effects have been known for a long time, in general, these effects have been minimally utilized to tune ferroelectric materials. In the few instances where these effects have been exploited they have had a significant influence on the structure and materials properties. For instance, thermal misfit strains have been shown to result in *c*-axis-orientated $PbTiO_3$ thin films when grown on single crystal MgO (001) substrates despite the tensile nature of lattice-misfit strains [341], and that it is possible to stabilize a tetragonal phase in $PbZr_{0.65}Ti_{0.35}O_3$ on $SrRuO_3/LaNiO_3$ buffered CaF_2 substrates [342] despite it being compositionally rhombohedral in the bulk. In addition, these thermal misfit strain effects can significantly impact the nature of the ferroelectric phase transition [343], and even provide additional and significant secondary contributions to pyroelectric responses [208, 344].

4.2. Orientation-driven strain control

Most research on epitaxial strain control of ferroelectricity in literature has been dominated by ferroelectric thin film heterostructures and devices grown on (00*l*)-oriented perovskite substrates. Nevertheless, there is increasing interest in the possibility of applying biaxial strain along other crystallographic planes to manipulate the nature of the ferroelectric phase and also engineer complex domain morphologies that are inaccessible in (001)-oriented films [345, 346]. In particular, it has been known that complex domain structures with highly-enhanced dielectric and piezoelectric susceptibilities can be engineered by electrically poling bulk single-crystal ferroelectrics along non-polar directions that form equivalent angles with at least two possible directions of spontaneous polarization (sometimes referred to as frustrated poling) [97, 347–350]. Appropriate choice of substrate-orientation, allows the combination of such electric poling-based approaches of domain engineering and biaxial-strain control of ferroelectric order to optimize desired functionalities.

In this regard, a number of theoretical studies have focused on the effect of epitaxial strain on (111)- and (110)-oriented epitaxial thin film ferroelectrics [200, 204, 350–352]. For instance, first-principles calculations have suggested that a complex phase transition process can occur in (111)-oriented $PbTiO_3$ and $BaTiO_3$ thin films [351], and that an unexpected triclinic phase and three distinct monoclinic phases may be possible in (110)-oriented $BaTiO_3$ films [200]. At the same time, for (101)-oriented $PbZr_{1-x}Ti_xO_3$ films with compositions near the MPB, phase-field simulations have predicted mobile two-domain configurations that can greatly enhance piezoelectricity. Recent work has compared the strain-composition phase diagram for (001)-, (110)-, and (111)-oriented $PbZr_{1-x}Ti_xO_3$ thin films using 3D, polydomain Ginzburg–Landau–Devonshire-based thermodynamic models [352]. These studies have shown that the use of film orientation can dramatically alter the energetics of competing ferroelectric phases with the potential to stabilize low-symmetry phases with highly-enhanced susceptibilities.

Driven by these theorietical studies, experimentalists have explored the role of film-orientation on the structure and properties of model ferroelectrics including $PbZr_{1-x}Ti_xO_3$ and $BiFeO_3$ [229, 353–355]. Recent work on (111)-oriented, tetragonal $PbZr_{0.2}Ti_{0.8}O_3$ films highlighted how domain-wall contributions to dielectric susceptibilities and ferroelectric

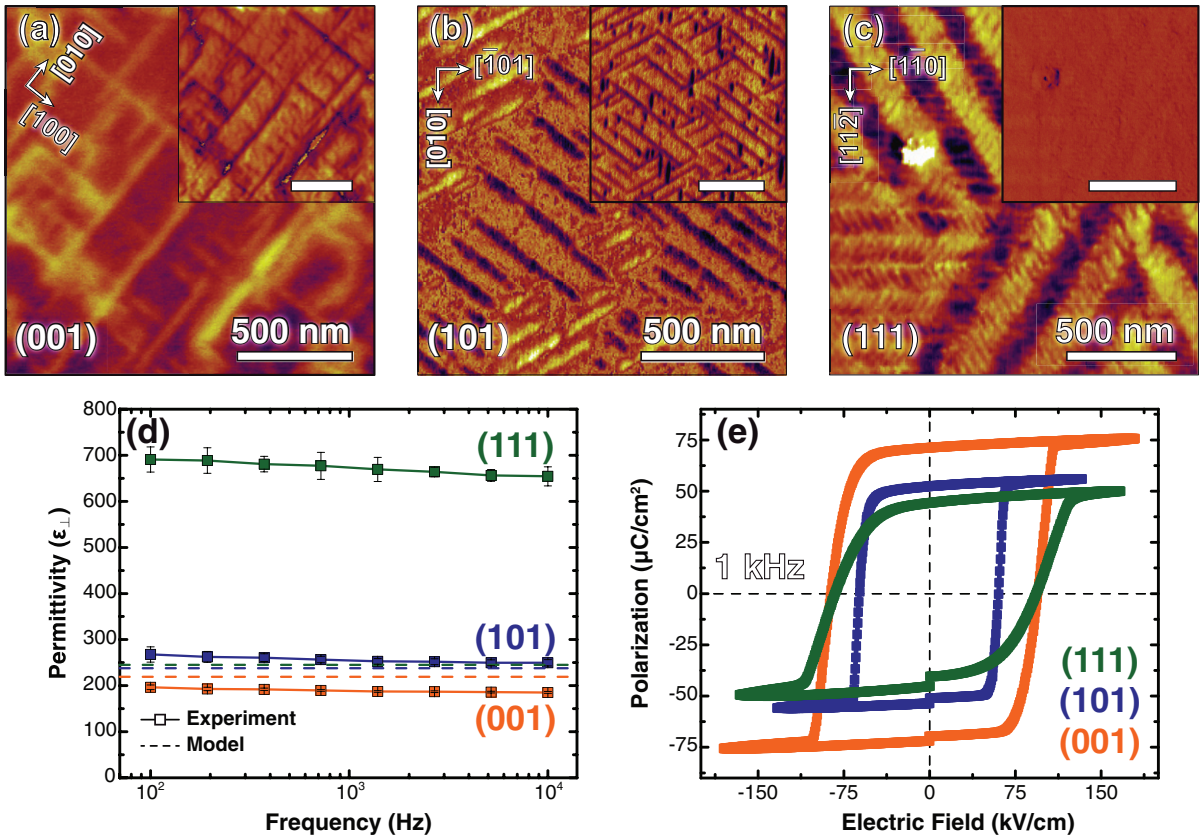

Figure 10. Lateral and vertical (*A*cosθ, combining phase θ and amplitude *A*, inset) PFM images for equilibrium domain structures of (a) (001)-, (b) (101)-, and (c) (111)-oriented $PbZr_{0.2}Ti_{0.8}O_3/La_{0.7}Sr_{0.3}MnO_3/SrTiO_3$ heterostructures. (d) The dielectric permittivity measured at an ac excitation voltage of 50 mV for (001)-, (101)-, and (111)-oriented $PbZr_{0.2}Ti_{0.8}O_3$ thin films (solid line). The dashed lines show the predicted permittivity (including intrinsic and extrinsic contributions) from GLD models. (e) Polarization - electric field hysteresis loops measured at 1 kHz for (001)-, (101)-, and (111)-oriented $PbZr_{0.2}Ti_{0.8}O_3$ thin films (Reprinted from [353, 354]. Copyright 2014 Nature Publishing Group).

switching characteristics can be dramatically tuned with film orientation [348, 349, 354]. First, the domain morphology for (001), (110)-, and (111)-oriented $PbZr_{0.2}Ti_{0.8}O_3$ thin films (figures 10(a)–(c), respectively) are dramatically different. Particularly, (111)-oriented films reveal a high-density, nanotwinned domain morphology and large enhancements in dielectric permittivity under low-field excitation (figure 10(d)). This effect can be understood as a result of so-called stationary or frozen contribution to the permittivity arising from the response of the volume of the ferroelectric material within the finite width of the domain walls [356–361], which has recently been found to be as much as 80-times larger than the intrinsic response [354]. Furthermore, different switching behaviors between (001)-/(101)- and (111)-oriented films were observed, with the latter exhibiting considerably broadened ferroelectric switching characteristics and lower threshold fields for the onset of nonlinearity (figure 10(e)). Both experiments and molecular dynamics simulations revealed the presence of 180° and multi-step 90° switching processes in (001)-/(101)- and (111)-oriented films, respectively. This multistep switching process was attributed to the presence of nanotwinned domain structure consisting of degenerate polarization variants that alter the elastic boundary conditions and reduce the substrate clamping [353]. Such 90°-switching-mediated domain reversal also provides new avenues to achieve low-power, multi-state switching processes for next-generation memory applications. These studies will undoubtably motivate additional studies of ferroelectric thin films with non-standard orientations (including those grown on highly miscut substrates) as a means to control crystal structure and domain morphology.

4.3. Chemical- and defect-induced strain

While chemistry has been traditionally used to manipulate material properties, it can also be used to access and manipulate novel strain states. Rare-earth doping in $BiFeO_3$, for instance, has been found to give rise to an MPB consisting of coexisting rhombohedral and orthorhombic domains [362–369]. For instance, in the case of Sm-doped $BiFeO_3$ thin films, the crystal structure evolves from rhombohedral to orthorhombic with increasing Sm-content. At the same time, the ferroelectric hysteresis loop shape transitioned from a standard single ferroelectric loop for Sm composition <13% to a double-loop for Sm-compositions >14% (figure 11(a)). On the other hand, films doped with rare-earths with comparable ionic radius to Bi^{3+}, such as La^{3+}, do not give rise to MPB-like coexistence, and ferroelectric double loops are not observed (figure 11(b)) [367–369]. Comprehensive investigations using several different rare-earth dopants have revealed a universal behavior for the presence of this phase boundary with enhanced dielectric and piezoelectric responses (figures 11(c) and (d) respectively),

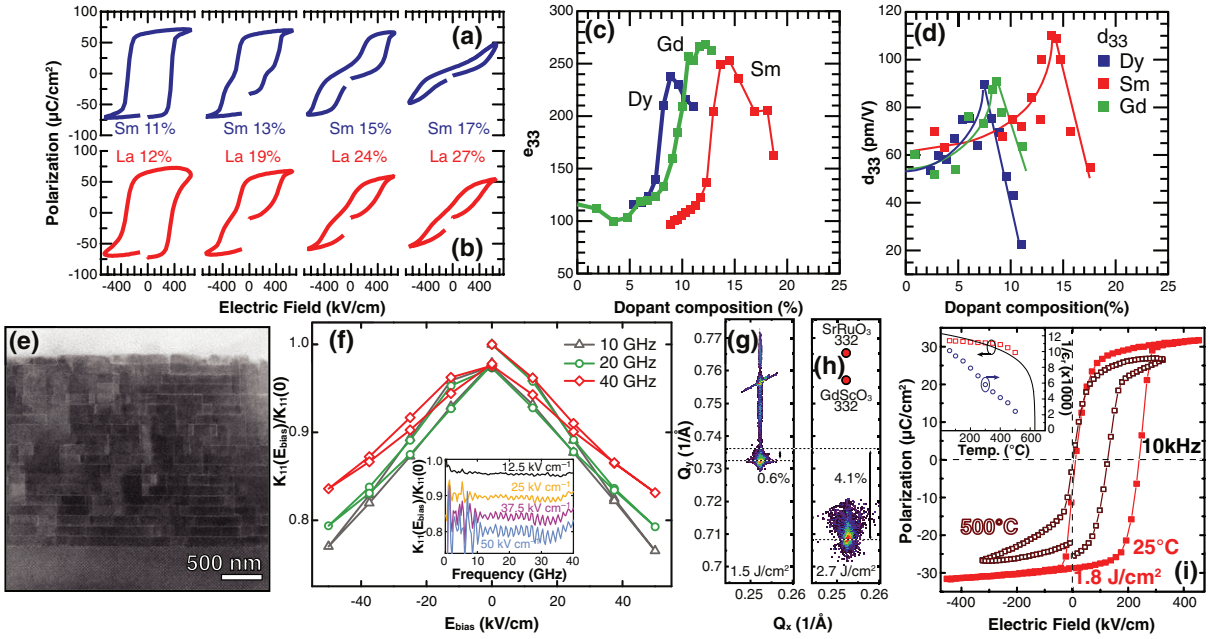

Figure 11. (a) Polarization-electric field hyseteresis loops for Sm-doped $BiFeO_3$ films showing a clear transition from ferroelectric to antiferroelectric behavior with increasing Sm-content. Such behavior is not observed in (b) La-doped $BiFeO_3$ due to the smaller ionic radius of the dopant ions (Reprinted with permission from [367]. Copyright 2011 AIP Publishing LLC). Both (c) ε_{33} and (d) d_{33} improve as a function of rare-earth dopant-concentration to the respective MPB compositions (Reprinted with permission from [369]. Copyright 2010 AIP Publishing LLC). (e) Bright-field STEM image of a $Sr_{n+1}Ti_nO_{3n+1}$ thin film with $n = 6$ showing alternating perovskite (dark) and SrO_2 (light) layers. (f) In-plane dielectric tunability of the same $Sr_{n+1}Ti_nO_{3n+1}$ thin films with $n = 6$ at microwave frequencies and (inset) frequency-dependent dielectric response at various applied bias fields (Reprinted with permission from [370]. Copyright 2013 Nature Publishing Group). Reciprocal space maps about the 103-diffraction condition of $BaTiO_3$ films grown at laser fluence of (g) 1.5 and (h) 2.7 J cm^{-2} that reveal that lattice expansion can be tuned using the growth process by >4%. (i) Ferroelectric hysteresis loops of $BaTiO_3$ films measured at 10 kHz which show ferroelectric behavior up to 500 °C and (inset) revealing the temperature dependent evolution of the polarization and dielectric constant from 25 to 500 °C (Adapted with permission from [380]. Copyright 2014 John Wiley and Sons).

wherein the structural and functional properties can be described simply by chemical strain, with the averaged *A*-site ionic radius as the primary controlling parameter [362, 363, 365–369].

Concurrently, engineered defect structures have also garnered attention as another route to control strain and functionality in ferroelectric materials. For instance, researchers have controllably inserted defect-layers of SrO_2 (that preferentially form under Sr-excess conditions) into a $SrTiO_3$ lattice at regular intervals to create low-loss Ruddlesden–Popper planes (figure 11(e)) [370]. When the number of perovskite layers between $(SrO)_2$ layers (n) is sufficiently large, the centrosymmetry of the $Sr_{n+1}TinO_{3n+1}$ system can be broken under biaxial tensile strain to give rise to a local ferroelectric instability, and highly enhanced dielectric responses. Furthermore, the tendency to form low-loss $(SrO)_2$ planar defects to accomodate non-stoichiometry related defects mitigates point defect formation in these systems and minimizes related dielectric losses. In turn, these films have figures of merit higher than any other tunable dielectric material at room temperature and comparable applied field (figure 11(f)) [370]. This study underscores the importance of the combination of defect- and strain-control in ferroelectric thin films and complements the growing evidence that small changes in the chemistry and defect structures can have a marked influence on ferroic properties [371–375].

In another instance, it has been recently shown that that previously observed anomalous lattice expansion in $Ba_xSr_{1-x}TiO_3$ thin films [376–379] are related to defect complexes that can be accessed through careful control of growth processes [380]. These defect complexes possess both an elastic and an electrical dipole that couples to the epitaxial strain and ferroelectric polarization, respectively, and can be preferentially aligned to produce large anisotropic lattice deformations and enhanced deformations states. The strain-induced alignment of defect-dipoles was exploited to induce deterministic additional out-of-plane strains in epitaxial $BaTiO_3$ thin films to controllably enhance the T_C to temperatures as high as 800–1000 °C without any need to change substrates (figures 11(g)–(i)) [380]. Such combined control of epitaxial strain and growth-induced defect-structures offers a potential pathway, decoupled from expensive oxide substrates, to strain engineer materials.

4.4. Ferroelectric nanocomposites

Self-assembled, ferroelectric nanocomposites offer a route to achieve strong elastic coupling between components due to the increased interfacial area (between the matrix and the ferroelectric) compared to the area of the substrate-film interface. The most widely used method to synthesize nanocomposite oxide materials is to deposit a mixture of the two component materials, often a perovskite and a spinel (although other mixtures are possible), with the desired ratio of the two phases. During the growth process the co-deposited phases separate due to immiscibility or a spinodal instability [381]. The resulting architecture of such nanocomposites generally falls into

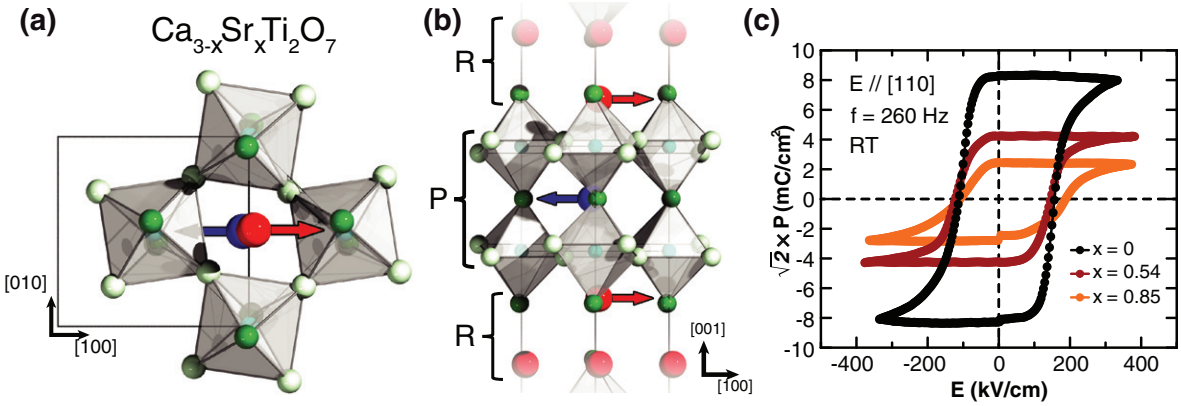

Figure 12. (a) and (b) Crystallographic structure of $Ca_{3-x}Sr_xTi_2O_7$ with the orthorhombic $A2_1am$ space group. The red (blue), white (dark green), and light-blue spheres represent Ca/Sr in the rock-salt (R) block and perovskite (P) block, planar (apical) oxygen of the TiO_6 octahedra, and Ti at the center of the TiO_6 octahedra, respectively. The red and blue arrows depict Ca/Sr displacement along [100] ∥ a in the R and the P block, respectively. (c) Polarization-electric field hysteresis loops for $Ca_{3-x}Sr_xTi_2O_7$ ($x = 0$, 0.54, 0.85) single crystals at room temperature with electric fields applied along the [110] (along the twin boundaries) at frequency $f = 260$ Hz. (Reprinted with permission from [395]. Copyright 2015 Nature Publishing Group).

one of three types: (1) nanoparticles of one phase embedded in a matrix of the other, (2) a lamellar structure reminiscent of traditional heteroepitaxial multilayers, or (3) a vertical array of columns of one phase embedded in a matrix of the other. The architecture of a given nanocomposite system is dictated by the ratio and relative interfacial energies of the two phases. Unlike pure-phase perovskite or traditional heteroepitaxial multilayers, nanocomposites are typically unable to maintain coherent in-plane strain to the substrate beyond a few tens of nanometers due to the massive interfacial area between the two composite phases. Allowing large interfacial strain due to out-of-plane lattice-mismatch between the two composite phases that can be maintained to films thickness in excess of a micron. For example, in the $BiFeO_3$–Sm_2O_3 system, vertical strains of up to 1.5% have been achieved in films up to 150 nm thick [382–384]. As a result, the dielectric permittivity is enhanced and the dielectric losses are suppressed as compared to pure $BiFeO_3$. This effect can be further enhanced by decreasing the column width and increasing the interfacial area (achieved by increasing the growth rate) [381–383, 385]. Building on the vertical strain stabilization observed in the $BiFeO_3$–Sm_2O_3 system, work on the $BaTiO_3$–Sm_2O_3 system revealed that vertical strains as large as 2.35% can be maintained in $BaTiO_3$ even in films >1 μm thick. In such structures, the tetragonality of the $BaTiO_3$, an indicator of potential ferroelectricity, was maintained up to 800 °C (well above the bulk T_C), due to the large vertical strain imposed by the stiffer Sm_2O_3 matrix [384, 385]. In addition to improved dielectric performance, nanocomposite films can be engineered to exhibit enhanced magnetic responses, such as in the $BiFeO_3$–Fe_3O_4 system [386–388] wherein the room-temperature magnetization of the nanocomposite film is nearly four times that of a pure-Fe_3O_4 film. Furthermore, the polar response of the $BiFeO_3$ phase is retained, causing the composite film to simultaneously exhibit strong ferromagnetic and ferroelectric ordering at room temperature. The large interfacial area of the nanocomposite architecture provides promise for enhanced magnetoelectric effects and coupling, such as those previously observed in $BaTiO_3$–$CoFe_2O_4$ and $BiFeO_3$–$CoFe_2O_4$ [389–391] nanocomposites. The ability to obtain such strong coupling between ferroelectric and non-ferroelectric components of nanocomposites provides promise significantly enhance our ability to engineer materials with strong magnetoelectric coupling.

4.5. Interface-, surface-, and octahedral-rotation-driven states

Ferroelectricity is usually induced by polar displacements of second-order Jahn–Teller active cations on the B-site (commonly d^0 transition metals ions, such as Ti^{4+}) and/or on the A-site (lone-pair active cations, such as Pb^{2+} and Bi^{3+}) [31]. The cation displacements that induce ferroelectricity (i.e., proper ferroelectricity), however, are often incompatible with and/or weakly coupled to magnetic ordering (which requires partially filled orbitals), making multiferroics rare in nature [392]. In 2011, theoretical studies posited a new type of ferroelectricity, so called "hybrid improper ferroelectricity," which could be induced by engineering the oxygen octahedra rotations in perovskite-derived structures [317]. The key observation was that the rotation distortion is a combination of two nonpolar modes with different symmetries. Soon after, a generic design algorithm for the development of such octahedral-rotation-induced ferroelectrics was reported [393]. In turn, this led to the articulation of another related pathway to ferroelectricity whereby a spontaneous and switchable polarization emerges from the destruction of an antiferroelectric state due to octahedral rotations and ordered cation sublattices [394]. Recent studies have provided the first experimental demonstration of room-temperature switchable polarization (figures 12(a)–(c)) in Ruddlesden–Popper compounds $Ca_3Ti_2O_7$, as well as Sr-doped $Ca_3Ti_2O_7$ [395]. Furthermore, the planar domain structure observed in $(Ca,Sr)_3Ti_2O_7$ accompanies abundant charged domain walls with conducting head–head and insulating tail–tail configurations, exhibiting a conduction difference of two orders of magnitude. Moreover, unlike proper ferroelectricity, hybrid-improper ferroelectricity does not require B-site cations with d^0 electronic configuration. Cations with strong magnetic interactions, are thus able to coexist and

couple to sizable electric polarizations; thus centric octahedral rotation-induced ferroelectricity provides a plausible route to achieving robust multiferroics. This was experimentally confirmed recently by using crystal chemistry to engineer specific atomic displacements and octahedral rotation in $(Ca_ySr_{1-y})_{1.15}Tb_{1.85}Fe_2O_7$, where it was shown that the polarization and magnetization can co-exist in a layered perovskite at room temperature [396].

In a similar spirit, there is growing work on the role of interface symmetry, chemistry, and octahedral rotational mismatches and how these effects can induce deterministic changes in ferroelectrics [397–400]. For instance, the direction of ferroelectric polarization can be tuned by precisely changing the atomic-scale interface between the ferroelectric ($BiFeO_3$) and the bottom electrode ($La_{0.7}Sr_{0.3}MnO_3$) [401]. Specifically, by switching the termination of the $La_{0.7}Sr_{0.3}MnO_3$ from $La_{0.7}Sr_{0.3}O$- to MnO_2-terminated surfaces and exploiting interfacial valence mismatch, one can influence the electrostatic potential step across the interface and thus the preferred direction of ferroelectric polarization. Further atomic-resolution scanning TEM studies mapped the lattice parameters and oxygen octahedral rotations across the ferroelectric-bottom electrode interface and discovered a mesoscopic antiferrodistortive phase transition near the interface in $BiFeO_3$ showing changes in electronic properties in interface adjacent layers [402]. As new ways of quantifying and inducing such octahedral rotations are further developed, this field could represent an exciting new arena for ferroelectric materials design. For example, in $BiFeO_3$ new results suggest that the monoclinic distortion of scandate substrates, resulting from oxygen octahedral rotation, is the driving force for domain variant down-selection. Using ultrathin, cubic $SrTiO_3$ buffer layers, researchers isolated the effect of "symmetry mismatch" from "lattice mismatch" on domain formation and showed that two-variant stripe domains are observed in films grown directly on orthorhombic $DyScO_3$, while four-variant domains are observed in films grown on $SrTiO_3$-buffered $DyScO_3$ when the buffer layer is >2 nm thick [227].

4.6. Strain gradients and flexoelectricity

Conventionally strain effects are considered only in the context of homogenous strains; however, recently it has been observed that large strain gradients (commonly on the order of 10^5 m^{-1}) can exist in thin films and can give rise to unconventional effects [169, 403–407]. The presence of strain gradients are particularly interesting because of the potential for strong so-called flexoelectric effects [408]. Flexoelectricity refers to the linear coupling of a strain gradient ($\partial\varepsilon_{ij}/\partial x_k$) and the polarization ($P_i$) of a material; an interaction mediated by the fourth-rank flexoelectric tensor (μ_{ijkl}). Flexoelectricity can be understood by considering convex bending of a thin film such that the top of the film is under tension and the bottom is under compression, thereby generating a strain gradient (figure 13(a)). Upon bending, the *B*-site cation (whose displacement is related to the polarization) can move within the unit-cell generating a polarization even in centrosymmetric materials or modifying the polarization in ferroelectrics. These flexoelectric effects (or effects that mimic those arising from flexoelectricity) can alter the ferroic response of materials [409, 410], allow for mechanically-induced ferroelectric switching [397, 411, 412], drive horizontal shifts of ferroelectric hysteresis loops [403, 404, 413–415], and allow for independent tuning of typically coupled ferroelectric susceptibilities [169, 403].

At first pass, one might assume that flexoelectricity could be easily studied by applying an external inhomogeneous strain to a material, and initially, researchers took this approach [397, 416–424]. While it was possible for researchers to measure changes in polarization and extract a value of the flexoelectric coefficient, these experiments were imprecise, with even the best experimental designs having limited control and ability to measure the strain and electric field gradients necessary to accurately measure flexoelectricity [420, 422]. In turn, these measurements commonly resulted in flexoelectric coefficients which varied by more than an order of magnitude between studies [423, 424]. The discussion is further complicated by the fact that experimentally measured values of flexoelectric coefficients are typically orders of magnitude larger [421, 425–427] than theoretically predicted values [425, 428, 429]. This has led many to hypothesize as to the origin of this discrepancy including suggestions of the role of polar clusters/nanoregions [430–433], inhomogenously distributed electronic/ionic defects [434], polarization gradients (in the presence of screening charges which minimize depolarization fields) [435], surface piezoelectricity [410, 436, 437], dynamic piezoelectricity [438–441], and other forms of macroscopic symmetry breaking [442], yet there is still no way to truly reconcile this discrepancy [429, 443].

Even if the magnitude or the sign of these effects are difficult to understand, the influence of flexoelectricity on material structure and responses are starting to be understood. To begin, it is important to be able to controllably engineer strain gradients in ferroelectric thin films, and one of the most developed approaches to do this involves generating a defect gradient, producing a strain gradient (as graphically depicted, figure 13(b)). This approach has been successfully employed to produce strain gradients on the order of 10^5 m^{-1} in $HmMnO_3$ by varying the oxygen partial pressure during growth [405, 406] and in $BiFeO_3$ by varying film thickness and temperature [444]. In an alternative approach, large strain gradients have been generated by growing compositionally-graded heterostructures where "chemical pressure" imposed by the lattice parameter evolution with composition can be used to generate large strain gradients in coherently strained films (shown graphically in the $PbZr_{1-x}Ti_xO_3$ system, figure 13(c)) [403, 404, 415]. Recently, detailed scanning TEM and geometric phase analysis studies has also revealed that polarization rotation and large strain gradients (once again on the order of 10^5) can exist at ferroelastic domains walls [409, 445]. The most pronounced strain gradient (or flexoelectric) effect is the presence of voltage shifted ferroelectric hysteresis loops. The shift, or the so-called built-in potential, is typically quantified in terms of the midpoint of the coercive fields and has been reported to be as large as 30 kV cm^{-1} (0.75 V) in $BiFeO_3$ [444], 50 kV cm^{-1} (1.75 V) in $HoMnO_3$ [406], 100 kV cm^{-1} (1.5 V) in $BaTiO_3$ [380], and 200 kV cm^{-1} (2 V) in compositionally-graded $PbZr_{1-x}Ti_xO_3$ (figure 13(d)) [404]. In addition, the strain gradients that result

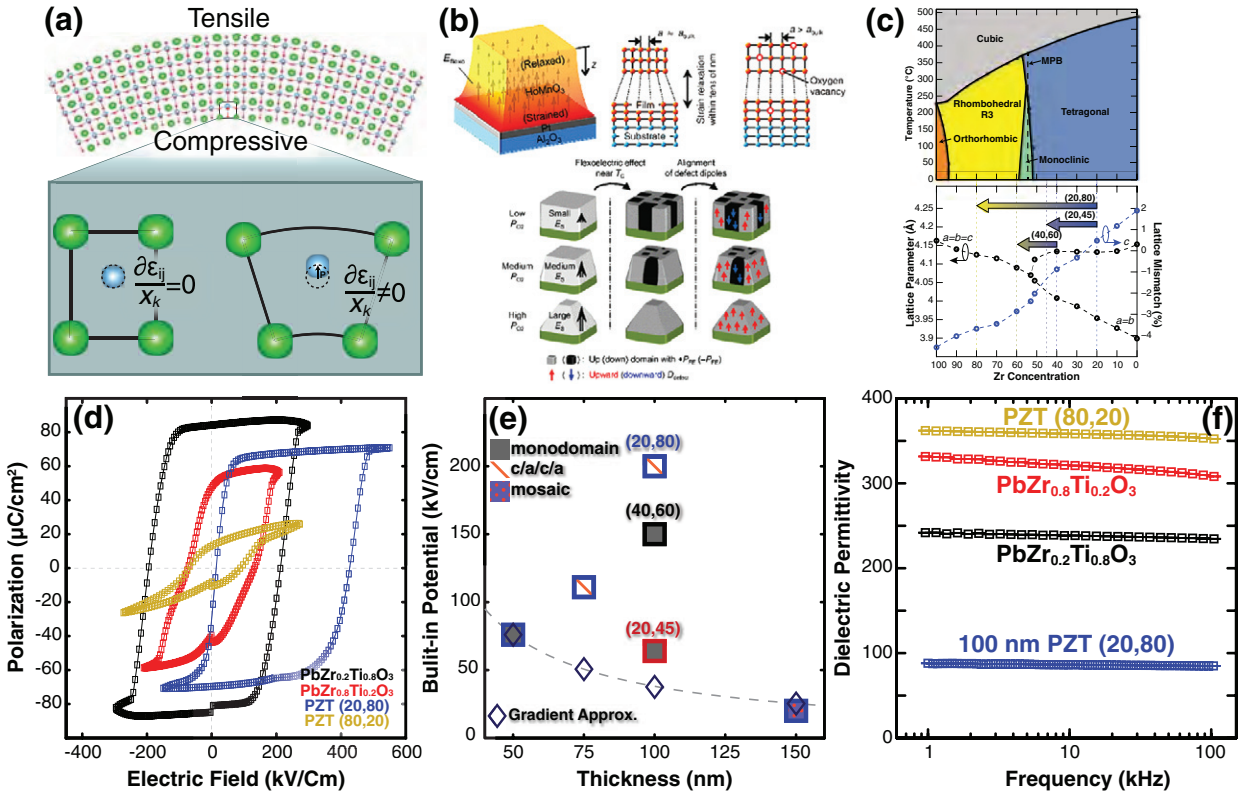

Figure 13. (a) Schematic illustration indicating the fundamental principles of flexoelectricity. (b) Illustration of methodologies for generating strain gradients through controlled defects. The top shows a diagram indicating strain relaxation caused by oxygen vacancies in $HoMnO_3$; the bottom, indicates how growth pressure can be used to tune the magnitude of strain relaxation and, in turn, the flexoelectric effects (reproduced from Reprinted with permission from [405]. Copyright 2012 American Chemical Society. Reprinted with permission from [406]. Copyright 2011 by the American Physical Society). (c) Phase diagram and lattice parameter evolution within the $PbZr_{1-x}Ti_xO_3$ system which indicates how compositionally-graded heterostructures with large strain gradients can be formed (Reprinted with permission from [415]. Copyright 2015 American Chemical Society). (d) Polariation-electric field hysteresis loops of various single-composition and compositionally-graded heterostructures demonstrating the influence of flexoelectric effects in generating large built in potentials (Adapted from [403]. Copyright 2013 American Chemical Society). (e) Plot of measured built-in potential as a function of film thickness for compositionally-graded heterostructures of various thickness and compositional-gradient form. The dashed line and small diamond markers represents an estimation of the built-in potentials based on the *flexo-chemo-electric* coefficient of the 50 nm (20,80) heterostructures. This work indicates that the built-in potentials are significantly enhanced by the presence of large local strain gradients such as those arising from ferroelastic domains walls and/or transitions through the MPB (Reprinted with permission from [415]. Copyright 2015 American Chemical Society). (f) Low-field dielectric permittivity measured as a function of frequency for various single-layer and compositionally-graded heterostructures highlighting the role of the built-in potential in significantly suppressing the intrinsic and extrinsic contributions to the dielectric permittivity (Reprinted with permission from [404]. Copyright 2013 John Wiley & Sons).

from defect segregation can produce non-switchable rectifying diode behavior [444, 446].

Using compositionally-graded heterostructures as a model system, it was observed that the flexoelectric effects (as measured through the built-in potential) do not follow simple predictions based on the chemical and strain gradient form, and instead is enhanced by the inclusion of the morphotropic phase boundary (where the lattice parameter evolution and dielectric constant are the greatest) and/or when ferroelastic domains are present (figure 13(e)) [415]. These extra, symmetry breaking contributions (which can mimic flexoelectricity) and are typically included in experimental measurements could potentially resolve the discrepancy between the theoretical and experimental measures of flexoelectric effects. Regardless of the origin, the built-in potentials alter the material response in a manner similar to an externally applied electric field, causing the suppression of the intrinsic and extrinsic contributions to the dielectric permittivity [403, 447], while having minimal detrimental influence to ferroelectric polarization. Using this approach, it has been shown that it is possible to achieve responses significantly lower than the intrinsic response (figure 13(f)). For instance, in compositionally-graded heterostructures, the lowest reported dielectric permittivity in $PbZr_{1-x}Ti_xO_3$ of ~64 at 10 kHz has been achieved without impact on the magnitude of the polarization [415]. This combination of properties is particularly useful to optimize the figure of merit of these materials for a range of advanced applications where the electromechanical [448–450] ($k^2 = e^2/c\varepsilon_r\varepsilon_0$, where e is the direct-effect piezoelectric coefficient and c is the material stiffness, ε_r is the dielectric permittivity, and ε_0 is the permittivity of free space) and thermal [449, 451, 452] ($k^2 = \pi^2 T/C_p\varepsilon_r\varepsilon_0$, where π is the pyroelectric coefficient, T is the temperature of operation, and C_p is the heat capacity) device efficiency is defined by so-called coupling factors. Routes to tune material stiffness, heat capacity, etc. are limited and thus the ability to tune these figures of merit is confined to routes, such as through flexoelectric

effects that decouple the piezoelectric or pyroelectric coefficients from the permittivity. In this regard, it has recently been shown that because the built-in potential significantly reduces the dielectric permittivity while having minimal impact on the pyroelectric coefficient resulting in a significant improvement in the figures of merit compared to $PbZr_{1-x}Ti_xO_3$ heterostructures without strain gradients, which are even greater than commonly used pyroelectric single crystals such as $LiNbO_3$, and $LiTaO_3$ [403].

5. Strain-driven developments in ferroelectric applications

In the previous sections we have discussed in detail the recent developments in strain-based routes to tune ferroelectric responses and even create new functionalities in materials. These studies while meritorious on their own are most important when they can be utilized to achieve a new or improved functional device. Here we highlight some of the most exciting works which utilized strain-tuned ferroelectric materials to create functional devices.

5.1. Integration of strained ferroelectrics in microelectronic devices

To realize strain-effects in ferroelectric-based microelectronic devices requires the ability to incorporate strained ferroelectric materials in a way compatible with industry standards and fabrication processes (at the wafer, chip, and package levels) as the semiconductor industry is notoriously reluctant to integrate new materials and processes. Such devices cannot rely on the convenient platform of single-crystal perovskite substrates and routes need to be developed to integrate strained ferroelectrics on semiconductor substrates (e.g., Si, Ge, GaAs, and others; for recent reviews see [453, 454]). The growth of perovskite ferroelectrics on semiconductor substrates is inherently complex due to the large differences in chemical composition, crystallographic structure, and thermal expansion coefficients. In this regard, several seminal works have focused on how to grow and control the interface of perovskite buffer layers to facilitate the growth of strained ferroelectric epilayers. These works include the growth of $SrTiO_3$ (and other oxides) on silicon and germanium [455, 456] and the utilization of such $SrTiO_3$-buffered silicon to grow $PbZr_{1-x}Ti_xO_3$ [457, 458]. Using similar approaches researchers have also produced epitaxial, *c*-axis oriented $BaTiO_3$ films using $SrTiO_3$ [459, 460] and $Ba_xSr_{1-x}TiO_3$ buffer layers [461]. Building off of this success, researchers experimentally replicated strain-induced ferroelectricity in $SrTiO_3$ [26, 110–112] demonstrating the efficacy of this approach in imposing epitaxial strain on ferroelectrics intergraded on silicon [462, 463]. Recently, there has been a renewed focus on such systems with demonstrations of ferroelectricity in $BaTiO_3$ films grown on *p*- and *n*-type $SrTiO_3$ buffer layers and directly on Ge (100), (110), and (111) [464–466]. Thus far researchers have produced $SrTiO_3$ [467, 468], $BaTiO_3$ [469], $PbZr_{1-x}Ti_xO_3$ [470–473], $BiFeO_3$ [474–476], and others using these techniques. At the same time, recent efforts using atomic layer deposition (ALD) methodologies for the growth of oxide perovskites on semiconductor substrates offer promise for the integration of strained ferroelectric thin films in semiconductor applications in a process that is both economic and scalable [477].

In turn, these advances are poised to play a very important role in redefining the next-generation of memory and transistor technologies [478–481]. For instance the ability to achieve robust ferroelectric materials with known crystallographic orientation is of paramount importance for fabricating ferroelectric random access memory (FRAMs, based on polarization reversal by an external electrical field in one transistor), as well as for ferroelectric field-effect transistor (FeFET)–based non-volatile memory devices that allow the advantage of non-destructive read out over conventional FRAMs [482]. Another promising candidate for emerging non-volatile memory technologies are ferroelectric tunnel junctions (FTJs) where quantum tunneling of electrons through ultrathin ferroelectric films is controlled by the ferroelectric polarization state and the study of strain-based routes to control these effects are anxiously awaiting discovery [481, 483]. Peering further into the future, strain-based routes to create materials with so-called negative-capacitance field-effect-transistors (NCFET) [484], where the gate-stack is modified with a ferroelectric layer in series, can potentially address voltage-scaling challenges in CMOS technologies related to the subthreshold slope of 60 mV/decade in conventional CMOS transitors. Despite disagreements toward the feasibility of a truly negative-capacitance ferroelectric state [485], encouraging experimental reports supporting the realization of such devices [486–488], along with the recently reported direct measurements of transient negative-capacitance [489] during ferroelectric switching have consolidated support for this concept in the research community.

Another area of interest for strain-tuned ferroelectric materials has been the integration of ferroelectric thin films in microelectromechanical systems (MEMS) and microfluidic devices [18, 490, 491] including micro-cantilever devices for data storage [492] and optical scanning [493], piezoelectric MEMS generators that can convert ambient vibrational energy into electricity [494, 495], and microfluidic pumps and mixers [496, 497]. Additionally, the ability to use strain to tune the strong electro-optic properties inherent in ferroelectric materials provides promise for their use and integration in wideband Si-integrated photonic circuits [498], high-speed optical switches, and electro-optic waveguide modulators [9, 499–501] to create multifunctional devices.

5.2. Strain-control of ferroelectric-ferromagnetic heterostructures

The ability to control ferromagnetism using electric fields holds promise for applications in low-power write operations in spintronic data storage and logic [502, 503]. Multiferroic materials, where the ferroelectric and (anti) ferromagnetic order parameters are intrinsically coupled have been aggressively pursued [504], however, in general, strong magnetic and ferroelectric polarization in materials tends to be mutually exclusive [392]. Alternatively, composites made by combining ferromagnetic materials (e.g., $CoFeO_4$, Terfenol-D, $La_{1-x}Sr_xMnO_3$, FeRh, etc.) and ferroelectric materials provides a simple route to generate

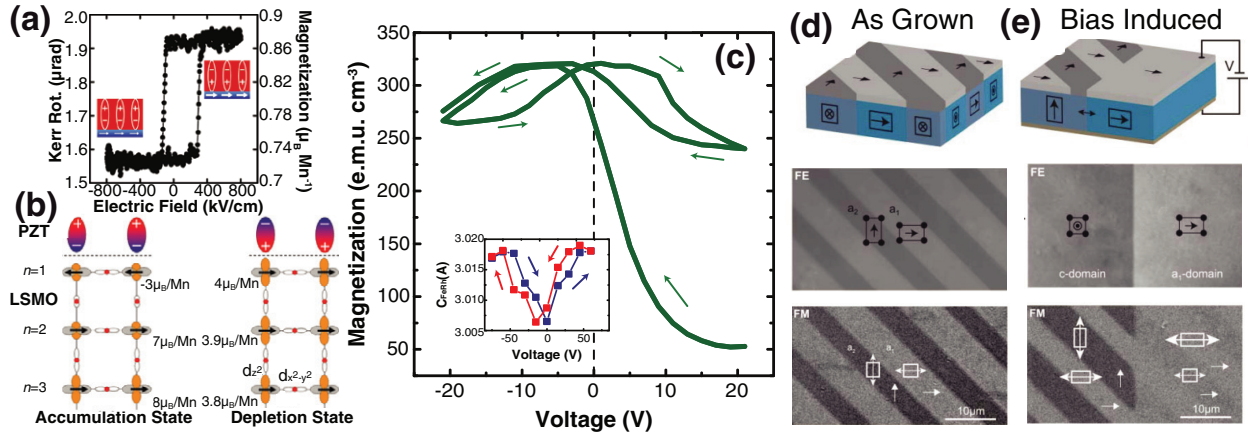

Figure 14. (a) Magnetoelectric hysteresis curve at 100 K showing the magnetic response of a $PbZr_{0.2}Ti_{0.8}O_3/La_{0.2}Sr_{0.8}MnO_3$ heterostructure as a function of applied electric field. The two magnetization values correspond to the modulation of the magnetization of the $La_{0.2}Sr_{0.8}MnO_3$ layer. The inset represents the magnetic and electric states of the $La_{0.2}Sr_{0.8}MnO_3$ and $PbZr_{0.2}Ti_{0.8}O_3$ layers, respectively. The size of the arrows indicates, qualitatively, the magnetization amplitude (Reprinted with permission from [509]. Copyright 2009 John Wiley and Sons). (b) Schematic model of the spin configurations in $La_{0.2}Sr_{0.8}MnO_3$ at the $PbZr_{0.2}Ti_{0.8}O_3$ interface for the depletion and accumulation states, showing the changes in the Mn and O orbital states and the expected changes in the magnetic moment per layer. The arrows indicate the spin orientation in the Mn cations and n denotes number of unit cells below the $PbZr_{0.2}Ti_{0.8}O_3$ layer. The Mn *d* orbitals are drawn in orange and grey, and the lobes of the *p* orbitals are shown around the oxygen atoms (red) (Reprinted figure with permission from [510]. Copyright 2010 by the American Physical Society). (c) Variation of the magnetization in FeRh/$BaTiO_3$ heterostructure with the applied voltage at 385 K, after heating under an external voltage of +21 V. The symmetric dependence of magnetization indicates that the voltage-induced strain effect from the ferroelectric $BaTiO_3$ dominates the magnetoeletric response. The inset shows the voltage dependence of the out-of-plane parameter of FeRh at 390 K (Reprinted with permission from [514]. Copyright 2014 Nature Publishing Group). (d) Ferroelectric (FE) and ferromagnetic (FM) microstructure after CoFe film growth on $BaTiO_3$ and (e) after the application of an out-of-plane electric field of 10 kV cm^{-1}; imaged using optical polarization microscopy. The polarization direction and lattice elongation of the $BaTiO_3$ substrate is indicated by black rectangles with arrows, whereas the orientation of the strain-induced magnetic easy axis is indicated by the white rectangles with double-headed arrows, and the magnetization direction in zero applied magnetic field is indicated by the white arrows. Exact correlation between the ferroic domains patterns can be seen due to the strain transfer at the heterostructure interface (Reprinted with permission from [516]. Copyright 2012 Nature Publishing Group).

large coupling of ferroelectric and magnetic order at room temperature [505]. Following pioneering experiments on $CoFe_2O_4/BaTiO_3$ nanostructures [389], a variety of ferromagnetic/ferroelectric composites such as $CoFe_2O_4/BiFeO_3$ [389], $Zn_{0.1}Fe_{2.9}O_4/(x)PbMg_{1/3}Nb_{2/3}O_3–(1-x)PbTiO_3$ [506], $Fe_3O_4/CoFe_2O_4/PbZr_{1-x}Ti_xO_3$ [507], $La_{1-x}Sr_xMnO_3/BaTiO_3$ [508] have been fabricated in the quest to find new ways to achieve large magnetoelectric coupling. To try and create multiferroic-like responses using ferroelectric–ferromagnetic heterostructures, a thorough understanding of nature of the interaction or coupling between the two layers is of paramount importance. In this regard, there have been efforts to understand how the ferroelectric polarization induced modulation of charge carriers (ferroelectric field effect) at the interface can affect the ferromagnetic moments at the interface (figures 14(a) and (b)) [509–511]. Recently, it has been observed that it was possible to switch the magnetization in $La_{0.7}Sr_{0.3}MnO_3$ films grown on $(x)PbMg_{1/3}Nb_{2/3}O_3–(1-x)PbTiO_3$ single crystal using an electric field as a result of elastic coupling/strain between the layers [512], leading it to be considered the dominant coupling mechanism in such heterostructures. This theory was supported by *in situ* Lorentz microscopy studies of $Fe_{0.7}Ga_{0.3}$ film on mechanically released $BaTiO_3$ films which provided direct observations of strain-driven magnetic switching and domain wall motion under static electric field [513]. Using a similar approach it has been demonstrated that epitaxial FeRh on $BaTiO_3$ single crystals can exhibit a nearly symmetric dependence of the magnetization on the electric field (figure 14(c)) [514] and that the antiferromagnetic and ferromagnetic lamellae of FeRh can be driven to phase separate by the underlying ferroelastic domain structure altering the magnetic response of the FeRh [515]. Similar observations were also reported in $BaTiO_3/CoFe_2O_4$ heterostructures where the strong degree of elastic coupling causes the ferromagnetic domains to mimic the ferroelectric domain structure under an applied electric field (figures 14(d) and (e)) [516].

Interfacial strain has also been used to impact the electronic structure of ferromagnet layers, altering their transport properties. For instance, colossal magnetoresistance in $La_{2/3}Ca_{1//3}MnO_3$ films [517] and large changes in the magnetic anisotropy in Sr_2CrReO_6 heterostructures supported on $BaTiO_3$ [518] have been achieved. These studies of multiferroic heterostructures have just scratched the surface of what is possible, more complex heterostructure designs or even composite systems provide an auspicious pathway to achieve strong muiltiferroic-like responses.

5.3. Domain-wall nanoelectronic devices

In addition to the effects of ferroelectric domains on the macroscopic response it has been recognized that abrupt changes in symmetry at ferroelectric domain boundaries (or domains walls) can result in interesting new functionalities and researchers have sought routes to control and utilize these

boundaries to create nanoscale functional devices [519, 520]. To probe such functionalities at domain walls, new metrology capable of observing phenomena on the nanoscale is needed and a range of techniques have been employed or developed including: conventional and multidimensional band excitation PFM (BE-PFM) [521–523], conductive atomic force microscopy (c-AFM), scanning tunneling microscopy (STM) [524], TEM [402, 525] with *in situ* mechanical and/or electrical perturbation [215, 526, 527], low-energy electron microscopy (LEEM) [528, 529], photoemission electron microscopy (PEEM) [530], and *ab initio* methods [531, 532]. Of the many domain wall functionalities studied, the overwhelming majority of the work has focused on variations in electronic conductivity which exist at domain walls. Differential conductivity at domain walls was first discovered at deoxygenated ferroelastic domain walls in WO_3, where it was found that domain walls could be preferentially doped to become superconducting [533]. Since then various modes of domain wall conduction in a wide variety of materials has been observed including: $BiFeO_3$ [226, 534–539], $AMnO_3$ (A = Y, Er, Ho,…) [540–542], $PbZr_{1-x}Ti_xO_3$ [543], $LiNbO_3$ [544], $BaTiO_3$ [350, 545, 546], and it has been shown that the conduction is dependent on the type and form of the domain wall [547, 548]. More recently, interest has focused on how to externally modulate the conductivity at domains walls including electrically writing domain walls [214, 219, 535, 549–553], moving domain walls [552], and/or altering domain wall geometry [554] using a scanning probe, by generating local chemical defects [555], and other forms of electrical modulation [556]. For example, it has been shown that by writing circular 180° domain walls that the conductivity of the domain wall can be controlled, where the conductivity of the head–head domain wall is significantly higher than the tail–tail domain wall (figures 15(a)–(d)) [554].

In designing domain wall-based devices, the domain walls must be indexable (capable of having a known position in space) such that they can be probed or perturbed (or moved), and in turn, this has motivated the study and development of techniques to make controlled patterns of domains by controlling thickness, thermal annealing, and controlled writing [219, 557] as well as routes to increase the mobility of domain walls [214, 219, 550–552]. In this regard, it has been demonstrated that heterostructures with aligned ferroelastic domains can be formed by kinetically-controlled growth and that these ferroelectric domain walls can be controllably moved and patterned by applying voltage pulses using the right electrode structure [214]. Recently it has been shown that the convergence of strain gradients and ferroelastic domains can generate needle-like ferroelastic domains (figure 15(e)) which are highly-labile and move in a deterministic fashion (in the out-of-plane direction, figures 15(f) and (g)) giving rise to locally enhanced piezoresponse [558]. Such domain structures are also indexable, providing new routes to design ferroelastic domain structures and responses with the directive of creating new domain wall functionalities. In spite of these successes there has been minimal demonstration of operational domain wall devices on the research level (of which most are based on magnetic domain walls) [559, 560]; with no devices being commercially available. The future is bright, however, as new reports of many interesting observations of unique domain wall functionalities are coming each day and, soon, the advances required to enable domain-wall based devices will be achieved.

5.4. Ferroelectric-based photovoltaics

Ferroelectrics are also being pursued for photovoltaic applications due to the novel functionalities provided by their unusual light-response and polarization that does not exist in classical semiconductors. It has been known for decades that ferroelectric crystals, when illuminated with light of energy at or above the band gap (E_g), can produce a steady-state photocurrent parallel to the polarization axis, along with anomalously high photovoltages (as high as 3-orders-of-magnitude larger than the band gap, as observed in $BaTiO_3$, $LiNbO_3$, $LiTaO_3$, and others [561–564]). This effect, also known as the bulk photovoltaic effect, arises from asymmetric scattering centers in materials [565] and asymmetric electrostatic potential (created by the presence of a polarization) that causes excited carriers to drift in a specific direction related to the polarization [566, 567]. At the same time, it has also been proposed that in ferroelectric heterojunction devices, the polarization can change the device band structure altering photovoltaic effects [568–570]. $BiFeO_3$, with a E_g of ~2.7 eV, was demonstrated to produce a switchable photovoltaic current under illumination of visible light without any need for doping and associated losses [571, 572], and has been considered to be a promising candidate to exploit such effects. A breakthrough in thin-film ferroelectric photovoltaics was achieved by using strain-engineered epitaxial thin films of $BiFeO_3$ possessing 1D 71° domain wall arrays and an in-plane electrode configuration to produce photovoltages up to six-times the E_g under illumination of white light [573]. The precise mechanism for such effects has been developed in recent studies of epitaxial $BiFeO_3$ films grown on (001)- and (111)-oriented $SrTiO_3$ substrates, using in-plane electrodes and illumination by linearly polarized light, wherein the photovoltaic current generated was observed to vary with sample and light-polarization rotation, confirming the tensorial nature of the photovoltaic response in these materials. Furthermore, using the combination of two sample orientations and the variation in photocurrent with light-polarization rotation, all the components of the bulk photovoltaic tensor of $BiFeO_3$ were calculated and found to be five orders-of-magnitude larger than other typical ferroelectric materials [574, 575]. With this understanding of the mechanism of the photovoltaic response, researchers are now working towards routes to enhance device performance, for example increasing the current collection efficiency by 7 orders-of-magnitude using multiple AFM tips [576], exploring new low bandgap polar materials [577], and finding other possible applications of the photovoltaic response of $BiFeO_3$, such as the variation in photocurrent with ferroelectric polarization as a way to read bits in a non-volatile memory device [578].

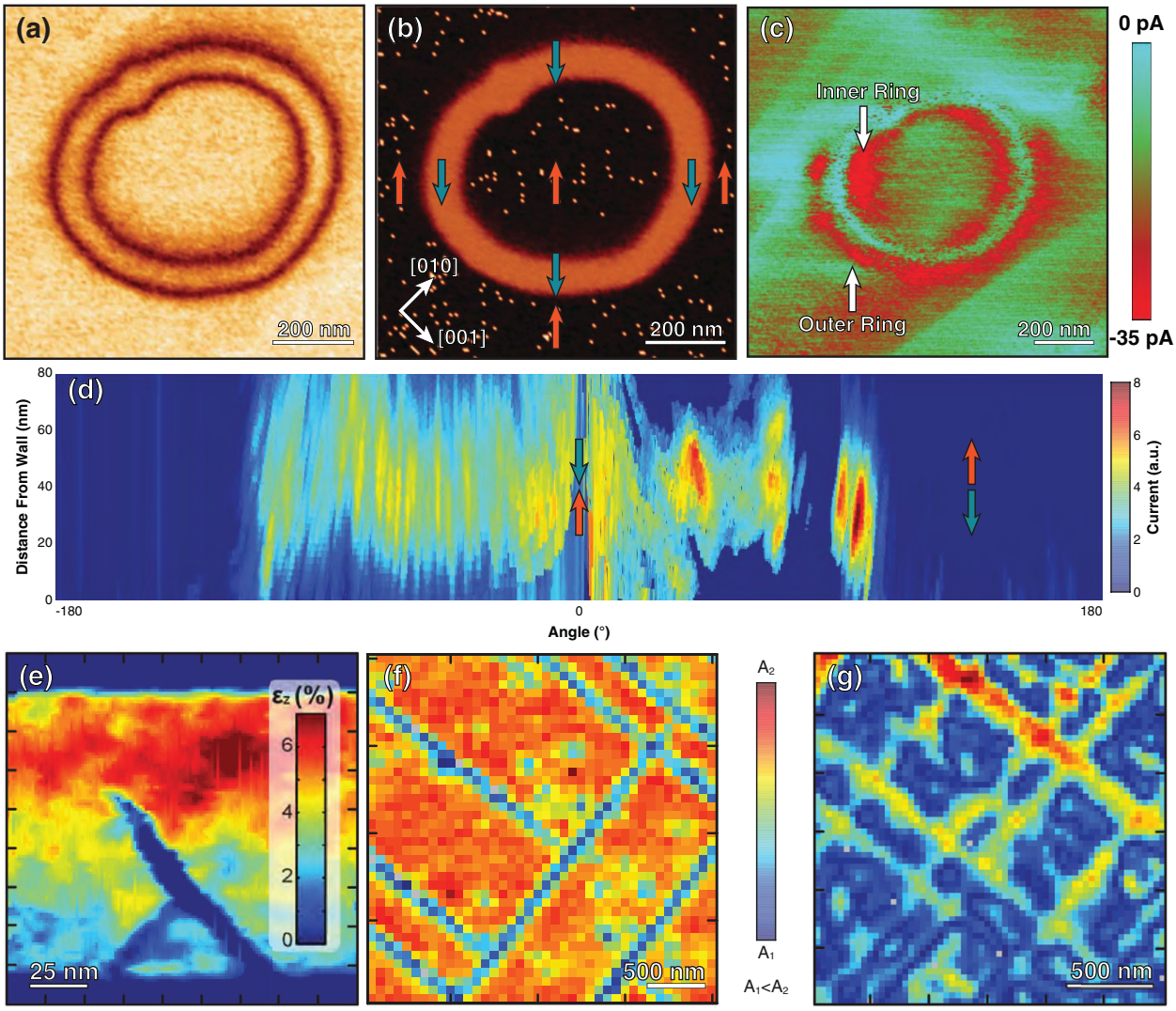

Figure 15. Topological control of conduction states in artificially created 180° domain walls due to head–head and tail–tail driven charge segregation as imaged via (a) vertical amplitude and (b) vertical phase images of a ring written in $BiFeO_3$ by application of +9 V within a single lateral domain. Polarization vectors are shown in the phase image. (c) c-AFM image of the written ring domain taken using tip bias of −2.8 V. (d) Spectrogram of the current as a function of angle and distance from the outer ring of the ferroelectric domains wall (Reprinted with permission from [554]. Copyright 2012 American Chemical Society). (e) Nanobeam electron diffraction strain mapping image of the out-of-plane strain (relative to the substrate $GdScO_3$) in compositionally-graded $PbZr_{1-x}Ti_xO_3$ heterostructures. The image shows that large out-of-plane strain gradients stabilize needle-like ferroelastic domain structures. High-field (~1/2 E_c) out-of-plane band excitation PFM amplitude images of (f) homogeneous $PbZr_{0.2}Ti_{0.8}O_3$ and (g) compositionally-graded heterostructures. These images reveal that the needle-like ferroelastic domains are highly labile in the out-of-plane direction, giving rise to locally enhanced piezoresponse (Reprinted with permission from [558]. Copyright 2016 Nature Publishing Group).

5.5. Thermal-based applications of ferroelectrics

The strongly coupled thermal and electrical responses in ferroelectric materials has spurred interest in how to use these effects for a wide variety of applications including infrared imaging [579], electron emission [580], cryogenic and solid state cooling [10, 581], and waste-heat energy conversion [582, 583]. Based on a strong theoretical foundation, researchers have explored computationally the effect of domain walls and domain structures [210, 212], thin-film thickness and strain state [584–589], thermal-mismatch strains [590–593], chemical and other gradients [435, 594], multilayer structures [344, 595], and much more [428] on the electrocaloric and pyroelectric responses of these materials, and in general, it was found that the pyroelectric (electrocaloric) responses are enhanced close to phase/domain boundaries where large changes in polarization (entropy) can be driven by small changes in temperature (electric field).

While the pyroelectric effect is arguably the most experimentally accessible thermal response of ferroelectric materials, measuring pyroelectric response (accurately) in thin films is difficult leading some to call it “one of the least-known properties of solid materials” [596]. While there are adequate techniques to measure pyroelectric response in bulk materials, including extraction of remanent polarization from temperature-dependent hysteresis loops [19, 597, 598], laser-induced sample heating [599], and linear resistive heating methods [600]; these techniques lack sufficient temperature stability and are unable to properly exclude thermally

stimulated currents, complicating their implementation in thin films [601]. Nevertheless, these approaches have still been applied to thin films [19, 597, 598, 602–604]. More recently researchers have developed phase-sensitive pyroelectric measurement techniques, including those based on microfabricated resistive heater-based 2ω measurements [605, 606] and modulated laser-based approaches [607–609] to achieve a more accurate measure of pyroelectric response in thin films. Using these approaches researchers were able to clarify the relative importance of a number of contributions to overall pyroelectric response including so-called intrinsic, extrinsic, and secondary pyroelectric effects in $PbZr_{1-x}TixO_3$ (section 3.2, figures 4(f) and (g)) [213]. Beyond just the magnitude of the pyroelectric response it is also important to consider the overall efficiency of the device typically quantified in terms of the pyroelectric figures of merit [418, 597, 610, 611]. In general, optimization of the figures of merit requires that one enhance the pyroelectric coefficient and suppress the dielectric permittivity. To decouple the seemingly correlated trends in ferroelectric susceptibilities, new forms of strain-control involving a combination of flexoelectric (strain-gradient) and composition-gradient based routes [211, 403, 415] (refer section 3.2 for details, figure 13) that decouple the pyroelectric and dielectric susceptibilities has been realized, producing thin films with figures of merit comparable or better than the commonly used pyroelectric materials today.

Recently there have also been reports of large electrocaloric effects in thin films of $PbZr_{0.95}Ti_{0.05}O_3$ [597], relaxor ferroelectrics such as $(1-x)PbMg_yNb_{1-y}O_3$–$(x)PbTiO_3$ [612], and $SrBi_2Ta_2O_9$ [613] which have led to a rejuvenation of interest in the study of these effects. An increasing number of publications including several reviews [10, 581, 610, 611, 614–616] have been written over the last few years. Materials of interest are those at the vicinity of temperature- and field-induced phase transitions where large entropy changes are achievable through the desired phase change [581–583, 614]. For instance, large electrocaloric responses are possible in antiferroelectrics via field-induced antiferroelectric to ferroelectric transitions [617]. In general, ferroelectric compositions near a MPB are sources of high entropy originating from multiple domain and polarization states as well as phase transitions that are induced by applied electric fields [618]. Large electrocaloric responses are also possible from entropy changes associated with 1st-order phase transitions as has been demonstrated in $BaTiO_3$ single-crystals [615] and in magnetoelectrically-coupled $La_{0.7}Ca_{0.3}MnO_3/BaTiO_3$ [616]. In this regard, the strain-induced mixed-phase structures in highly-compressively strained $BiFeO_3$ (refer to section 3.3) demonstrate large temperature- and field-induced changes in structure and polarization, as well as several near-room temperature first-order phase transitions, which are promising for thermal-based applications.

Despite these seemly successful and exciting results there are some question relating to the accuracy and methodologies of the approaches used to quantify the electrocaloric responses in these materials. Typically to quantify the electrocaloric response, the pyroelectric response is measured and the electrocaloric response is inferred through thermodynamic Maxwell relations that estimate the adiabatic temperature or isothermal entropy change (measure of the electrocaloric effect). Such *indirect* measurements require careful acknowledgement and understanding of the boundary conditions of the materials [607]. In an alternative approach, *direct* measurements of electrocaloric responses have been attempted, but are inherently difficult due to the small size and low thermal mass of thin film-based devices wherein the electocaloric temperature changes are typically well below the resolution of off-the-shelf thermocouple-based capabilities. Additionally, one must also consider effects such as Joule heating (from current flow through the material) which can alter the temperature change in direct measurements. Comparisons of direct and indirect methods have shown that in some cases the two techniques yield similar results [452, 619–621], but can also vary dramatically in others [607, 622] and this has been a cause for concern in the field. The development of measurement capabilities that allow reliable and direct measurements of pyroelectric and electrocaloric effects in thin-film are needed to truly understand the magnitude and mechanisms of these responses. Over the last few years, researchers have been adapting new measurement strategies for the direct characterization of pyroelectric and electrocaloric effects in thin-film. This includes the use of microfabricated resistive heater-based 2ω measurements [605, 606], modulated laser-based approaches with phase sensitive detection [607–609], measurements of electrocaloric temperature changes using scanning thermal microscopy and infrared imaging [621], and differential scanning calorimetry [623]. These techniques once fully developed and vetted provide promise to probe the role of strain, crystal and domain structure on the thermal susceptibilities in these materials.

6. New horizons for ferroelectrics—looking ahead

In this review we have touched on a number of exciting observations and developments in the field of ferroelectrics over the last decade. To conclude, let us shift gears to looking towards the future of what research in ferroelectrics might hold.

6.1. High-throughput functional materials discovery

The strong investment in advanced materials-by-design approaches and Materials Genome concepts stand poised to expand the known world of functional materials [624, 625]. As the methodologies and approaches mature, the ability to solve for complex material properties will grow, begetting new discoveries and predictions of potential interesting materials. For ferroelectrics, the potential for high-throughput Berry-phase analysis and other first-principles approaches could produce new candidate materials at an unprecedented rate. This, in turn, requires that experimental approaches keep pace and develop routes to greatly shorten the time to discovery and testing of high-quality materials.

6.2. New strain-based approaches to materials discovery and design

Here we have already discussed traditional strain control of materials and recent advances in strain control of materials and thus one can speculate a number of routes that might be possible in the future. One includes expanding work on free-standing thin-film heterostructures where 'on-demand' and tunable strain is possible. In essence, can we create advanced micro-/nano-electromechanical systems (MEMS/NEMS) based on ferroelectric materials where new regimes of magnitude- and time-varying strains can be used to produce exotic functionality? There has been some work on the production of such free-standing complex oxides [107, 626–631], but it begs the question of what is possible in the future? One sneak peak, showed routes to greatly enhanced piezoelectric coefficients and figures of merit for vibrational energy harvesting systems [632]. At the same time, the development of new substrates—both different lattice parameters for perovskite-based systems as well as non-perovskite substrates—could usher in a new golden age of ferroelectric thin films.

6.3. In operando, dynamic, and ultrafast studies of ferroelectrics

As noted at the start of this review, development in both modeling and characterization methods have greatly expanded the time- and length-scales over which one can probe materials. Theoreticians have innovatively simulated many aspects of *in operando* conditions. Using first-principles thermodynamics [633], changes in surface composition and defect concentrations can be probed [634, 635]. Epitaxial strain and interfacial effects are included directly, as are surface interactions with water and other molecules [636–640]. The influence of compositional disorder on temporal- and spatial-dependent dielectric response of relaxors and other ferroelectrics can now be modeled through molecular dynamics simulations of large supercells [641–647]. Ferroelectric and multiferroic domain dynamics under driving fields are simulated with phase field and molecular dynamics simulations. Advances in hardware and the application of novel transmission electron microscopy methods have also provided not only atomic-scale insights, but real-time probes of ferroelectrics under applied fields [527, 648–652]. In the coming years, new advances in hardware, data analysis, and big-data approaches are poised to provide unprecedented information about ferroelectrics. In particular, faster frame-rates during high-resolution imaging may open up doors for extensive work on the nature of ferroelectric switching. Another development that is already beginning to change the way we study and understand ferroelectrics under applied fields is an advanced scanning-probe microscopy operation mode known as band excitation [521, 653–656]. This technique enables the real-time, *in operando* study of ferroelectric switching with nanoscale resolution as well as the quantification and extraction of extensive data about the nature of the processes. This technique is inherently a 'big data' approach and in the coming years application of advanced statistical analysis and data mining may provide new insights. Likewise, synchrotron- and ultra-fast probes of ferroelectrics are rapidly developing [657]. Studies have utilized bright-light sources to enable *in operando* studies of devices under applied fields [191, 658–660], detailed structural study of ultrathin ferroelectric films [661–663], studies of the evolution of ferroelectrics under different environmental conditions [664, 665], and, increasingly, ultrafast probes of dynamic response in these materials [309, 666–670]. Using ultrafast probes is it possible to strongly perturb materials ($>$MV cm^{-1}) on time scales $<$ps. These studies could lead to new insights about the physics of ferroelectricity and the observation of novel states of matter.

6.4. Topologically protected states in ferroelectrics

With the intense study of skyrmion and other topologically protected states in magnet systems, researchers have begun to investigate such topics in ferroelectric systems [671, 672]. A number of theoretical studies have suggested that there is potential for exotic physical phenomena including topological structures such as vortices, waves, and skyrmions in ferroelectric materials [297, 320–323] which are just now being observed experimentally [324]. Topological insulators have different band topologies in the Brillouin zone than do conventional insulators, and as a result the interfaces between topological and conventional insulators must always be conductive [673–675]. This fundamental characteristic can potentially have an intriguing and synergistic interaction with ferroelectrics, since ferroelectric nanomaterials require conductive surfaces to compensate the bound charge and reduce the depolarizing field [676]. Previous recent work has discovered topological insulators [677–680] and topological crystalline insulators [681, 682] that break inversion symmetry, but none of these are switchable. A recent proposal [683] suggests that $CsPbI_3$ under pressure could exhibit transition to a topological insulating phase and to a switchable ferroelectric phase, but more work in this area could yield exciting functional materials.

7. Conclusion

Ferroelectrics (and ferroics in general) have been one of the most important classes of materials over the last half century. The techniques developed for this field are, in turn, applied other condensed matter physics realms with great success. Ultimately the diverse functionality of ferroelectrics means that they likely have staying power as we aim to improve their performance in existing devices and dream about novel applications in the years to come. In the end, breakthroughs in ferroelectrics will be poised to impact across society—from energy, to medicine, to information, to communications, and beyond.

Acknowledgments

The authors acknowledges support from the Army Research Office under grant W911NF-14-1-0104, the Department of

Energy under grant DE-SC0012375, the National Science Foundation under grants DMR-1124696, DMR-1451219, CMMI-1434147, and OISE-1545907, the Office of Naval Research under grant N00014-10-1-0525, and the Air Force Office of Scientific Research under grant FA9550-12-1-0471. The authors have benefited from numerous collaborations within the programs at the University of California, Berkeley and the University of Illinois, Urbana-Champaign as well as numerous other valued collaborators around the world.

References

[1] Francombe M H 1972 *Thin Solid Films* **13** 413
[2] Eaton S S, Butler D B, Parris M, Wilson D and McNeillie H 1988 A ferroelectric nonvolatile memory *ISSCC Digest of Technical Papers* (IEEE) p 130
[3] Busch G 1987 *Ferroelectrics* **74** 267
[4] Cross L E and Newnham R E 1987 *History of Ferroelectrics* ed W D Kingery and E Lense (Westerville, OH: American Ceramic Society) p 289
[5] Cross L E and Newnham R E 1987 *High Technology Ceramics: Past, Present and Future* ed W D Kingery and E Lense (Ann Arbor, MI: University of Michigan) p 289
[6] Auciello O, Scott J F and Ramesh R 1998 *Phys. Today* **51** 22
[7] Haertling G H 1999 *J. Am. Ceram. Soc.* **82** 797
[8] Scott J F 2000 *Ferroelectric Memories* ed K Itoh (Germany: Springer)
[9] Wessels B W 2007 *Annu. Rev. Mater. Res.* **37** 659
[10] Scott J F 2011 *Annu. Rev. Mater. Res.* **41** 229
[11] Sharma B S, Vogel S F and Prentky P I 1973 *Ferroelectrics* **5** 69
[12] de Araujo C P, Taylor G W and Scott J F 1996 *Ferroelectric Thin Films: Synthesis and Basic Principles* ed L A Shuvalov (Amsterdam: Gordon and Breach) p 580
[13] Blum J B and Gurkovich S R 1985 *J. Mater. Sci.* **20** 4479
[14] Budd K D, Key S and Payne D 1985 *J. Brit. Ceram. Proc.* **1** 107
[15] Ramesh R 1997 *Thin Film Ferroelectric Materials and Devices* ed H L Tuller (New York: Springer) p 249
[16] Damjanovic D 1998 *Rep. Prog. Phys.* **61** 1267
[17] Tagantsev A K, Sherman V O, Astafiev K F, Venkatesh J and Setter N 2003 *J. Electroceram.* **11** 5
[18] Muralt P and Muralt P 2000 *J. Micromech. Microeng.* **10** 136
[19] Zhang Q and Whatmore R W 2003 *J. Appl. Phys.* **94** 5228
[20] Schlom D G, Chen L, Pan X, Schmehl A and Zurbuchen M A 2008 *J. Am. Ceram. Soc.* **91** 2429
[21] Christen H M and Eres G 2008 *J. Phys.: Condens. Matter* **20** 264005
[22] Martin L W, Chu Y H and Ramesh R 2010 *Mater. Sci. Eng.* R **68** 89
[23] Shaw T M, Trolier-McKinstry S and McIntyre P C 2000 *Annu. Rev. Mater. Sci.* **30** 263
[24] Ahn C H, Rabe K M and Triscone J M 2004 *Science* **303** 488
[25] Setter N 2006 *J. Appl. Phys.* **100** 051606
[26] Schlom D G, Chen L Q, Eom C B, Rabe K M, Streiffer S K and Triscone J M 2007 *Annu. Rev. Mater. Res.* **37** 589
[27] Schlom D G, Chen L Q, Fennie C J, Gopalan V, Muller D A, Pan X, Ramesh R and Uecker R 2014 *MRS Bull.* **39** 118
[28] Giencke J E, Folkman C M, Baek S and Eom C 2014 *Curr. Opin. Solid State Mater. Sci.* **18** 39
[29] Spaldin N A 2004 *Science* **304** 1606
[30] Cohen R E and Krakauer H 1990 *Phys. Rev.* B **42** 6416
[31] Cohen R E 1992 *Nature* **358** 136
[32] Roytburd A L 1998 *J. Appl. Phys.* **83** 228
[33] Pertsev N A, Zembilgotov Z G and Tagantsev A K 1999 *Ferroelectrics* **223** 79
[34] Bellaiche L, Garcia A and Vanderbilt D 2000 *Phys. Rev. Lett.* **84** 5427
[35] Grinberg I, Cooper V R and Rappe A M 2002 *Nature* **419** 909
[36] Sepliarsky M, Wu Z, Asthagiri A and Cohen R E 2004 *Ferroelectrics* **301** 55
[37] Shin Y, Cooper V R, Grinberg I and Rappe A M 2005 *Phys. Rev.* B **71** 054104
[38] Resta R and Vanderbilt D 2007 *Theory of Polarization: a Modern Approach* ed C H Ahn *et al* (Berlin: Springer)
[39] Rabe K M, Ahn C H and Triscone J M 2007 *Physics of Ferroelectrics: a Modern Perspective* ed K M Rabe *et al* (Berlin: Springer) p 389
[40] Diéguez O and Vanderbilt D 2008 *Phase Transit.* **81** 607
[41] Liu S, Grinberg I and Rappe A M 2013 *J. Phys.: Condens. Matter* **25** 102202
[42] Dawber M, Rabe K M and Scott J F 2005 *Rev. Mod. Phys.* **77** 1083
[43] Fatuzzo E and Merz W J 1967 *Ferroelectricity* (Amsterdam: North Holland) p 289
[44] Mitsui T, Tatsuzaki I and Nakamura E 1976 *An Introduction to the Physics of Ferroelectricity* (London: Gordon and Breach) p 443
[45] Lines M E and Glass A M 1979 *Principles and Applications of Ferroelectrics and Related Materials* ed M E Lines and A M Glass (New York: Oxford University Press) p 680
[46] Nye J F 1957 *Physical Properties of Crystals: Their Representation by Tensors and Matrices* (Oxford: Clarendon)
[47] Goldschmidt V 1926 *Naturwissenschaften* **14** 477
[48] Jahn H A 1938 *Proc. R. Soc.* A **164** 0117
[49] Jahn H A and Teller E 1937 *Proc. R. Soc.* A **161** 220
[50] Opik U and Pryce M H L 1957 *Proc. R. Soc.* A **238** 425
[51] Seshadri R and Hill N A 2001 *Chem. Mater.* **13** 2892
[52] Kay H F and Vousden P 1949 *London Edinburgh Dublin Phil. Mag. J. Sci.* **40** 1019
[53] Merz W J 1949 *Phys. Rev.* **75** 687
[54] Matthias B and Vonhippel A 1948 *Phys. Rev.* **73** 1378
[55] Ramesh R, Sands T and Keramidas V G 1993 *Appl. Phys. Lett.* **63** 731
[56] Tuttle B A, Garino T J, Voigt J A, Headly T J, Dimos D and Eatouch M O 1995 *Relationships Between Ferroelectric 90° Domain Formation and Electrical Properties of Chemically Prepared Pb(Zr,Ti)O_3 Thin Films* ed O Auciello and R Waser (Berlin: Springer) p 117
[57] Xu F, Trolier-McKinstry S, Ren W, Xu B, Xie Z L and Hemker K J 2001 *J. Appl. Phys.* **89** 1336
[58] Kim D J, Maria J P, Kingon A I and Streiffer S K 2003 *J. Appl. Phys.* **93** 5568
[59] Nagarajan V, Roytburd A, Stanishevsky A, Prasertchoung S, Zhao T, Chen L, Melngailis J, Auciello O and Ramesh R 2003 *Nat. Mater.* **2** 43
[60] Lee K and Baik S 2006 *Annu. Rev. Mater. Res.* **36** 81–116
[61] Wada S, Muraishi T, Yokoh K, Yako K, Kamemoto H and Tsurumi T 2007 *Ferroelectrics* **355** 37
[62] Xu Y 2013 *Ferroelectric Materials and Their Applications* ed Y Xu (Amsterdam: Elsevier)
[63] Tagantsev A K, Cross L E and Fousek J 2010 *Domains in Ferroic Crystals and Thin Films* ed A K Tagantsev (Berlin: Springer)
[64] Scheel H J, Bednorz J G and Dill P 1976 *Ferroelectrics* **13** 507
[65] Bednorz J G and Scheel H J 1977 *J. Cryst. Growth* **41** 5
[66] Sandstrom R L, Giess E A, Gallagher W J, Segmuller A, Cooper E I, Chisholm M F, Gupta A, Shinde S and Laibowitz R B 1988 *Appl. Phys. Lett.* **53** 1874
[67] Asano H, Kubo S, Michikami O, Satoh M and Konaka T 1990 *Japan. J. Appl. Phys.* **29** L1452
[68] Brown R, Pendrick V, Kalokitis D and Chai B H T 1990 *Appl. Phys. Lett.* **57** 1351

[69] Berkstresser G W, Valentino A J and Brandle C D 1991 *J. Cryst. Growth.* **109** 457
[70] Hontsu S, Ishii J, Kawai T and Kawai S 1991 *Appl. Phys. Lett.* **59** 2886
[71] Mateika D, Kohler H, Laudan H and Volkel E 1991 *J. Cryst. Growth* **109** 447
[72] Miyazawa Y, Toshima H and Morita S 1993 *J. Cryst. Growth* **128** 668
[73] Berkstresser G W, Valentino A J and Brandle C D 1993 *J. Cryst. Growth* **128** 684
[74] Marti W, Fischer P, Altorfer F, Scheel H J and Tadin M 1994 *J. Phys.: Condens. Matter* **6** 127
[75] Britten J F, Dabkowska H A, Dabkowski A B, Greedan J E, Campbell J L and Teesdale W J 1995 *Acta Crystallogr.* C **51** 1975
[76] Petrosyan A G, Shirinyan G O, Pedrini C, Durjardin C, Ovanesyan K L, Manucharyan R G, Butaeva T I and Derzyan M V 1998 *Cryst. Res. Technol.* **33** 241
[77] Chakoumakos B C, Schlom D G, Urbanik M and Luine J 1998 *J. Appl. Phys.* **83** 1979
[78] Ovanesyan K L, Petrosyan A G, Shirinyan G O, Pedrini C and Zhang L 1999 *J. Cryst. Growth* **198** 497
[79] Nabokin P I, Souptel D and Balbashov A M 2003 *J. Cryst. Growth* **250** 397
[80] Liferovich R P and Mitchell R H 2004 *J. Solid State Chem.* **177** 2188
[81] Zhao J, Ross N L and Angel R J 2004 *J. Phys.: Condens. Matter* **16** 8763
[82] Pawlak D A, Ito M, Dobrzycki L, Wozniak K, Oku M, Shimamura K and Fukuda T 2005 *J. Mater. Res.* **20** 3329
[83] Uecker R, Wilke H, Schlom D G, Velickov B, Reiche P, Polity A, Bernhagen M and Rossberg M 2006 *J. Cryst. Growth* **295** 84
[84] Johnston K E, Mitchell M R, Blanc F, Lightfoot P and Ashbrook S E 2013 *J. Phys. Chem.* C **117** 2252
[85] Ohnishi T, Takahashi K, Nakamura M, Kawasaki M, Yoshimoto M and Koinuma H 1999 *Appl. Phys. Lett.* **74** 2531
[86] Chang J, Park Y and Kim S 2008 *Appl. Phys. Lett.* **92** 152910
[87] Ngai J H, Schwendemann T C, Walker A E, Segal Y, Walker F J, Altman E I and Ahn C H 2010 *Adv. Mater.* **22** 2945
[88] Kleibeuker J E *et al* 2010 *Adv. Funct. Mater.* **20** 3490
[89] Biswas A, Rossen P B, Yang C H, Siemons W, Jung M H, Yang I K, Ramesh R and Jeong Y H 2011 *Appl. Phys. Lett.* **98** 051904
[90] Blok J L, Wan X, Koster G, Blank D H A and Rijnders G 2011 *Appl. Phys. Lett.* **99** 151917
[91] Hegde M S, Satyalakshmi K M, Manoharan S S and Kumar D 1995 *Mater. Sci. Eng.* B **32** 239
[92] Yasukawa M, Ioroi A, Ikeuchi K and Kono T 2004 *Mater. Lett.* **58** 3536
[93] Jona F and Shirane G 1962 *Ferroelectric Crystals* ed F Jona and G Shirane (New York: McMillan) p 402
[94] Dorrian J F, Newnham R E, Smith D K and Kay M I 1972 *Ferroelectrics* **3** 17
[95] Torardi C C, Subramanian M A, Calabrese J C, Gopalakrishnan J, Mccarron E M, Morrissey K J, Askew T R, Flippen R B, Chowdhry U and Sleight A W 1988 *Phys. Rev.* B **38** 225
[96] Rae A D, Thompson J G and Withers R L 1992 *Acta Crystallogr.* B **48** 418
[97] Park S E, Wada S, Cross L E and Shrout T R 1999 *J. Appl. Phys.* **86** 2746
[98] Joseph J, Vimala T M, Sivasubramanian V and Murthy V R K 2000 *J. Mater. Sci.* **35** 1571
[99] Slodczyk A, Kania A, Daniel P and Ratuszna A 2005 *J. Phys. D: Appl. Phys.* **38** 2910
[100] Baettig P, Seshadri R and Spaldin N A 2007 *J. Am. Chem. Soc.* **129** 9854
[101] Belik A A, Iikubo S, Kodama K, Igawa N, Shamoto S and Takayama-Muromachi E 2008 *Chem. Mater.* **20** 3765
[102] Prodjosantoso A K, Zhou Q and Kennedy B J 2013 *J. Solid State Chem.* **200** 241
[103] Koehler J, Dinnebier R and Bussmann-Holder A 2012 *Phase Transit.* **85** 949
[104] Pertsev N A, Zembilgotov A G and Tagantsev A K 1998 *Phys. Rev. Lett.* **80** 1988
[105] Zembilgotov A G, Pertsev N A, Kohlstedt H and Waser R 2002 *J. Appl. Phys.* **91** 2247
[106] Beach R S, Borchers J A, Matheny A, Erwin R W, Salamon M B, Everitt B, Pettit K, Rhyne J J and Flynn C P 1993 *Phys. Rev. Lett.* **70** 3502
[107] Gan Q, Rao R A, Eom C B, Garrett J L and Lee M 1998 *Appl. Phys. Lett.* **72** 978
[108] Bozovic I, Logvenov G, Belca I, Narimbetov B and Sveklo I 2002 *Phys. Rev. Lett.* **89** 107001
[109] Lock J M 1951 *Proc. R. Soc.* A **208** 391
[110] Pertsev N A, Tagantsev A K and Setter N 2000 *Phys. Rev.* B **61** R825
[111] Li Y L *et al* 2006 *Phys. Rev.* B **73** 184112
[112] Haeni J H *et al* 2004 *Nature* **430** 758
[113] Choi K J *et al* 2004 *Science* **306** 1005
[114] Biegalski M D, Jia Y, Schlom D G, Trolier-McKinstry S, Streiffer S K, Sherman V, Uecker R and Reiche P 2006 *Appl. Phys. Lett.* **88** 192907
[115] Meyer B and Vanderbilt D 2001 *Phys. Rev.* B **63** 205426
[116] Souza I, Iniguez J and Vanderbilt D 2002 *Phys. Rev. Lett.* **89** 117602
[117] Neaton J B and Rabe K M 2003 *Appl. Phys. Lett.* **82** 1586
[118] Resta R 2003 *Modelling Simul. Mater. Sci. Eng.* **11** R69
[119] Dieguez O, Rabe K M and Vanderbilt D 2005 *Phys. Rev.* B **72** 144101
[120] Kolpak A M, Sai N and Rappe A M 2006 *Phys. Rev.* B **74** 054112
[121] Zhong W, Vanderbilt D and Rabe K M 1995 *Phys. Rev.* B **52** 6301
[122] Waghmare U V and Rabe K M 1997 *Phys. Rev.* B **55** 6161
[123] Walizer L, Lisenkov S and Bellaiche L 2006 *Phys. Rev.* B **73** 144105
[124] Kornev I A, Bellaiche L, Janolin P E, Dkhil B and Suard E 2006 *Phys. Rev. Lett.* **97** 157601
[125] Paul J, Nishimatsu T, Kawazoe Y and Waghmare U V 2007 *Phys. Rev. Lett.* **99** 077601
[126] Dieguez O, Tinte S, Antons A, Bungaro C, Neaton J B, Rabe K M and Vanderbilt D 2004 *Phys. Rev.* B **69** 212101
[127] Tinte S, Stachiotti M G, Phillpot S R, Sepliarsky M, Wolf D and Migoni R L 2004 *J. Phys.: Condens. Matter* **16** 3495
[128] Sepliarsky M and Cohen R E 2011 *J. Phys.: Condens. Matter* **23** 435902
[129] Asthagiri A, Wu Z, Choudhury N and Cohen R E 2006 *Ferroelectrics* **333** 69
[130] Sepliarsky M, Asthagiri A, Phillpot S R, Stachiotti M G and Migoni R L 2005 *Curr. Opin. Solid State Mater. Sci.* **9** 107
[131] Shin Y, Son J, Lee B, Grinberg I and Rappe A M 2008 *J. Phys.: Condens. Matter* **20** 015224
[132] Liu S, Grinberg I, Takenaka H and Rappe A M 2013 *Phys. Rev.* B **88** 104102
[133] Liu J M, Wang X, Chan H L W and Choy C L 2004 *Phys. Rev.* B **69** 094114
[134] Schorn P J, Bottger U and Waser R 2005 *Appl. Phys. Lett.* **87** 242902
[135] Li B L, Liu X P, Fang F, Zhu J L and Liu J M 2006 *Phys. Rev.* B **73** 014107
[136] Xue F, Gao X S and Liu J 2009 *J. Appl. Phys.* **106** 114103
[137] Li Y L, Hu S Y, Liu Z K and Chen L Q 2001 *Appl. Phys. Lett.* **78** 3878

[138] Chen L Q 2002 *Annu. Rev. Mater. Res.* **32** 113
[139] Li Y L, Choudhury S, Liu Z K and Chen L Q 2003 *Appl. Phys. Lett.* **83** 1608
[140] Chen L 2008 *J. Am. Ceram. Soc.* **91** 1835
[141] Sheng G, Zhang J X, Li Y L, Choudhury S, Jia Q X, Liu Z K and Chen L Q 2008 *Appl. Phys. Lett.* **93** 232904
[142] Ederer C and Spaldin N 2005 *Phys. Rev. Lett.* **95** 257601
[143] Lee H N, Nakhmanson S M, Chisholm M F, Christen H M, Rabe K M and Vanderbilt D 2007 *Phys. Rev. Lett.* **98** 217602
[144] Sando D *et al* 2014 *Phil. Trans. R. Soc.* A **372** 20120438
[145] Infante I C *et al* 2010 *Phys. Rev. Lett.* **105** 057601
[146] Kartavtseva M S, Gorbenko O Y, Kaul A R and Murzina T V 2010 *Thin Solid Films* **518** 4750
[147] Daumont C *et al* 2012 *J. Phys.: Condens. Matter* **24** 162202
[148] Ishikawa K, Nomura T, Okada N and Takada K 1996 *Japan. J. Appl. Phys.* **35** 5196
[149] Zhong W L, Jiang B, Zhang P L, Ma J M, Cheng H M, Yang Z H and Li L X 1993 *J. Phys.: Condens. Matter* **5** 2619
[150] Tybell T, Ahn C H and Triscone J M 1999 *Appl. Phys. Lett.* **75** 856
[151] Ghosez P and Rabe K M 2000 *Appl. Phys. Lett.* **76** 2767
[152] Junquera J and Ghosez P 2003 *Nature* **422** 506
[153] Fong D D, Stephenson G B, Streiffer S K, Eastman J A, Auciello O, Fuoss P H and Thompson C 2004 *Science* **304** 1650
[154] Munkholm A, Streiffer S K, Murty M V R, Eastman J A, Thompson C, Auciello O, Thompson L, Moore J F and Stephenson G B 2002 *Phys. Rev. Lett.* **88** 016101
[155] Streiffer S K, Eastman J A, Fong D D, Thompson C, Munkholm A, Murty M V R, Auciello O, Bai G R and Stephenson G B 2002 *Phys. Rev. Lett.* **89** 067601
[156] Scott J F 2001 *Ferroelectrics* **260** 649
[157] Han H, Kim Y, Alexe M, Hesse D and Lee W 2011 *Adv. Mater.* **23** 4599
[158] Lee W, Han H, Lotnyk A, Schubert M A, Senz S, Alexe M, Hesse D, Baik S and Gosele U 2008 *Nat. Nanotechnol.* **3** 402
[159] Saad M M, Baxter P, Bowman R M, Gregg J M, Morrison F D and Scott J F 2004 *J. Phys.: Condens. Matter* **16** L451
[160] Stengel M and Spaldin N A 2006 *Nature* **443** 679
[161] Chang L W, McMillen M, Morrison F D, Scott J F and Gregg J M 2008 *Appl. Phys. Lett.* **93** 132904
[162] Zhou C and Newns D M 1997 *J. Appl. Phys.* **82** 3081
[163] Vendik O G, Zubko S P and Ter-Martirosayn L T 1998 *Appl. Phys. Lett.* **73** 37
[164] Vendik O G and Zubko S P 2000 *J. Appl. Phys.* **88** 5343
[165] Tyunina M and Levoska J 2006 *Appl. Phys. Lett.* **88** 262904
[166] Gerra G, Tagantsev A K, Setter N and Parlinski K 2006 *Phys. Rev. Lett.* **96** 107603
[167] Choi D K, Kim B S, Son S Y, Oh S H and Park K W 1999 *J. Appl. Phys.* **86** 3347
[168] Sinnamon L J, Saad M M, Bowman R M and Gregg J M 2002 *Appl. Phys. Lett.* **81** 703
[169] Catalan G, Sinnamon L J and Gregg J M 2004 *J. Phys.: Condens. Matter* **16** 2253
[170] Bratkovsky A M and Levanyuk A P 2005 *Phys. Rev. Lett.* **94** 107601
[171] Gerra G, Tagantsev A K and Setter N 2007 *Phys. Rev. Lett.* **98** 207601
[172] Majdoub M S, Maranganti R and Sharma P 2009 *Phys. Rev.* B **79** 115412
[173] Stengel M, Vanderbilt D and Spaldin N A 2009 *Nat. Mater.* **8** 392
[174] Chang L, Alexe M, Scott J F and Gregg J M 2009 *Adv. Mater.* **21** 4911
[175] Berger V 1998 *Phys. Rev. Lett.* **81** 4136
[176] Kalinin S V, Bonnell D A, Alvarez T, Lei X, Hu Z, Shao R and Ferris J H 2004 *Adv. Mater.* **16** 795
[177] Waser R 2012 *Nanoelectronics and Information Technology* vol 1, ed R Waser (New York: Wiley) p 1040
[178] Fousek J and Janovec V 1969 *J. Appl. Phys.* **40** 135
[179] Sapriel J 1975 *Phys. Rev.* B **12** 5128
[180] Janovec V 1976 *Ferroelectrics* **12** 43
[181] Strukov B A and Levanyuk A P 1998 *Ferroelectric Phenomena in Crystals* vol 1, ed B A Strukov and A P Levanyuk (Berlin: Springer) p 308
[182] Streiffer S K, Parker C B, Romanov A E, Lefevre M J, Zhao L, Speck J S, Pompe W, Foster C M and Bai G R 1998 *J. Appl. Phys.* **83** 2742
[183] Fousek J and Safranko M 1965 *Japan. J. Appl. Phys.* **4** 403
[184] Pompe W, Gong X, Suo Z and Speck J S 1993 *J. Appl. Phys.* **74** 6012
[185] Roytburd A L 1993 *Phase Transit.* **45** 1
[186] Kalinin S and Gruverman A 2007 *Scanning Probe Microscopy* vol 1, ed S Kalinin and A Gruverman (Berlin: Springer) p 980
[187] Kalinin S V, Borisevich A and Fong D 2012 *ACS Nano* **6** 10423
[188] Lichtensteiger C, Triscone J M, Junquera J and Ghosez P 2005 *Phys. Rev. Lett.* **94** 047603
[189] Fuoss P H and Brennan S 1990 *Annu. Rev. Mater. Sci.* **20** 365
[190] Stephenson G B *et al* 2003 *Physica B: Condens. Matter* **336** 81
[191] Do D H, Evans P G, Isaacs E D, Kim D M, Eom C B and Dufresne E M 2004 *Nat. Matter.* **3** 365
[192] Stemmer S, Streiffer S K, Ernst F and Ruehle M 1995 *Phys. Status Solidi* **147** 135
[193] Zheng H, Meng Y S and Zhu Y 2015 *MRS Bull.* **40** 12
[194] Alpay S P and Roytburd A L 1998 *J. Appl. Phys.* **83** 4714
[195] Roytburd A L, Alpay S P, Bendersky L A, Nagarajan V and Ramesh R 2001 *J. Appl. Phys.* **89** 553
[196] Roytburd A L, Roytburd V and Slutsker J 2009 *Appl. Phys. Lett.* **94** 152904
[197] Roitburd A L 1976 *Phys. Status Solidi* A **37** 329
[198] Li Y L, Hu S Y, Liu Z K and Chen L Q 2002 *Acta Mater.* **50** 395
[199] Yu J, Wu Z, Liu Z, Yan Q, Wu J and Duan W 2008 *J. Phys.: Condens. Matter* **20** 135203
[200] Gui Z, Prosandeev S and Bellaiche L 2011 *Phys. Rev.* B **84** 214112
[201] Li Y L, Hu S Y and Chen L Q 2005 *J. Appl. Phys.* **97** 034112
[202] Choudhury S, Li Y L and Chen L Q 2005 *J. Am. Ceram. Soc.* **88** 1669
[203] Li Y L and Chen L Q 2006 *Appl. Phys. Lett.* **88** 072905
[204] Zhang J X, Li Y L, Choudhury S, Chen L Q, Chu Y H, Zavaliche F, Cruz M P, Ramesh R and Jia Q X 2008 *J. Appl. Phys.* **103** 094111
[205] Ganpule C S, Nagarajan V, Hill B K, Roytburd A L, Williams E D, Ramesh R, Alpay S P, Roelofs A, Waser R and Eng L M 2002 *J. Appl. Phys.* **91** 1477
[206] Roelofs A, Pertsev N A, Waser R, Schlaphof F, Eng L M, Ganpule C, Nagarajan V and Ramesh R 2002 *Appl. Phys. Lett.* **80** 1424
[207] Lee K S, Choi J H, Lee J Y and Baik S 2001 *J. Appl. Phys.* **90** 4095
[208] Karthik J, Damodaran A and Martin L 2012 *Phys. Rev. Lett.* **108** 167601
[209] Karthik J, Damodaran A R and Martin L W 2012 *Adv. Mater.* **24** 1610
[210] Karthik J and Martin L W 2011 *Appl. Phys. Lett.* **99** 032904
[211] Karthik J, Mangalam R V K, Agar J C and Martin L W 2013 *Phys. Rev.* B **87** 024111
[212] Karthik J and Martin L 2011 *Phys. Rev.* B **84** 024102

[213] Karthik J, Agar J C, Damodaran A R and Martin L W 2012 *Phys. Rev. Lett.* **109** 257602
[214] Feigl L, McGilly L J, Sandu C S and Setter N 2014 *Appl. Phys. Lett.* **104** 172904
[215] Gao P, Britson J, Jokisaari J R, Nelson C T, Baek S, Wang Y, Eom C, Chen L and Pan X 2013 *Nat. Commun.* **4** 2791
[216] Le Rhun G, Vrejoiu I, Pintilie L, Hesse D, Alexe M and Gosele U 2006 *Nanotechnology* **17** 3154
[217] Vrejoiu I, Le Rhun G, Zakharov N D, Hesse D, Pintilie L and Alexe M 2006 *Phil. Mag.* **86** 4477
[218] Chen L, Ouyang J, Ganpule C S, Nagarajan V, Ramesh R and Roytburd A L 2004 *Appl. Phys. Lett.* **84** 254
[219] Feigl L, Yudin P, Stolichnov I, Sluka T, Shapovalov K, Mtebwa M, Sandu C S, Wei X, Tagantsev A K and Setter N 2014 *Nat. Commun.* **5** 4677
[220] Matzen S, Nesterov O, Rispens G, Heuver J A, Biegalski M, Christen H M and Noheda B 2014 *Nat. Commun.* **5** 4415
[221] Borodavka F, Gregora I, Bartasyte A, Margueron S, Plausinaitiene V, Abrutis A and Hlinka J 2013 *J. Appl. Phys.* **113** 187216
[222] Feigl L, McGilly L J and Setter N 2014 *Ferroelectrics* **465** 36
[223] Eerenstein W, Mathur N D and Scott J F 2006 *Nature* **442** 759
[224] Martin L W and Schlom D G 2012 *Curr. Opin. Solid State Mater. Sci.* **16** 199
[225] Catalan G and Scott J F 2009 *Adv. Mater.* **21** 2463
[226] Chu Y H 2006 *Adv. Mater.* **18** 2307
[227] Chen Z H, Damodaran A R, Xu R, Lee S and Martin L W 2014 *Appl. Phys. Lett.* **104** 182908
[228] Das R R *et al* 2006 *Appl. Phys. Lett.* **88** 242904
[229] Chu Y H, Cruz M P, Yang C H, Martin L, Yang P L, Zhang J X, Lee K, Yu P, Chen L Q and Ramesh R 2007 *Adv. Mater.* **19** 2662
[230] Winchester B, Wu P and Chen L Q 2011 *Appl. Phys. Lett.* **99** 052903
[231] Jang H W *et al* 2009 *Adv. Mater.* **21** 817
[232] Park J W, Baek S H, Wu P, Winchester B, Nelson C T, Pan X Q, Chen L Q, Tybell T and Eom C B 2010 *Appl. Phys. Lett.* **97** 212904
[233] Baek S, Folkman C M, Park J, Lee S, Bark C, Tybell T and Eom C 2011 *Adv. Mater.* **23** 1621
[234] Baek S H *et al* 2010 *Nat. Mater.* **9** 309
[235] Chu Y, He Q, Yang C, Yu P, Martin L W, Shafer P and Ramesh R 2009 *Nano Lett.* **9** 1726
[236] Folkman C M *et al* 2009 *Appl. Phys. Lett.* **94** 251911
[237] Daraktchiev M, Catalan G and Scott J F 2008 *Ferroelectrics* **375** 122
[238] Martin L W, Chu Y, Zhan Q, Ramesh R, Han S, Wang S X, Warusawithana M and Schlom D G 2007 *Appl. Phys. Lett.* **91** 172513
[239] Martin L W, Chu Y, Holcomb M B, Huijben M, Yu P, Han S, Lee D, Wang S X and Ramesh R 2008 *Nano Lett.* **8** 2050
[240] Bea H, Bibes M, Ott F, Dupe B, Zhu X H, Petit S, Fusil S, Deranlot C, Bouzehouane K and Barthelemy A 2008 *Phys. Rev. Lett.* **100** 017204
[241] Chen Z, Liu J, Qi Y, Chen D, Damodaran A R, He X, Xu R, N’Diaye A T, Rockett A and Martin L W 2015 *Nano Lett.* **15** 6506
[242] Cazorla C and Iniguez J 2013 *Phys. Rev.* B **88** 214430
[243] Haumont R, Kreisel J and Bouvier P 2006 *Phase Transit.* **79** 1043
[244] Palai R, Katiyar R S, Schmid H, Tissot P, Clark S J, Robertson J, Redfern S A T, Catalan G and Scott J F 2008 *Phys. Rev.* B **77** 014110
[245] Haumont R, Bouvier P, Pashkin A, Rabia K, Frank S, Dkhil B, Crichton W A, Kuntscher C A and Kreisel J 2009 *Phys. Rev.* B **79** 184110
[246] Selbach S M, Tybell T, Einarsrud M and Grande T 2008 *Adv. Mater.* **20** 3692
[247] Guennou M, Bouvier P, Chen G S, Dkhil B, Haumont R, Garbarino G and Kreisel J 2011 *Phys. Rev.* B **84** 174107
[248] Sando D, Barthélémy A and Bibes M 2014 *J. Phys.: Condens. Matter* **26** 473201
[249] Zeches R J *et al* 2009 *Science* **326** 977
[250] Jaffe B, Cook W R and Jaffe H 1971 *Piezoelectric Ceramics* vol 3, ed B Jaffe *et al* (London: Elsevier) p 328
[251] Cross E 2004 *Nature* **432** 24
[252] Noheda B and Cox D E 2006 *Phase Transit.* **79** 5
[253] Ahart M, Somayazulu M, Cohen R E, Ganesh P, Dera P, Mao H, Hemley R J, Ren Y, Liermann P and Wu Z 2008 *Nature* **451** 545
[254] Saito Y, Takao H, Tani T, Nonoyama T, Takatori K, Homma T, Nagaya T and Nakamura M 2004 *Nature* **432** 84
[255] Nagarajan V *et al* 2004 *Appl. Phys. Lett.* **84** 5225
[256] Yun K Y, Ricinschi D, Kanashima T, Noda M and Okuyama M 2004 *Japan. J. Appl. Phys.* **43** L647
[257] Yun K Y, Ricinschi D, Kanashima T and Okuyama M 2006 *Appl. Phys. Lett.* **89** 192902
[258] Ricinschi D, Yun K Y and Okuyama M 2006 *J. Phys.: Condens. Matter* **18** L97
[259] Ravindran P, Vidya R, Kjekshus A, Fjellvåg H and Eriksson O 2006 *Phys. Rev.* B **74** 224412
[260] Bea H *et al* 2009 *Phys. Rev. Lett.* **102** 217603
[261] Hatt A J, Spaldin N A and Ederer C 2010 *Phys. Rev.* B **81** 054109
[262] Damodaran A R, Liang C W, He Q, Peng C Y, Chang L, Chu Y H and Martin L W 2011 *Adv Mater.* **23** 3170
[263] Kumar A, Denev S, Zeches R J, Vlahos E, Podraza N J, Melville A, Schlom D G, Ramesh R and Gopalan V 2010 *Appl. Phys. Lett.* **97** 112903
[264] Dupé B, Infante I C, Geneste G, Janolin P E, Bibes M, Barthélémy A, Lisenkov S, Bellaiche L, Ravy S and Dkhil B 2010 *Phys. Rev.* B **81** 144128
[265] Chen Z *et al* 2010 *Appl. Phys. Lett.* **97** 242903
[266] Wojdel J C and Iniguez J 2010 *Phys. Rev. Lett.* **105** 037208
[267] Mazumdar D, Shelke V, Iliev M, Jesse S, Kumar A, Kalinin S V, Baddorf A P and Gupta A 2010 *Nano Lett.* **10** 2555
[268] Iliev M N, Abrashev M V, Mazumdar D, Shelke V and Gupta A 2010 *Phys. Rev.* B **82** 014107
[269] Christen H M, Nam J H, Kim H S, Hatt A J and Spaldin N A 2011 *Phys. Rev.* B **83** 144107
[270] Chen Z *et al* 2011 *Adv. Funct. Mater.* **21** 133
[271] Siemons W, Biegalski M D, Nam J H and Christen H M 2011 *Appl. Phys. Express* **4** 095801
[272] Liu H *et al* 2012 *Phys. Rev.* B **85** 014104
[273] Woo C *et al* 2012 *Phys. Rev.* B **86** 054417
[274] Zhang J X *et al* 2011 *Phys. Rev. Lett.* **107** 147602
[275] Kuo H Y, Shu Y C, Chen H Z, Hsueh C J, Wang C H and Chu Y H 2011 *J. Eur. Ceram. Soc.* **31** 3063
[276] Chen Z *et al* 2011 *Phys. Rev.* B **84** 094116
[277] Diéguez O, González-Vázquez O E, Wojdeł J C and Íñiguez J 2011 *Phys. Rev.* B **83** 094105
[278] Chen Y *et al* 2012 *Adv. Mater.* **24** 3070
[279] Beekman C *et al* 2013 *Adv. Mater.* **25** 5561
[280] Pailloux F *et al* 2014 *Phys. Rev.* B **89** 104106
[281] Damodaran A, Lee S, Karthik J, MacLaren S and Martin L 2012 *Phys. Rev.* B **85** 024113
[282] Damodaran A R, Breckenfeld E, Choquette A K and Martin L W 2012 *Appl. Phys. Lett.* **100** 082904
[283] Bruinsma R and Zangwill A 1986 *J. Phys.* **47** 2055
[284] Ouyang J, Zhang W, Huang X and Roytburd A L 2011 *Acta Mater.* **59** 3779
[285] Vasudevan R K, Liu Y, Li J, Liang W I, Kumar A, Jesse S, Chen Y C, Chu Y H, Nagarajan V and Kalinin S V 2011 *Nano Lett.* **11** 3346

[286] Zhang J X *et al* 2011 *Nat. Nanotechnol.* **6** 98
[287] He Q *et al* 2011 *Nat. Commun.* **2** 225
[288] Ko K T *et al* 2011 *Nat. Commun.* **2** 567
[289] Infante I C *et al* 2011 *Phys. Rev. Lett.* **107** 237601
[290] Kreisel J, Jadhav P, Chaix-Pluchery O, Varela M, Dix N, Sanchez F and Fontcuberta J 2011 *J. Phys.: Condens. Matter* **23** 342202
[291] MacDougall G J, Christen H M, Siemons W, Biegalski M D, Zarestky J L, Liang S, Dagotto E and Nagler S E 2012 *Phys. Rev.* B **85** 100406
[292] Zubko P, Gariglio S, Gabay M, Ghosez P and Triscone J M 2011 *Annu. Rev. Condens. Mater. Phys.* **2** 141
[293] Dawber M, Stucki N, Lichtensteiger C, Gariglio S and Triscone J M 2008 *J. Phys.: Condens. Matter* **20** 264015
[294] Li S, Eastman J A, Vetrone J M, Newnham R E and Cross L E 1997 *Phil. Mag.* B **76** 47
[295] Sai N, Meyer B and Vanderbilt D 2000 *Phys. Rev. Lett.* **84** 5636
[296] Nakhmanson S M, Rabe K M and Vanderbilt D 2005 *Appl. Phys. Lett.* **87** 102906
[297] Choudhury N, Walizer L, Lisenkov S and Bellaiche L 2011 *Nature.* **470** 513
[298] Aguado-Puente P, García-Fernández P and Junquera J 2011 *Phys. Rev. Lett.* **107** 217601
[299] Aguado-Puente P and Junquera J 2012 *Phys. Rev.* B **85** 184105
[300] Tabata H, Tanaka H and Kawai T 1994 *Appl. Phys. Lett.* **65** 1970
[301] Tabata H and Kawai T 1997 *Appl. Phys. Lett.* **70** 321
[302] O’Neill D, Bowman R M and Gregg J M 2000 *Appl. Phys. Lett.* **77** 1520
[303] Kim J, Kim Y, Kim Y S, Lee J, Kim L and Jung D 2002 *Appl. Phys. Lett.* **80** 3581
[304] Sigman J, Norton D P, Christen H M, Fleming P H and Boatner L A 2002 *Phys. Rev. Lett.* **88** 097601
[305] Dawber M, Lichtensteiger C, Cantoni M, Veithen M, Ghosez P, Johnston K, Rabe K M and Triscone J M 2005 *Phys. Rev. Lett.* **95** 177601
[306] Bousquet E, Dawber M, Stucki N, Lichtensteiger C, Hermet P, Gariglio S, Triscone J M and Ghosez P 2008 *Nature* **452** 732
[307] Tenne D A *et al* 2006 *Science* **313** 1614
[308] Zubko P, Stucki N, Lichtensteiger C and Triscone J M 2010 *Phys. Rev. Lett.* **104** 187601
[309] Jo J Y, Chen P, Sichel R J, Callori S J, Sinsheimer J, Dufresne E M, Dawber M and Evans P G 2011 *Phys. Rev. Lett.* **107** 055501
[310] Callori S J, Gabel J, Su D, Sinsheimer J, Fernandez-Serra M and Dawber M 2012 *Phys. Rev. Lett.* **109** 067601
[311] Sinsheimer J, Callori S J, Bein B, Benkara Y, Daley J, Coraor J, Su D, Stephens P W and Dawber M 2012 *Phys. Rev. Lett.* **109** 167601
[312] Warusawithana M P, Colla E V, Eckstein J N and Weissman M B 2003 *Phys. Rev. Lett.* **90** 036802
[313] Lee H N, Christen H M, Chisholm M F, Rouleau C M and Lowndes D H 2005 *Nature.* **433** 395
[314] Rogdakis K, Seo J W, Viskadourakis Z, Wang Y, Ah Qune L F N, Choi E, Burton J D, Tsymbal E Y, Lee J and Panagopoulos C 2012 *Nat.Commun.* **3** 1064
[315] Sai N, Fennie C J and Demkov A A 2009 *Phys. Rev. Lett.* **102** 107601
[316] Ghosez P and Triscone J 2011 *Nat Mater.* **10** 269
[317] Benedek N A and Fennie C J 2011 *Phys. Rev. Lett.* **106** 107204
[318] Chen P, Cosgriff M P, Zhang Q, Callori S J, Adams B W, Dufresne E M, Dawber M and Evans P G 2013 *Phys. Rev. Lett.* **110** 047601
[319] Tang Y L *et al* 2015 *Science* **348** 547
[320] Naumov I I, Bellaiche L and Fu H 2004 *Nature* **432** 737
[321] Ponomareva I, Naumov I I and Bellaiche L 2005 *Phys. Rev.* B **72** 214118
[322] Prosandeev S and Bellaiche L 2007 *Phys. Rev.* B **75** 094102
[323] Prosandeev S, Ponomareva I, Naumov I, Kornev I and Bellaiche L 2008 *J. Phys.: Condens. Matter* **20** 193201
[324] Yadav A K *et al* 2016 *Nature* **530** 198
[325] Wright D C and Mermin N D 1989 *Rev. Mod. Phys.* **61** 385
[326] Prosandeev S, Malashevich A, Gui Z, Louis L, Walter R, Souza I and Bellaiche L 2013 *Phys. Rev.* B **87** 195111
[327] Fennie C J and Rabe K M 2006 *Phys. Rev. Lett.* **97** 267602
[328] Lee J H *et al* 2010 *Nature* **466** 954
[329] Tyunina M, Narkilahti J, Plekh M, Oja R, Nieminen R M, Dejneka A and Trepakov V 2010 *Phys. Rev. Lett.* **104** 227601
[330] Belik A A, Kolodiazhnyi T, Kosuda K and Takayama-Muromachi E 2009 *J. Mater. Chem.* **19** 1593
[331] De Luca G M, Preziosi D, Chiarella F, Di Capua R, Gariglio S, Lettieri S and Salluzzo M 2013 *Appl. Phys. Lett.* **103** 062902
[332] Dieguez O and Iniguez J 2015 *Phys. Rev.* B **91** 184113
[333] Reyes-Lillo S E and Rabe K M 2013 *Phys. Rev.* B **88** 180102
[334] Bhattacharjee S, Bousquet E and Ghosez P 2009 *Phys. Rev. Lett.* **102** 117602
[335] Bousquet E, Spaldin N A and Ghosez P 2010 *Phys. Rev. Lett.* **104** 037601
[336] Sviridov E V, Alyoshin V A, Golovko Y I, Zakharchenko I N, Mukhortov V M and Dudkevich V P 1990 *Phys. Status Solidi* A **121** 157
[337] Mehrotra V, Kaplan S, Sievers A J and Giannelis E P 1993 *J. Mater. Res.* **8** 1209
[338] Speck J S, Daykin A C, Seifert A, Romanov A E and Pompe W 1995 *J. Appl. Phys.* **78** 1696
[339] Srikant V, Tarsa E J, Clarke D R and Speck J S 1995 *J. Appl. Phys.* **77** 1517
[340] Taylor T R, Hansen P J, Acikel B, Pervez N, York R A, Streiffer S K and Speck J S 2002 *Appl. Phys. Lett.* **80** 1978
[341] Ogawa T, Senda A and Kasanami T 1991 *Japan. J. Appl. Phys.* **30** 2145
[342] Ehara Y, Yasui S, Ishii K and Funakubo H 2012 *Japan. J. Appl. Phys.* **51** 09LA14
[343] Tenne D *et al* 2004 *Phys. Rev.* B **69** 2
[344] Kesim M T, Zhang J, Alpay S P and Martin L W 2014 *Appl. Phys. Lett.* **105** 052901
[345] Saito K, Kurosawa T, Akai T, Oikawa T and Funakubo H 2003 *J. Appl. Phys.* **93** 545
[346] Funakubo H *et al* 2008 *Phase Transit.* **81** 667
[347] Wada S, Yako K, Kakemoto H, Tsurumi T and Kiguchi T 2005 *J. Appl. Phys.* **98** 014109
[348] Hlinka J, Ondrejkovic P and Marton P 2009 *Nanotechnology* **20** 105709
[349] Bernal A, Zhang S, Zhang S and Bassiri-Gharb N 2009 *Appl. Phys. Lett.* **95** 142911
[350] Sluka T, Tagantsev A K, Damjanovic D, Gureev M and Setter N 2012 *Nat. Commun.* **3** 748
[351] Oja R, Johnston K, Frantti J and Nieminen R M 2008 *Phys. Rev.* B **78** 094102
[352] Xu R, Zhang J, Chen Z and Martin L W 2015 *Phys. Rev.* B **91** 144106
[353] Xu R, Liu S, Grinberg I, Karthik J, Damodaran A R, Rappe A M and Martin L W 2015 *Nat. Mater.* **14** 79
[354] Xu R, Karthik J, Damodaran A R and Martin L W 2014 *Nat. Commun.* **5** 3120
[355] Ouyang J, Slusker J, Levin I, Kim D, Eom C, Ramesh R and Roytburd A L 2007 *Adv. Funct. Mater.* **17** 2094
[356] Fousek J 1965 *Czech. J. Phys.* **15** 412
[357] Nettleton R E 1966 *J. Phys. Soc. Japan* **21** 1633
[358] Lawless W N 1968 *Phys. Rev.* **175** 619
[359] Lawless W N and Fousek J 1970 *J. Phys. Soc. Japan* **28** 419

[360] Rao W F and Wang Y U 2007 *Appl. Phys. Lett.* **90** 041915
[361] Morozovska A N, Eliseev E A, Varenyk O V and Kalinin S V 2013 *J. Appl. Phys.* **113** 187222
[362] Fujino S, Murakami M, Anbusathaiah V, Lim S, Nagarajan V, Fennie C J, Wuttig M, Salamanca-Riba L and Takeuchi I 2008 *Appl. Phys. Lett.* **92** 202904
[363] Cheng C J, Kan D, Lim S H, McKenzie W R, Munroe P R, Salamanca-Riba L G, Withers R L, Takeuchi I and Nagarajan V 2009 *Nano Lett.* **80** 014109
[364] Emery S B, Cheng C, Kan D, Rueckert F J, Alpay S P, Nagarajan V, Takeuchi I and Wells B O 2010 *Appl. Phys. Lett.* **97** 152902
[365] Cheng C, Borisevich A Y, Kan D, Takeuchi I and Nagarajan V 2010 *Chem. Mater.* **22** 2588
[366] Kan D, Anbusathaiah V and Takeuchi I 2011 *Adv. Mater.* **23** 1765
[367] Kan D, Cheng C, Nagarajan V and Takeuchi I 2011 *J. Appl. Phys.* **110** 014106
[368] Kan D, Pálová L, Anbusathaiah V, Cheng C J, Fujino S, Nagarajan V, Rabe K M and Takeuchi I 2010 *Adv. Funct. Mater.* **20** 1108
[369] Cheng C J, Kan D, Anbusathaiah V, Takeuchi I and Nagarajan V 2010 *Appl. Phys. Lett.* **97** 212905
[370] Lee C *et al* 2013 *Nature* **502** 532
[371] Breckenfeld E, Wilson R, Karthik J, Damodaran A R, Cahill D G and Martin L W 2012 *Chem. Mater.* **24** 331
[372] Breckenfeld E, Wilson R B and Martin L W 2013 *Appl. Phys. Lett.* **103** 082901
[373] Breckenfeld E, Chen Z, Damodaran A R and Martin L W 2014 *ACS Appl. Mater. Interfaces* **6** 22436
[374] Breckenfeld E, Shah A B and Martin L W 2013 *J. Mater. Chem.* C **1** 8052
[375] Breckenfeld E, Bronn N, Mason N and Martin L W 2014 *Appl. Phys. Lett.* **105** 121610
[376] Mukhortov V M, Golovko Y I, Mukhortov V M and Dudkevich V P 1981 *Sov. Phys. J.* **24** 102
[377] Mukhortov V M, Golovko Y I, Aleshin V A, Sviridov E V, Mukhortov V M, Dudkevich V P and Fesenko E G 1983 *Phys. Status Solidi* A **77** K37
[378] Abe K, Komatsu S, Yanase N, Sano E and Kawakubo T 1997 *Japan. J. Appl. Phys.* **36** 5575
[379] Kawakubo T, Komatsu S, Abe K, Sano K, Yanase N and Fukushima N 1998 *Japan. J. Appl. Phys.* **37** 5108
[380] Damodaran A R, Breckenfeld E, Chen Z, Lee S and Martin L W 2014 *Adv. Mater.* **26** 6341
[381] MacManus-Driscoll J L 2010 *Adv. Funct. Mater.* **20** 2035
[382] MacManus-Driscoll J L, Zerrer P, Wang H, Yang H, Yoon J, Fouchet A, Yu R, Blamire M G and Jia Q 2008 *Nat. Mater.* **7** 314
[383] Yang H, Wang H, Zou G, Jain M, Suvorova N, Feldmann D, Dowden P, DePaula R, MacManus-Driscoll J and Taylor A 2008 *Appl. Phys. Lett.* **93** 142904
[384] Harrington S A *et al* 2011 *Nat. Nanotechnol.* **6** 491
[385] Fouchet A, Wang H, Yang H, Yoon J, Jia Q and MacManus-Driscoll J L 2009 *IEEE Trans. Ultrason. Ferroelectr. Freq. Control* **56** 1534
[386] Weal E, Patnaik S, Bi Z, Wang H, Fix T, Kursumovic A and Driscoll J M 2010 *Appl. Phys. Lett.* **97** 153121
[387] Choi E, Weal E, Bi Z, Wang H, Kursumovic A, Fix T, Blamire M G and MacManus-Driscoll J L 2013 *Appl. Phys. Lett.* **102** 012905
[388] Qu T, Zhao Y, Yu P, Zhao H, Zhang S and Yang L 2012 *Appl. Phys. Lett.* **100** 242410
[389] Zheng H *et al* 2004 *Science* **303** 661
[390] Zheng H, Straub F, Zhan Q, Yang P, Hsieh W, Zavaliche F, Chu Y, Dahmen U and Ramesh R 2006 *Adv. Mater.* **18** 2747
[391] Zavaliche F, Zheng H, Mohaddes-Ardabili L, Yang S, Zhan Q, Shafer P, Reilly E, Chopdekar R, Jia Y and Wright P 2005 *Nano Lett.* **5** 1793
[392] Hill N A 2000 *J. Phys. Chem.* B **104** 6694
[393] Rondinelli J M and Fennie C J 2012 *Adv. Mater.* **24** 1961
[394] Mulder A T, Benedek N A, Rondinelli J M and Fennie C J 2013 *Adv. Funct. Mater.* **23** 4810
[395] Oh Y S, Luo X, Huang F, Wang Y and Cheong S 2015 *Nat. Mater.* **14** 407
[396] Pitcher M J, Mandal P, Dyer M S, Alaria J, Borisov P, Niu H, Claridge J B and Rosseinsky M J 2015 *Science* **347** 420
[397] Lu H, Bark C, Esque de los Ojos D, Alcala J, Eom C B, Catalan G and Gruverman A 2012 *Science* **336** 59
[398] Yu P, Chu Y H and Ramesh R 2012 *Mater. Today* **15** 320
[399] Yin Y W *et al* 2013 *Nat. Mater.* **12** 397
[400] Lichtensteiger C, Fernandez-Pena S, Weymann C, Zubko P and Triscone J M 2014 *Nano Lett.* **14** 4205
[401] Yu P *et al* 2012 *Proc. Natl Acad. Sci.* **109** 9710
[402] Borisevich A Y *et al* 2010 *ACS Nano* **4** 6071
[403] Mangalam R V K, Agar J C, Damodaran A R, Karthik J and Martin L W 2013 *ACS Appl. Mater. Interfaces* **5** 13235
[404] Mangalam R V K, Karthik J, Damodaran A R, Agar J C and Martin L W 2013 *Adv. Mater.* **25** 1761
[405] Lee D, Yang S M, Yoon J and Noh T W 2012 *Nano Lett.* **12** 6436
[406] Lee D, Yoon A, Jang S Y, Yoon J G, Chung J S, Kim M, Scott J F and Noh T W 2011 *Phys. Rev. Lett.* **107** 057602
[407] Catalan G, Noheda B, McAneney J, Sinnamon L J and Gregg J M 2005 *Phys. Rev.* B **72** 020102
[408] Indenbom V L, Loginov E B and Osipov M A 1981 *Kristallografiya* **26** 1157
[409] Catalan G, Lubk A, Vlooswijk A H G, Snoeck E, Magen C, Janssens A, Rispens G, Rijnders G, Blank D H A and Noheda B 2011 *Nat. Mater.* **10** 963
[410] Yudin P V and Tagantsev A K 2013 *Nanotechnology* **24** 432001
[411] Wen Z, Qiu X, Li C, Zheng C, Ge X, Li A and Wu D 2014 *Appl.Phys.Lett.* **104** 042907
[412] Gruverman A, Rodriguez B J, Kingon A I, Nemanich R J, Tagantsev A K, Cross J S and Tsukada M 2003 *Appl. Phys. Lett.* **83** 728
[413] Mantese J V, Schubring N W, Micheli A L and Catalan A B 1995 *Appl. Phys. Lett.* **67** 721
[414] Mantese J V, Schubring N W, Micheli A L, Catalan A B, Mohammed M S, Naik R and Auner G W 1997 *Appl. Phys. Lett.* **71** 2047
[415] Agar J C, Damodaran A R, Velarde G A, Pandya S, Mangalam R V K and Martin L W 2015 *ACS Nano* **9** 7332
[416] Ma W H and Cross L E 2006 *Appl. Phys. Lett.* **88** 232902
[417] Ma W H and Cross L E 2002 *Appl. Phys. Lett.* **81** 3440
[418] Ma W and Cross L E 2001 *Appl. Phys. Lett.* **79** 4420
[419] Ma W H and Cross L E 2001 *Appl. Phys. Lett.* **78** 2920
[420] Fu J Y, Zhu W, Li N and Cross L E 2006 *J. Appl. Phys.* **100** 024112
[421] Fu J Y, Zhu W, Li N, Smith N B and Cross L E 2007 *Appl. Phys. Lett.* **91** 182910
[422] Baskaran S, He X, Chen Q and Fu J Y 2011 *Appl. Phys. Lett.* **98** 242901
[423] Hana P, Marvan M, Burianova L, Zhang S J, Furman E and Shrout T R 2006 *Ferroelectrics* **336** 137
[424] Hana P 2007 *Ferroelectrics* **351** 196
[425] Cross L E 2006 *J. Mater. Sci.* **41** 53
[426] Ma W H and Cross L E 2005 *Appl. Phys. Lett.* **86** 072905
[427] Chu B, Zhu W, Li N and Cross L E 2009 *J. Appl. Phys.* **106** 104109
[428] Ponomareva I and Lisenkov S 2012 *Phys. Rev. Lett.* **108** 167604
[429] Hong J and Vanderbilt D 2013 *Phys. Rev.* B **88** 174107
[430] Frenkel A I, Ehre D, Lyahovitskaya V, Kanner L, Wachtel E and Lubomirsky I 2007 *Phys. Rev. Lett.* **99** 215502

[431] Kleemann W, Schafer F J and Fontana M D 1984 *Phys. Rev.* B **30** 1148
[432] Aktas O, Carpenter M A and Salje E K H 2013 *Appl. Phys. Lett.* **103** 142902
[433] Burns G and Dacol F H 1983 *Phys. Rev.* B **28** 2527
[434] Aschauer U, Pfenninger R, Selbach S M, Grande T and Spaldin N A 2013 *Phys. Rev.* B **88** 054111
[435] Zhang J, Xu R, Damodaran A R, Chen Z H and Martin L W 2014 *Phys. Rev.* B **89** 224101
[436] Stengel M 2013 *Nat. Commun.* **4** 2693
[437] Tagantsev A K and Yurkov A S 2012 *J. Appl. Phys.* **112** 044103
[438] Axe J D, Harada J and Shirane G 1970 *Phys. Rev.* B **1** 1227
[439] Farhi E, Tagantsev A K, Currat R, Hehlen B, Courtens E and Boatner L A 2000 *Eur. Phys. J.* B **15** 615
[440] Hehlen B, Arzel L, Tagantsev A K, Courtens E, Inaba Y, Yamanaka A and Inoue K 1998 *Phys. Rev.* B **57** 13989
[441] Mirzade F K 2007 *Phys. Status Solidi* B **244** 529
[442] Biancoli A, Fancher C M, Jones J L and Damjanovic D 2015 *Nat. Mater.* **14** 224
[443] Yudin P V, Ahluwalia R and Tagantsev A K 2014 *Appl. Phys. Lett.* **104** 082913
[444] Lee D *et al* 2014 *Adv. Mater.* **26** 5005
[445] Jia C, Urban K W, Alexe M, Hesse D and Vrejoiu I 2011 *Science* **331** 1420
[446] Lee D, Baek S H, Kim T H, Yoon J, Folkman C M, Eom C B and Noh T W 2011 *Phys. Rev.* B **84** 125305
[447] Narayanan M, Tong S, Liu S, Ma B and Balachandran U 2013 *Appl. Phys. Lett.* **102** 062906
[448] Nakamura K and Kawamura Y 2000 *IEEE Trans. Ultrason. Ferroelectr. Freq. Control* **47** 750
[449] Sebald G, Lefeuvre E and Guyomar D 2008 *IEEE Trans. Ultrason. Ferroelectr. Freq. Control* **55** 538
[450] Wang Q M, Du X H, Xu B M and Cross L E 1999 *IEEE Trans. Ultrason. Ferroelectr. Freq. Control* **46** 638
[451] Navid A and Pilon L 2011 *Smart Mater. Struct.* **20** 025012
[452] Sebald G, Seveyrat L, Guyomar D, Lebrun L, Guiffard B and Pruvost S 2006 *J. Appl. Phys.* **100** 124112
[453] Reiner J W, Kolpak A M, Segal Y, Garrity K F, Ismail-Beigi S, Ahn C H and Walker F J 2010 *Adv. Mater.* **22** 2919
[454] Mazet L, Yang S M, Kalinin S V, Schamm-Chardon S and Dubourdieu C 2015 *Sci. Technol. Adv. Mater.* **16** 036005
[455] McKee R A, Walker F J and Chisholm M F 1998 *Phys. Rev. Lett.* **81** 3014
[456] McKee R A, Walker F J and Chisholm M F 2001 *Science* **293** 468
[457] Lin A, Hong X, Wood V, Verevkin A A, Ahn C H, McKee R A, Walker F J and Specht E D 2001 *Appl. Phys. Lett.* **78** 2034
[458] Kim D M, Eom C B, Nagarajan V, Ouyang J, Ramesh R, Vaithyanathan V and Schlom D G 2006 *Appl. Phys. Lett.* **88** 142904
[459] Niu F and Wessels B W 2007 *J. Vac. Sci. Technol.* B **25** 1053
[460] Niu G, Yin S, Saint-Girons G, Gautier B, Lecoeur P, Pillard V, Hollinger G and Vilquin B 2011 *Microelectron. Eng.* **88** 1232
[461] Vaithyanathan V *et al* 2006 *J. Appl. Phys.* **100** 024108
[462] Woicik J C, Li H, Zschack P, Karapetrova E, Ryan P, Ashman C R and Hellberg C S 2006 *Phys. Rev.* B **73** 024112
[463] Warusawithana M P *et al* 2009 *Science* **324** 367
[464] Hudait M K, Zhu Y, Jain N, Maurya D, Zhou Y, Varghese R and Priya S 2013 *ACS Appl. Mater. Interfaces* **5** 11446
[465] Hudait M K, Zhu Y, Jain N, Maurya D, Zhou Y and Priya S 2013 *J. Appl. Phys.* **114** 024303
[466] Fredrickson K D, Ponath P, Posadas A B, McCartney M R, Aoki T, Smith D J and Demkov A A 2014 *Appl. Phys. Lett.* **104** 242908
[467] Vehkamäki M, Hatanpää T, Hänninen T, Ritala M and Leskelä M 1999 *Electrochem. Solid State Lett.* **2** 504
[468] Yim C J, Kim S U, Kang Y S, Cho M H and Ko D H 2011 *Electrochem. Solid State Lett.* **14** G45
[469] Vehkamäki M, Hatanpää T, Ritala M, Leskelä M, Väyrynen S and Rauhala E 2007 *Chem. Vapor Depos.* **13** 239
[470] Weon Hwang G, Ju Lee H, Lee K and Seong Hwang C 2007 *J. Electrochem. Soc.* **154** G69
[471] Watanabe T, Hoffmann-Eifert S, Hwang C S and Waser R 2008 *J. Electrochem. Soc.* **155** D715
[472] Zhang F, Perng Y C, Choi J H, Wu T, Chung T K, Carman G P, Locke C, Thomas S, Saddow S E and Chang J P 2011 *J. Appl. Phys.* **109** 124109
[473] Choi J H, Zhang F, Perng Y C and Chang J P 2013 *J. Vac. Sci. Technol.* B **31** 012207
[474] Akbashev A R, Chen G and Spanier J E 2014 *Nano Lett.* **14** 44
[475] Zhang F *et al* 2013 *J. Phys. Chem.* C **117** 24579
[476] Liu Y T, Ku C S, Chiu S J, Lee H Y and Chen S Y 2014 *ACS Appl. Mater. Interfaces* **6** 443
[477] McDaniel M D, Ngo T Q, Hu S, Posadas A, Demkov A A and Ekerdt J G 2015 *Appl. Phys. Rev.* **2** 041301
[478] Scott J F 2007 *Science* **315** 954
[479] Theis T N and Solomon P M 2010 *Proc. IEEE* **98** 2005
[480] Theis T N and Solomon P M 2010 *Science* **327** 1600
[481] Tsymbal E Y and Gruverman A 2013 *Nat. Mater.* **12** 602
[482] Liao L *et al* 2009 *ACS Nano* **3** 700
[483] Ionescu A M 2012 *Nat. Nanotechnol.* **7** 83
[484] Salahuddin S and Dattat S 2008 *Nano Lett.* **8** 405
[485] Krowne C M, Kirchoefer S W, Chang W, Pond J M and Alldredge L M B 2011 *Nano Lett.* **11** 988
[486] Khan A I, Bhowmik D, Yu P, Kim S J, Pan X, Ramesh R and Salahuddin S 2011 *Appl. Phys. Lett.* **99** 113501
[487] Appleby D J R, Ponon N K, Kwa K S K, Zou B, Petrov P K, Wang T, Alford N M and O'Neill A 2014 *Nano Lett.* **14** 3864
[488] Gao W, Khan A, Marti X, Nelson C, Serrao C, Ravichandran J, Ramesh R and Salahuddin S 2014 *Nano Lett.* **14** 5814
[489] Khan A I, Chatterjee K, Wang B, Drapcho S, You L, Serrao C, Bakaul S R, Ramesh R and Salahuddin S 2015 *Nat. Mater.* **14** 182
[490] Trolier-Mckinstry S and Muralt P 2004 *J. Electroceram.* **12** 7
[491] Zhang S, Li F, Jiang X, Kim J, Luo J and Geng X 2015 *Prog. Mater. Sci.* **68** 1
[492] Kim Y, Lee C S and Jin W 2005 *Sensors* **17** 57
[493] Maeda R, Tsaur J J, Lee S H and Ichiki M 2005 *Electroceramic-Based MEMS Fabrication-Technology and Applications* ed N Setter (New York: Springer) p 19
[494] Liu J Q, Fang H B, Xu Z Y, Mao X H, Shen X C, Chen D, Liao H and Cai B C 2008 *Microelectron. J.* **39** 802
[495] Saadon S and Sidek O 2011 *Energy Convers. Manage.* **52** 500
[496] Laser D J and Santiago J G 2004 *J. Micromech. Microeng.* **14** R35
[497] Woias P 2005 *Sensors Actuators* B **105** 28
[498] Abel S *et al* 2013 *Nat. Commun.* **4** 1671
[499] Petraru A, Schubert J, Schmid M and Buchal C 2002 *Appl. Phys. Lett.* **81** 1375
[500] Lin P T, Liu Z and Wessels B W 2009 *J. Opt.* A **11** 075005
[501] Abel S, Caimi D, Sousa M, Stöferle T, Rossel C, Marchiori C, Chelnokov A and Fompeyrine J 2012 *Proc. SPIE* **8263** 82630Y
[502] Fusil S, Garcia V, Barthélémy A and Bibes M 2014 *Annu. Rev. Mater. Res.* **44** 91
[503] Béa H, Gajek M, Bibes M and Barthélémy A 2008 *J. Phys.: Condens. Matter* **20** 434221

[504] Chu Y *et al* 2008 *Nat. Mater.* **7** 478
[505] Ma J, Hu J, Li Z and Nan C W 2011 *Adv. Mater.* **23** 1062
[506] Liu M, Obi O, Lou J, Stoute S, Cai Z, Ziemer K and Sun N X 2009 *J. Phys. D Appl. Phys.* **42** 045007
[507] Ren S and Wuttig M 2008 *Appl. Phys. Lett.* **92** 083502
[508] Eerenstein W, Wiora M, Prieto J L, Scott J F and Mathur N D 2007 *Nat. Mater.* **6** 348
[509] Molegraaf H J A, Hoffman J, Vaz C A F, Gariglio S, Van D M, Ahn C H and Triscone J M 2009 *Adv. Mater.* **21** 3470
[510] Vaz C A F, Hoffman J, Segal Y, Reiner J W, Grober R D, Zhang Z, Ahn C H and Walker F J 2010 *Phys. Rev. Lett.* **104** 127202
[511] Lu H *et al* 2012 *Appl. Phys. Lett.* **100** 232904
[512] Thiele C, Dörr K, Bilani O, Rödel J and Schultz L 2007 *Phys. Rev.* B **75** 054408
[513] Brintlinger T, Lim S H, Baloch K H, Alexander P, Qi Y, Barry J, Melngailis J, Salamanca-Riba L, Takeuchi I and Cumings J 2010 *Nano Lett.* **10** 1219
[514] Cherifi R O *et al* 2014 *Nat. Mater.* **13** 345
[515] Phillips L C *et al* 2015 *Sci. Rep.* **5** 10026
[516] Lahtinen T H E, Franke K and van Dijken S 2012 *Sci. Rep.* **2** 258
[517] Cheng Z X, Wang X L, Dou S X, Osada M and Kimura H 2011 *Appl. Phys. Lett.* **99** 19
[518] Czeschka F D, GeprÃgs S, Opel M, Goennenwein S T B and Gross R 2009 *Appl. Phys. Lett.* **95** 062508
[519] Catalan G, Seidel J, Ramesh R and Scott J F 2012 *Rev. Mod. Phys.* **84** 119
[520] Seidel J 2012 *J. Phys. Chem. Lett.* **3** 2905
[521] Jesse S and Kalinin S V 2011 *J. Phys.* D **44** 464006
[522] Kalinin S V, Rar A and Jesse S 2006 *IEEE Trans. Ultrason. Ferroelectr. Freq. Control* **53** 2226
[523] Kalinin S V, Morozovska A N, Chen L Q and Rodriguez B J 2010 *Rep. Prog. Phys.* **73** 056052
[524] Chiu Y P *et al* 2011 *Adv. Mater.* **23** 1530
[525] Lubk A, Rossell M D, Seidel J, He Q, Yang S Y, Chu Y H, Ramesh R, Hytch M J and Snoeck E 2012 *Phys. Rev. Lett.* **109** 047601
[526] Gao P *et al* 2014 *Nat. Commun.* **5** 3801
[527] Nelson C T *et al* 2011 *Science* **334** 968
[528] Barrett N *et al* 2013 *J. Appl. Phys.* **113** 187217
[529] Cherifi S, Hertel R, Fusil S, Bea H, Bouzehouane K, Allibe J, Bibes M and Barthelemy A 2010 *Phys. Status Solidi Lett.* **4** 22
[530] Seidel J, Yang S Y, Alarcón-Lladó E, Ager J W and Ramesh R 2012 *Ferroelectrics* **433** 123
[531] Meyer B and Vanderbilt D 2002 *Phys. Rev.* B **65** 104111
[532] Lubk A, Gemming S and Spaldin N A 2009 *Phys. Rev.* B **80** 104110
[533] Aird A and Salje E K H 1998 *J. Phys.: Condens. Matter* **10** L377
[534] Balke N *et al* 2012 *Nat. Phys.* **8** 81
[535] Maksymovych P, Seidel J, Chu Y H, Wu P, Baddorf A P, Chen L Q, Kalinin S V and Ramesh R 2011 *Nano Lett.* **11** 1906
[536] Seidel J *et al* 2010 *Phys. Rev. Lett.* **105** 197603
[537] Seidel J, Singh-Bhalla G, He Q, Yang S, Chu Y and Ramesh R 2013 *Phase Transit.* **86** 53
[538] Morozovska A N, Vasudevan R K, Maksymovych P, Kalinin S V and Eliseev E A 2012 *Phys. Rev.* B **86** 085315
[539] Farokhipoor S and Noheda B 2011 *Phys. Rev. Lett.* **107** 127601
[540] Meier D, Seidel J, Cano A, Delaney K, Kumagai Y, Mostovoy M, Spaldin N A, Ramesh R and Fiebig M 2012 *Nat. Mater.* **11** 284
[541] Du Y, Wang X L, Chen D P, Dou S X, Cheng Z X, Higgins M, Wallace G and Wang J Y 2011 *Appl. Phys. Lett.* **99** 252107
[542] Wu W, Horibe Y, Lee N, Cheong S W and Guest J R 2012 *Phys. Rev. Lett.* **108** 077203
[543] Guyonnet J, Gaponenko I, Gariglio S and Paruch P 2011 *Adv. Mater.* **23** 5377
[544] Schröder M, Haußmann A, Thiessen A, Soergel E, Woike T and Eng L M 2012 *Adv. Funct. Mater.* **22** 3936
[545] Sluka T, Tagantsev A K, Bednyakov P and Setter N 2013 *Nat. Commun.* **4** 1808
[546] Eliseev E A, Yudin P V, Kalinin S V, Setter N, Tagantsev A K and Morozovska A N 2013 *Phys. Rev.* B **87** 054111
[547] Eliseev E A, Morozovska A N, Svechnikov G S, Maksymovych P and Kalinin S V 2012 *Phys. Rev.* B **85** 045312
[548] Gureev M Y, Mokry P, Tagantsev A K and Setter N 2012 *Phys. Rev.* B **86** 104104
[549] Seidel J *et al* 2009 *Nat. Mater.* **8** 229
[550] Khan A I, Marti X, Serrao C, Ramesh R and Salahuddin S 2015 *Nano Lett.* **15** 2229
[551] Rojac T, Ursic H, Bencan A, Malic B and Damjanovic D 2015 *Adv. Funct. Mater.* **25** 2099
[552] McGilly L J, Yudin P, Feig l L, Tagantsev A K and Setter N 2015 *Nat. Nanotechnol.* **10** 145
[553] Maksymovych P, Morozovska A N, Yu P, Eliseev E A, Chu Y, Ramesh R, Baddorf A P and Kalinin S V 2012 *Nano Lett.* **12** 209
[554] Vasudevan R K, Morozovska A N, Eliseev E A, Britson J, Yang J, Chu Y, Maksymovych P, Chen L Q, Nagarajan V and Kalinin S V 2012 *Nano Lett.* **12** 5524
[555] Farokhipoor S and Noheda B 2012 *J. Appl. Phys.* **112** 052003
[556] Yang C H *et al* 2009 *Nat. Mater.* **8** 485
[557] Li D and Bonnell D A 2008 *Annu. Rev. Mater. Res.* **38** 351
[558] Agar J C *et al* 2016 *Nat Mater.* (http://www.nature.com/nmat/journal/vaop/ncurrent/full/nmat4567.html)
[559] Parkin S S P, Hayashi M and Thomas L 2008 *Science* **320** 190
[560] Yamanouchi M, Chiba D, Matsukura F and Ohno H 2004 *Nature* **428** 539
[561] Chynoweth A G 1956 *Phys. Rev.* **102** 705
[562] Fridkin V M and Popov B N 1978 *Sov. Phys.—Usp.* **21** 981
[563] Glass A M, Linde D V D and Negran T J 1974 *Appl. Phys. Lett.* **25** 233
[564] Brody P S and Crowne F 1975 *J. Electron. Mater.* **4** 955
[565] Belinicher V I and Sturman B I 1980 *Sov. Phys.—Usp.* **23** 199
[566] Young S M, Zheng F and Rappe A M 2012 *Phys. Rev. Lett.* **109** 236601
[567] Zenkevich A, Matveyev Y, Maksimova K, Gaynutdinov R, Tolstikhina A and Fridkin V 2014 *Phys. Rev.* B **90** 161409
[568] Pintilie L, Alexe M, Pintilie I and Botila T 1996 *Appl. Phys. Lett.* **69** 1571
[569] Pintilie L, Alexe M, Pignolet A and Hesse D 1998 *J. Phys.* IV **8** 101
[570] Pintilie L, Alexe M, Pignolet A and Hesse D 1998 *Appl. Phys. Lett.* **73** 342
[571] Yang S Y *et al* 2009 *Appl. Phys. Lett.* **95** 062909
[572] Ji W, Yao K and Liang Y C 2010 *Adv. Mater.* **22** 1763
[573] Yang S Y *et al* 2010 *Nat. Nanotechnol.* **5** 143
[574] Bhatnagar A, Chaudhuri A R, Kim Y H, Hesse D and Alexe M 2013 *Nat. Commun.* **4** 2835
[575] Ji W, Yao K and Liang Y C 2011 *Phys. Rev.* B **84** 094115
[576] Alexe M and Hesse D 2011 *Nat. Commun.* **2** 256
[577] Grinberg I *et al* 2013 *Nature* **503** 509
[578] Guo R, You L, Zhou Y, Lim Z S, Zou X, Chen L, Ramesh R and Wang J 2013 *Nat. Commun.* **4** 1990
[579] Whatmore R W 1986 *Rep. Prog. Phys.* **49** 1335
[580] Rosenman G, Shur D, Krasik Y E and Dunaevsky A 2000 *J. Appl. Phys.* **88** 6109
[581] Lu S and Zhang Q 2009 *Adv. Mater.* **21** 1983

[582] Olsen R B, Bruno D A and Briscoe J M 1985 *J. Appl. Phys.* **58** 4709
[583] Sebald G, Pruvost S and Guyomar D 2008 *Smart Mater. Struct.* **17** 015012
[584] Sharma A, Ban Z G and Alpay S P 2004 *J. Appl. Phys.* **95** 3618
[585] Akcay G, Misirlioglu I B and Alpay S P 2007 *J. Appl. Phys.* **101** 104110
[586] Akcay G, Alpay S P, Mantese J V and Rossetti G A 2007 *Appl. Phys. Lett.* **90** 252909
[587] Akcay G, Alpay S P, Rossetti G A and Scott J F 2008 *J. Appl. Phys.* **103** 024104
[588] Marathe M and Ederer C 2014 *Appl. Phys. Lett.* **104** 212902
[589] Liu Y, Infante I C, Lou X, Lupascu D C and Dkhil B 2014 *Appl. Phys. Lett.* **104** 012907
[590] Zhang J, Cole M W and Alpay S P 2010 *J. Appl. Phys.* **108** 054103
[591] Zhang J, Alpay S P and Rossetti G A 2011 *Appl. Phys. Lett.* **98** 132907
[592] Zhang J, Misirlioglu I B, Alpay S P and Rossetti G A 2012 *Appl. Phys. Lett.* **100** 222909
[593] Kesim M T, Zhang J, Trolier-McKinstry S, Mantese J V, Whatmore R W and Alpay S P 2013 *J. Appl. Phys.* **114** 204101
[594] Zhong S, Alpay S P, Ban Z G and Mantese J V 2005 *Appl. Phys. Lett.* **86** 092903
[595] Espinal Y, Kesim M T, Misirlioglu I B, Trolier-McKinstry S, Mantese J V and Alpay S P 2014 *Appl. Phys. Lett.* **105** 232905
[596] Lang S B 2005 *Phys. Today* **58** 31
[597] Mischenko A S, Zhang Q, Scott J F, Whatmore R W and Mathur N D 2006 *Science.* **311** 1270
[598] Mischenko A S, Zhang Q, Whatmore R W and Scott J F and Mathur N D 2006 *Appl. Phys. Lett.* **89** 242912
[599] Chynoweth A G 1956 *J. Appl. Phys.* **27** 78
[600] Byer R L and Roundy C 1972 *Ferroelectrics* **3** 333
[601] Zhao S, Zhang S, Liu W, Donnelly N, Xu Z and Randall C 2009 *J. Appl. Phys.* **105** 053705
[602] Takayama R and Tomita Y 1989 *J. Appl. Phys.* **65** 1666
[603] Liu W, Ko J S and Zhu W 2000 *Thin Solid Films* **371** 254
[604] Zhang Q and Whatmore R W 2001 *J. Phys.* D **34** 2296
[605] Bhatia B, Karthik J, Tong T, Cahill D G, Martin L W and King W P 2012 *J. Appl. Phys.* **112** 104106
[606] Bhatia B, Damodaran A R, Cho H, Martin L W and King W P 2014 *J. Appl. Phys.* **116** 194509
[607] Tong T, Karthik J, Mangalam R V K, Martin L W and Cahill D G 2014 *Phys. Rev.* B **90** 094116
[608] Botea M, Iuga A and Pintilie L 2013 *Appl. Phys. Lett.* **103** 232902
[609] Tong T, Karthik J, Martin L W and Cahill D G 2014 *Phys. Rev.* B **90** 155423
[610] Bowen C R, Taylor J, LeBoulbar E, Zabek D, Chauhan A and Vaish R 2014 *Energy Environ. Sci.* **7** 3836
[611] Moya X, Kar-Narayan S and Mathur N D 2014 *Nat. Mater.* **13** 439
[612] Correia T M, Young J S, Whatmore R W, Scott J F, Mathur N D and Zhang Q 2009 *Appl. Phys. Lett.* **95** 182904
[613] Chen H, Ren T, Wu X, Yang Y and Liu L 2009 *Appl. Phys. Lett.* **94** 182902
[614] Valant M 2012 *Prog. Mater. Sci.* **57** 980
[615] Correia T and Zhang Q 2014 *Electrocaloric Materials: New Generation of Coolers* vol 34, ed T Correia and Q Zhang (Berlin: Springer) p 253
[616] Alpay S P, Mantese J, Trolier-McKinstry S, Zhang Q and Whatmore R W 2014 *MRS Bull.* **39** 1099
[617] Peng B, Fan H and Zhang Q 2013 *Adv. Funct. Mater.* **23** 2987
[618] Chukka R, Cheah J W, Chen Z, Yang P, Shannigrahi S, Wang J and Chen L 2011 *Appl. Phys. Lett.* **98** 242902
[619] Guyomar D, Sebald G, Guiffard B and Seveyrat L 2006 *J. Phys.* D **39** 4491
[620] Kar-Narayan S and Mathur N D 2010 *J. Phys.* D **43** 032002
[621] Kar-Narayan S, Crossley S, Moya X, Kovacova V, Abergel J, Bontempi A, Baier N, Defay E and Mathur N D 2013 *Appl. Phys. Lett.* **102** 032903
[622] Lu S G, Rožič B, Zhang Q M, Kutnjak Z, Pirc R, Lin M, Li X and Gorny L 2010 *Appl. Phys. Lett.* **97** 202901
[623] Goupil F L, Berenov A, Axelsson A, Valant M and Alford N M 2012 *J. Appl. Phys.* **111** 124109
[624] Ceder G and Persson K 2013 *Sci. Am.* **309** 36
[625] Curtarolo S, Hart G L W, Nardelli M B, Mingo N, Sanvito S and Levy O 2013 *Nat. Mater.* **12** 191
[626] Lee L P, Burns M J and Char K 1992 *Appl. Phys. Lett.* **61** 2706
[627] Mechin L, Villegier J C and Bloyet D 1997 *J. Appl. Phys.* **81** 7039
[628] Kanno I, Fujii S, Kamada T and Takayama R 1997 *Appl. Phys. Lett.* **70** 1378
[629] Kim J H and Grishin A M 2005 *Appl. Phys. Lett.* **87** 033502
[630] Jang H W, Baek S H, Ortiz D, Folkman C M, Eom C B, Chu Y H, Shafer P, Ramesh R, Vaithyanathan V and Schlom D G 2008 *Appl. Phys. Lett.* **92** 062910
[631] Pellegrino L, Biasotti M, Bellingeri E, Bernini C, Siri A S and Marré D 2009 *Adv. Mater.* **21** 2377
[632] Baek S H *et al* 2011 *Science* **334** 958
[633] Reuter K and Scheffler M 2001 *Phys. Rev.* B **65** 035406
[634] He L and Vanderbilt D 2003 *Phys. Rev.* B **68** 134103
[635] Ederer C and Spaldin N 2005 *Phys. Rev.* B **71** 224103
[636] Li D, Zhao M H, Garra J, Kolpak A M, Rappe A M, Bonnell D A and Vohs J M 2008 *Nat. Mater.* **7** 473
[637] Kolpak A M, Li D, Shao R, Rappe A M and Bonnell D A 2008 *Phys. Rev. Lett.* **101** 036102
[638] Martirez J M P, Morales E H, Saidi W A, Bonnell D A and Rappe A M 2012 *Phys. Rev. Lett.* **109** 256802
[639] Morales E H, Martirez J M P, Saidi W A, Rappe A M and Bonnell D A 2014 *ACS Nano* **8** 4465
[640] Martirez J M P, Kim S, Morales E H, Diroll B T, Cargnello M, Gordon T R, Murray C B, Bonnell D A and Rappe A M 2015 *J. Am. Chem. Soc.* **137** 2939
[641] Spanier J E, Kolpak A M, Urban J J, Grinberg I, Ouyang L, Yun W S, Rappe A M and Park H 2006 *Nano Lett.* **6** 735
[642] Tinte S, Burton B P, Cockayne E and Waghmare U V 2006 *Phys. Rev. Lett.* **97** 137601
[643] Grinberg I, Juhas P, Davies P K and Rappe A M 2007 *Phys. Rev. Lett.* **99** 267603
[644] Grinberg I, Shin Y H and Rappe A M 2009 *Phys. Rev. Lett.* **103** 197601
[645] Pasciak M, Welberry T R, Kulda J, Kempa M and Hlinka J 2012 *Phys. Rev.* B **85** 224109
[646] Takenaka H, Grinberg I and Rappe A M 2013 *Phys. Rev. Lett.* **110** 147602
[647] Takenaka H, Grinberg I, Shin Y H and Rappe A M 2014 *Ferroelectrics* **469** 1
[648] Gao P, Nelson C T, Jokisaari J R, Baek S, Bark C W, Zhang Y, Wang E, Schlom D G, Eom C and Pan X 2011 *Nat. Commun.* **2** 591
[649] Gao P *et al* 2012 *Adv. Mater.* **24** 1106
[650] Winkler C R, Damodaran A R, Karthik J, Martin L W and Taheri M L 2012 *Micron* **43** 1121
[651] Winkler C R, Jablonski M L, Damodaran A R, Jambunathan K, Martin L W and Taheri M L 2012 *J. Appl. Phys.* **112** 052013
[652] Winkler C R *et al* 2014 *Nano Lett.* **14** 3617
[653] Jesse S, Kalinin S V, Proksch R, Baddorf A P and Rodriguez B J 2007 *Nanotechnology* **18** 435503
[654] Bintachitt P, Jesse S, Damjanovic D, Han Y, Reaney I M, Trolier-McKinstry S and Kalinin S V 2010 *Proc. Natl Acad. Sci.* **107** 7219

[655] Griggio F, Jesse S, Kumar A, Marincel D M, Tinberg D S, Kalinin S V and Trolier-McKinstry S 2011 *Appl. Phys. Lett.* **98** 212901
[656] Vasudevan R K, Zhang S, Ding J, Okatan M B, Jesse S, Kalinin S V and Bassiri-Gharb N 2015 *Appl. Phys. Lett.* **106** 222901
[657] Evans P G and Sichel-Tissot R J 2013 *Am. Ceram. Soc. Bull.* **92** 18
[658] Grigoriev A, Sichel R, Lee H N, Landahl E C, Adams B, Dufresne E M and Evans P G 2008 *Phys. Rev. Lett.* **100** 027604
[659] Do D H, Grigoriev A, Kim D M, Eom C, Evans P G and Dufresne E M 2008 *Integr. Ferroelectr.* **101** 174
[660] Highland M J, Fister T T, Richard M, Fong D D, Fuoss P H, Thompson C, Eastman J A, Streiffer S K and Stephenson G B 2010 *Phys. Rev. Lett.* **105** 167601
[661] Fong D D *et al* 2005 *Phys. Rev.* B **71** 144112
[662] Fong D D *et al* 2006 *Phys. Rev. Lett.* **96** 127601
[663] Hruszkewycz S O, Highland M J, Holt M V, Kim D, Folkman C M, Thompson C, Tripathi A, Stephenson G B, Hong S and Fuoss P H 2013 *Phys. Rev. Lett.* **110** 177601
[664] Wang R V *et al* 2009 *Phys. Rev. Lett.* **102** 047601
[665] Highland M J, Fister T T, Fong D D, Fuoss P H, Thompson C, Eastman J A, Streiffer S K and Stephenson G B 2011 *Phys. Rev. Lett.* **107** 187602
[666] Grigoriev A, Do D, Kim D M, Eom C, Adams B, Dufresne E M and Evans P G 2006 *Phys. Rev. Lett.* **96** 187601
[667] Daranciang D *et al* 2012 *Phys. Rev. Lett.* **108** 087601
[668] Wen H *et al* 2013 *Phys. Rev. Lett.* **110** 037601
[669] Schick D, Herzog M, Wen H, Chen P, Adamo C, Gaal P, Schlom D G, Evans P G, Li Y and Bargheer M 2014 *Phys. Rev. Lett.* **112** 097602
[670] Nah S, Kuo Y, Chen F, Park J, Sinclair R and Lindenberg A M 2014 *Nano Lett.* **14** 4322
[671] Dawber M, Gruverman A and Scott J F 2006 *J. Phys.: Condens. Matter* **18** L71
[672] Gregg J M 2012 *Ferroelectrics* **433** 74
[673] Kane C L and Mele E J 2005 *Phys. Rev. Lett.* **95** 146802
[674] Hasan M Z and Kane C L 2010 *Rev. Mod. Phys.* **82** 3045
[675] Qi X and Zhang S 2011 *Rev. Mod. Phys.* **83** 1057
[676] Wurfel P and Batra I P 1973 *Phys. Rev.* B **8** 5126
[677] Xiao D, Yao Y, Feng W, Wen J, Zhu W, Chen X, Stocks G M and Zhang Z 2010 *Phys. Rev. Lett.* **105** 096404
[678] Ishizaka K *et al* 2011 *Nat. Mater.* **10** 521
[679] Brune C *et al* 2011 *Phys. Rev. Lett.* **106** 126803
[680] Chen Y L *et al* 2013 *Nat. Phys.* **9** 704
[681] Plekhanov E, Barone P, Di Sante D and Picozzi S 2014 *Phys. Rev.* B **90** 161108
[682] Wang Q, Wu S, Felser C, Yan B and Liu C 2015 *Phys. Rev.* B **91** 165435
[683] Zheng F, Tan L Z, Liu S and Rappe A M 2015 *Nano Lett.* **15** 7794